2024

Breaking Down Microtubule Formation: Characterizing the Biochemical and Cellular Functions of the γ-Tubulin Ring Complex

Adi Y. Berman

BREAKING DOWN MICROTUBULE FORMATION:

CHARACTERIZING THE BIOCHEMICAL AND CELLULAR FUNCTIONS OF

THE γ-TUBULIN RING COMPLEX

A Thesis Presented to the Faculty of
The Rockefeller University
in Partial Fulfillment of the Requirements for
the degree of Doctor of Philosophy

By

Adi Y. Berman

June 2024

BREAKING DOWN MICROTUBULE FORMATION: CHARACTERIZING THE BIOCHEMICAL AND CELLULAR FUNCTIONS OF THE γ-TUBULIN RING COMPLEX

Adi Y. Berman, Ph.D.

The Rockefeller University 2024

The γ-Tubulin ring complex (γ-TuRC) is an essential regulator of the microtubule cytoskeleton. It is composed of >30 individual proteins that include the major component, γ-tubulin, as well as γ-tubulin complex proteins 2-6 (GCP2-6), mitotic-spindle organizing proteins associated with a ring of γ-tubulin proteins 1 and 2 (MOZART, or MZT1 and MZT2), and an actin molecule. This ~2.2MDa assembly regulates microtubule dynamics by facilitating the nucleation of new microtubules, modulating microtubule minus-end dynamics by acting as a minus-end cap, and anchoring microtubules to specify their cellular localization. These three major activities of the γ-TuRC, nucleation, capping, and anchoring, contribute to the dynamic nature of individual microtubules and of larger microtubule networks that are critical for cellular activities, including cell motility, intracellular trafficking, and cell division. In recent years, structural studies of the γ-TuRC have spurred biochemical and cellular characterization of its nucleation activity. However, it remains unclear how the remaining major γ-TuRC activities contribute to microtubule dynamics.

In the first part of this thesis, I characterize the capping activity of the γ-TuRC. Using biochemical assays, I examine the association of recombinantly expressed and purified γ-TuRC at microtubule minus-ends either following a nucleation event, or on pre-formed microtubules. Using total internal reflection fluorescence (TIRF) microscopy, the dynamics of this association can be quantified in terms of the number of microtubules that are capped, and the length of time the cap persists at the minus-end under these two conditions. Additionally, I purified a recombinant γ-TuRC composed of GTP-binding deficient γ-tubulin in order to examine the GTP-binding dependency of the γ-TuRC's capping activity. As opposed to the γ-TuRC's nucleation activity, which is GTP-binding dependent, I found that the γ-TuRC's capping activity is GTP-binding independent. By expressing GTP-binding deficient γ-tubulin in HeLa cells depleted of endogenous γ-tubulin protein, I characterized the role of the γ-TuRC's capping activity in dividing cells. While cells expressing the GTP-binding γ-tubulin mutant could not form bipolar mitotic spindles and became arrested in mitosis, fixed- and live-cell imaging experiments showed that expression of this mutant rescued non-centrosomal microtubule formation, which was lost under γ-tubulin knockdown conditions. Together, these data suggest that the γ-TuRC's capping activity is GTP-binding independent and plays a role in non-centrosomal microtubule formation during mitosis.

In the second part of my thesis, I perform studies towards further characterizing the γ-TuRC. First, I use affinity-purification followed by mass spectrometry to characterize the composition of γ-TuRCs purified from a HeLa cell line overexpressing GFP-tagged γ-tubulin. Further mass spectrometry analysis identified interacting proteins that co-purified with γ-tubulin, some of which have a known function related to the microtubule

cytoskeleton or cell division. Second, I performed cell biology experiments to examine how the composition of the γ-TuRC may affect its activities. Recent work has suggested that the N-terminal domains of GCP6, named the N-helical domains (NHD) and the "belt" domain, are needed to maintain the structural integrity of the γ-TuRC, and that without these domains, specific components of the complex are lost. Cells expressing these N-terminally truncated GCP6 constructs displayed partial γ-tubulin-containing complexes relative to cells expressing full-length GCP6. Furthermore, cells expressing GCP6 truncated of the NHDs and the belt domain showed loss of centrosomal GCP6 and γ-tubulin specifically during mitosis, while their centrosomal localization persisted during interphase. Together, these data suggest that different components of the γ-TuRC may mediate the localization and anchoring of the γ-TuRC at specific cellular sites, such as the centrosome.

To Shai and Yonah

Acknowledgements

I am incredibly thankful that I had the privilege to spend the last few years in the Kapoor lab. Every person that I have worked with has taught me so much, both at the bench and outside of the lab. I am particularly thankful to Dr. Michal Wieczorek, whose discoveries regarding the γ-TuRC and microtubules laid the foundation for the conception of these projects, and whose mentorship and guidance made me a better scientist. Additionally, I would like to thank Drs. Amol Aher, Lina Carlini, and Keith Mickolajczyk for everything they taught me regarding biochemistry, microscopy, and data analysis. Finally, thank you to my advisor, Tarun, for allowing me the opportunity to explore my scientific curiosities and expand my experimental capabilities. Your advice helped me navigate the obstacles I faced, whether inside or outside of the lab. Your mentorship, which coupled the highest of expectations with unwavering support, will impact my career for many years to come.

I would like to thank my committee members, Drs. Brian Chait, Gregory Alushin, and Yael David. Brian, thank you for opening your door to me whenever I asked. Your scientific expertise has been critical to my research, and your excitement has kept me motivated. Greg, your profound knowledge and insights regarding the cytoskeleton have provoked many thoughtful discussions regarding my work. Yael, your multidisciplinary expertise made you an invaluable member of my committee. Your questions during my committee meetings made me expand my way of thinking and approach my research in new ways, and your advice and support went beyond the scope of my research. I would also like to thank Dr. Iain Cheeseman for agreeing to serve as my external examiner. Your impactful work regarding cell division has been an important influence on my research.

I would also like to thank my collaborators in the Chait lab, Dr. P. Dominic Olinares and Dr. Wenzhu Zhang, for their important contributions to this work. Thank you as well to the Rockefeller University Electron Microscopy and Proteomics Resource Centers for all of their help and guidance.

Thank you to the TPCB administration and the Rockefeller graduate program for their support in my studies. In particular, thank you to Dr. Derek Tan for your dedication to making sure that every part of the graduate school experience, both science-related and in general, is taken care of. I am very grateful I had you to turn to whenever the need arose.

Thank you to my parents for always encouraging and enabling me to pursue my interests. Ima, your artistic creativity and ability to get everything done even when time shouldn't permit it, and Abba, your love for logical reasoning and mathematical analysis, have been key characteristics that shape who I am and the science that I do. Thank you to each member of my family for your constant support during the long hours, busy weekends, and for listening to my incessant ramblings about cell biology.

Thank you to my son, Yonah, for making every day filled with laughter and excitement. You motivate me to work harder, think more creatively, and push myself to learn new things.

Lastly, thank you to my husband, Shai. Thank you for becoming an unofficial scientist just so you could listen to hours of practice presentations, edit countless pages of scientific reports, and understand my experiments. I can't wait for all of the life-long discoveries we will continue to make together.

Table of Contents

List of Figures

List of Tables

List of Abbreviations

γ-TuRC	γ-Tubulin ring complex
γ-TuSC	γ-tubulin small complex
GCP	γ-Tubulin complex protein
MZT	Mitotic-spindle organizing proteins associated with a ring of γ-tubulin (MOZART)
TIRF	Total internal reflection fluorescence
NHD	N-helical domains
MTOC	Microtubule organizing centers
MAP	Microtubule associated proteins
CLASP	Cytoplasmic linker-associated protein
CAMSAP	Calmodulin-regulated spectrin-associated protein
ASPM	Abnormal spindle-like microcephaly associated
PCM	Pericentriolar material
LB	Luminal bridge
GFP	Green fluorescent protein
GMPCPP	Guanylyl-(α,β)-methylene-diphosphonate
LFQ	Label-free quantitation
CPC	Chromosome passenger complex
MTA	Metastatic tumor antigen
NuRD	Nucleosome remodeling and histone deacetylation

Chapter 1: Introduction

1.1 Overview of the microtubule cytoskeleton

Microtubules are one of the main elements of the cytoskeleton (Fig. 1.1 A and B). They are dynamic, tubular polymers that carry out several essential cellular functions, such as cell motility, defining the cell shape, and DNA segregation during cell division. Microtubules are built from α-tubulin and β-tubulin heterodimers that associate in a head-to-tail manner. The microtubule polymer is inherently polar, with α-tubulin being exposed at the minus-end, which is characterized by slower dynamics and is the origin of microtubule nucleation, and β-tubulin being exposed at the plus-end, which exhibits faster dynamics and is the direction of microtubule growth (Fig. 1.1 C).

This polarity is a defining feature of the microtubule cytoskeleton's cellular functions. Microtubule minus-ends are often anchored at specific cellular locations, called microtubule organizing centers (MTOCs), allowing for specialized organization of microtubule arrays, which will be discussed in detail below (Akhmanova and Kapitein 2022; Sanchez and Feldman 2017). The rapid growth and shrinkage of microtubule plus-ends allows for the execution of cellular functions, such as pushing the cell membrane or transporting cargo (Akhmanova and Steinmetz 2015). Because of their distinctive properties, microtubule associated proteins (MAPs) can often distinguish between the minus- and plus-ends, providing another level of specialized activities along the length of the microtubule and at the respective ends (Fig 1.1 C). Microtubule plus-end binding proteins constitute a major body of scientific work, and these important proteins have been reviewed elsewhere (Akhmanova and Steinmetz 2015). In this work, I focus on proteins that regulate the minus-ends of microtubules, in regard to their formation, stabilization, and

localization. Specifically, I will discuss relevant recent advances in our understanding of the γ-Tubulin Ring Complex (γ-TuRC), a protein complex that modulates these various aspects of microtubule minus-ends and works in concert with key minus-end binding proteins.

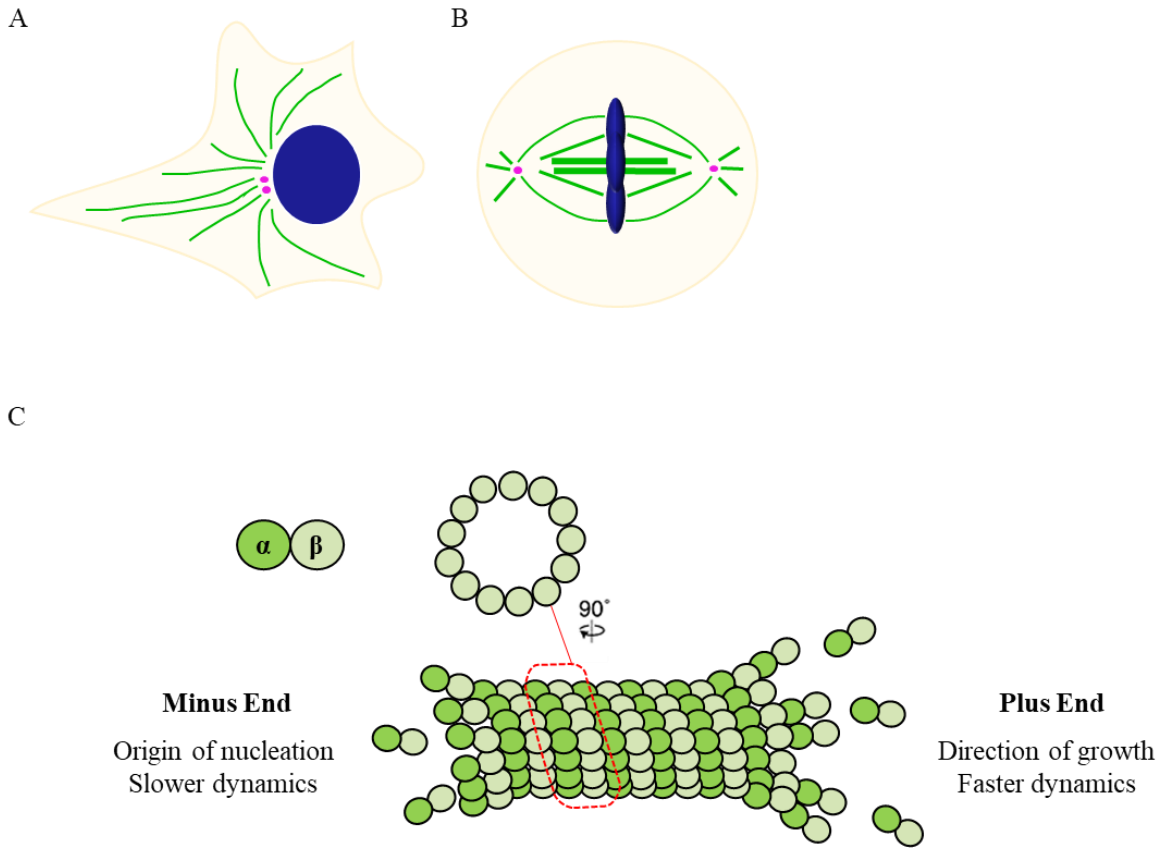

Figure 1.1 The microtubule cytoskeleton and microtubule architecture

(A and B) Microtubule cytoskeleton organization during interphase. Microtubules (green), DNA (blue), and centrosomes (pink) are included in the schematic. (A) and mitosis (B). (C) Schematic representation of the microtubule structure, highlighting the differences between the plus- and minus-ends.

1.2 The γ-TuRC is a master regulator of microtubule minus-end dynamics

1.2.1 Microtubule nucleation

How microtubules are formed and maintained has been a long-standing question in cell biology. Biochemical characterization has shown that purified tubulin dimers can undergo spontaneous microtubule nucleation. However, the conditions under which spontaneous nucleation occurs are inconsistent with the cellular environment for several reasons. First, typically at least 15-20μM of tubulin is required for *de novo* nucleation, while the cytoplasmic concentration of tubulin is 10μM (Fig. 1.2 A). This inconsistency may be accounted for by increasing local concentrations of tubulin, as has been proposed to occur at the centrosome (Baumgart et al. 2019; Woodruff et al. 2017), or by providing a template for tubulin dimers to bind to that mimics a microtubule end, as the concentration of tubulin needed for microtubule polymer elongation is lower (~10μM) than that needed for *de novo* nucleation (Fig. 1.2 A; Wieczorek et al. 2015).

Second, spontaneous nucleation is a kinetically complicated process. Tubulin dimers must form both longitudinal and lateral interactions in order to form a tubular, cylindrical polymer, which is inherently more complex than simple polymers such as helical actin filaments. A further complication is the strained bent-to-straight conformational change that tubulin dimers undergo as they oligomerize, which results in a kinetic penalty for the formation of lateral interactions (Fig. 1.2 B; Rice, Moritz, and Agard 2021; Ayaz et al. 2012; Rice, Montabana, and Agard 2008). Computational models predict an accretion model for *de novo* tubulin polymerization, as opposed to a simple nucleation-elongation model (Fig 1.2 C; Rice, Moritz, and Agard 2021). The accretion model proposes that establishing a critical nucleus for microtubule polymer formation is dictated by the number of contacts individual tubulin dimers can establish. Thus, smaller initial oligomers

form more slowly, and larger oligomers accrue tubulin dimers more quickly. Including a microtubule template in this computational model greatly accelerated assembly kinetics (Fig. 1.22 D; Rice, Moritz, and Agard 2021). Similarly, the cell must be able to overcome this kinetic barrier in order to limit the time and energy input required for microtubule nucleation to be compatible with cellular functions.

Third, spontaneously nucleated microtubules can be formed with different numbers of protofilaments, the parallel oligomers of longitudinally associated tubulin dimers, ranging from 10-16, whereas in the cellular environment, microtubule protofilament number is generally restricted to 13 (specialized microtubules may contain a different number of protofilaments; Chaaban et al. 2018; Kwiatkowska et al. 2006). As changes in protofilament number can structurally and functionally impact microtubules, the cell must employ a mechanism to specify the protofilament number of microtubules (Fig. 1.2 E; Chaaban and Brouhard 2017).

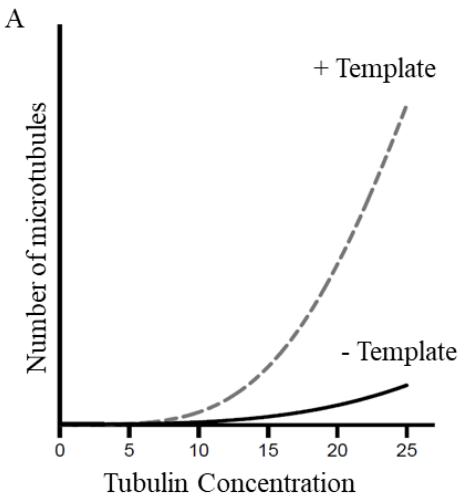
A
+ Template
Number of microtubules
- Template
0
5
10
15
20
25
Tubulin Concentration

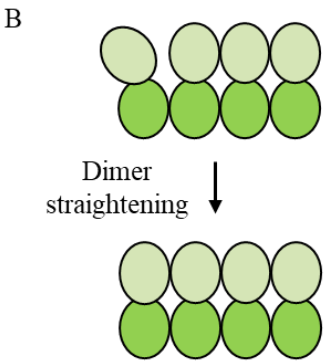
B
Dimer
straightening

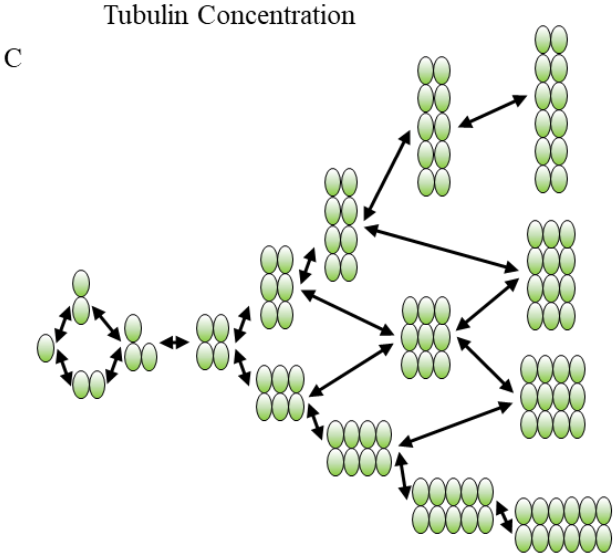
C

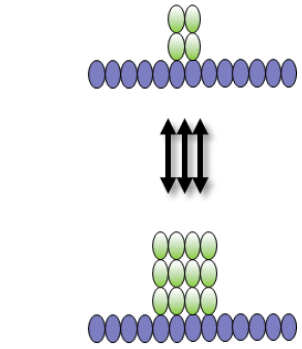
D

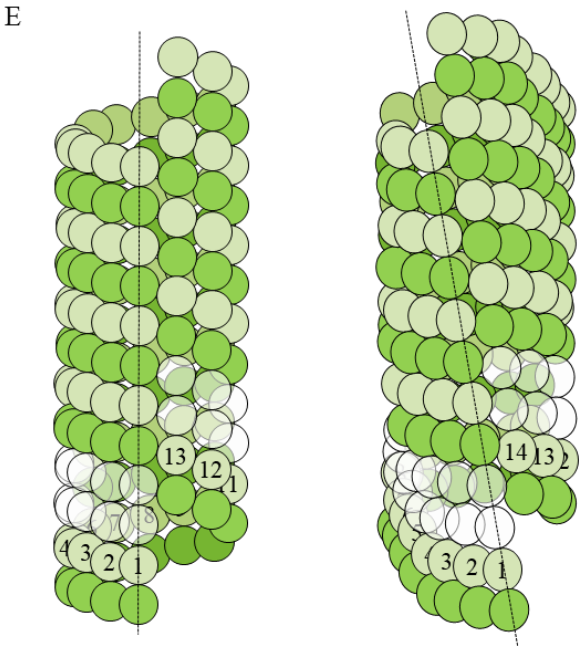
E
13
12
11
4
3
2
1
14
13
3
2
1

Figure 1.2 Biochemical barriers to microtubule nucleation

A) Plot depicting the number of microtubules nucleated when the tubulin concentration is increased, in the absence (solid line) or presence (dashed line) of a template. Adapted from Zheng et al. 1995. B) Schematic illustrating the kinetically unfavorable process required to straighten bent tubulin dimers during oligomerization. Adapted from Rice, Moritz, and Agard 2021. C) Accretion model of tubulin polymerization. Each oval unit represents a tubulin dimer. Adapted from Rice, Moritz, and Agard 2021. D) Accretion model in the presence of a template. Adapted from Rice, Moritz, and Agard 2021. E) Schematic of the microtubule lattice when the microtubule is composed of 13 (left) or 14 (right) protofilaments. While the protofilaments run straight in a 13-protofilament microtubule, they are tilted in a 14-protofilament microtubule. Adapted from Chaaban and Brouhard 2017.

The cell utilizes several different factors to overcome these obstacles. Primarily, however, the cell employs a large multi-protein complex called the γ-TuRC which can serve as a template for tubulin dimers to bind to and polymerize off of (Fig. 1.3 A). The γ-TuRC is composed of at least nine unique proteins. Its most abundant component is γ-tubulin, a member of the tubulin family, which was first discovered by a genetic screen in *Aspergillus nidulans*, where it acted as a suppressor of a growth inhibiting β-tubulin mutation (C. E. Oakley and Oakley 1989). It was later found that γ-tubulin associates with several other proteins to form a ring-shaped complex (Zheng et al. 1995). The human homologs of these proteins were termed γ-tubulin complex proteins, or GCPs, of which there are GCP2-6 (Murphy, Urbani, and Stearns 1998). Structural characterization of the γ-TuRC determined that the proteins MOZART1 and MOZART2A/B (MZT1 and MZT2A/B) and a single actin monomer, which had been known to associate with the γ-TuRC, are core components of the complex (Wieczorek, Huang, et al. 2020; Wieczorek, Urnavicius, et al. 2020; Consolati et al. 2020; Peng Liu et al. 2019; Choi et al. 2010; Teixido-Travesa et al. 2010; Hutchins et al. 2010).

Biochemical studies have found that purified recombinant or cellular γ-TuRCs can nucleate microtubules *in vitro* at tubulin dimer concentrations of 10-15μM, which is closer to the expected cytoplasmic concentration (Wieczorek et al. 2021; Consolati et al. 2020). The rate of microtubule nucleation is also increased in the presence of the γ-TuRC, as predicted by the accretion model (Wieczorek et al. 2021; Consolati et al. 2020).

A remaining open question is whether the γ-TuRC can nucleate microtubules with a preference for 13 protofilaments, as is seen in the majority of cellular microtubules. The cryo-EM structure of the γ-TuRC revealed that the complex contains 14 molecules of γ-

tubulin (Fig. 1.3 A and B; Wieczorek, Urnavicius, et al. 2020; Consolati et al. 2020; Peng Liu et al. 2019). If each γ-tubulin mediates an interaction with an α/β-tubulin dimer, this would result in a 14 protofilament microtubule, as opposed to 13. Additionally, the helical parameters of the γ-TuRC do not match those of a 13 protofilament microtubule, making it an imperfect template (Fig. 1.3 B; Wieczorek, Urnavicius, et al. 2020). It has been proposed that activation of the γ-TuRC, either by activating proteins or post-translational modifications (Sulimenko, Dráberová, and Dráber 2022), induces a conformational change where the first and 14th γ-tubulin molecules will overlap with one another, resulting in only 13 accessible γ-tubulins and a closer helical match between the γ-TuRC and a 13-protofilament microtubule (Wieczorek, Urnavicius, et al. 2020; Kollman et al. 2010). However, more work will be necessary to determine if this is indeed the case.

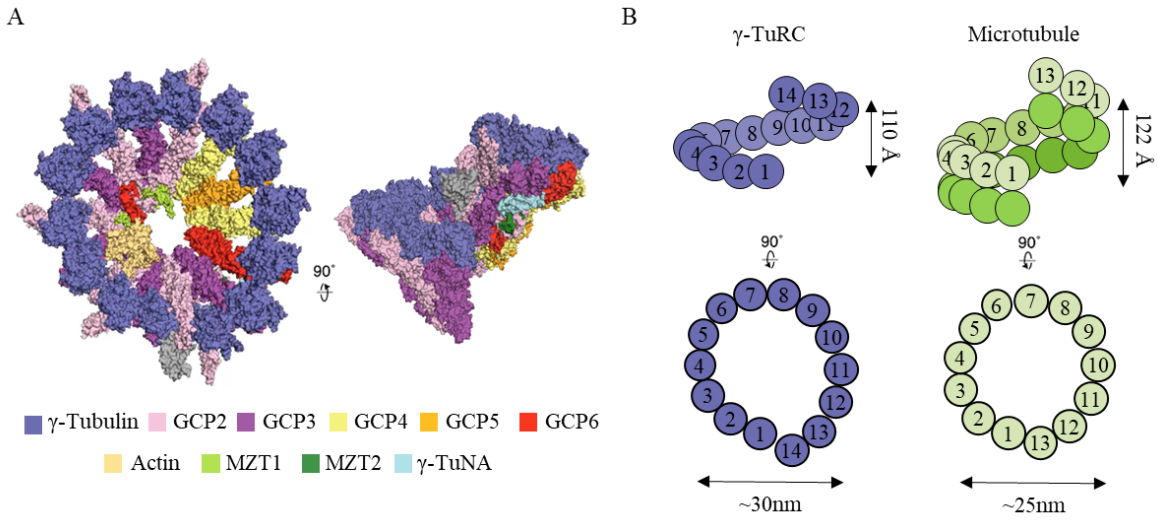

Figure 1.3 The structure of the γ-TuRC reveals a mismatch with the structure of 13-protofilament microtubules

(A) Surface representation of the 3D reconstruction of the native γ-TuRC solved using cryo-EM. PDB accession nos.: 6V6S, 6X0U, and 6X0V. Adapted from Wieczorek, Urnavicius, et al. 2020; Wieczorek, Huang, et al. 2020. (B) Schematic illustrating the structural mismatch between the γ-TuRC and the lattice of a 13-protofilament microtubule, both in terms of helical parameters and diameter. Adapted from Wieczorek, Urnavicius, et al. 2020.

In recent years, it has become clear that the cell possesses other microtubule nucleation factors that act either in parallel to or synergistically with the γ-TuRC. The examination of these pathways is critical, as cell biology and biochemical data have shown that microtubules form in the presence of other nucleation factors even in the absence of γ-TuRC proteins, and that the γ-TuRC alone is an inefficient nucleator *in* vitro (Tsuchiya and Goshima 2021; Wieczorek et al. 2021; Consolati et al. 2020; Ramírez Cota et al. 2017;

O'Toole et al. 2012; Hannak et al. 2002). While γ-TuRC-dependent microtubule nucleation may be the dominant cellular pathway, it is important to understand the relative contributions of other nucleation factors and investigate how they shape the microtubule cytoskeleton.

As previously mentioned, pathways that locally increase the tubulin concentration can favor microtubule nucleation, either independently or in concert with the γ-TuRC. For example, it has been proposed that certain centrosomal proteins form phase separated compartments which can recruit, and effectively concentrate, tubulin dimers and perhaps other microtubule associated proteins, such as the γ-TuRC (X. Jiang et al. 2021; Woodruff et al. 2017). This would increase the efficiency of γ-TuRC-mediated microtubule nucleation, but also provide a means for the centrosome to nucleate microtubules independently of the γ-TuRC. This is consistent with the observations that the centrosomal concentration of soluble tubulin is ~10-fold higher than the cytoplasmic concentration, and that in systems depleted of γ-tubulin or other γ-TuRC proteins, centrosomal microtubules are still formed (Tsuchiya and Goshima 2021; Baumgart et al. 2019; Ramírez Cota et al. 2017; McKinley and Cheeseman 2017; Hannak et al. 2002). Other MAPs, such as the neuronal microtubule regulator, tau, and the mitotic spindle associated protein, TPX2, have been proposed to act by a similar mechanism (M. R. King and Petry 2020; Hernández-Vega et al. 2017). However, as the condensate-forming properties of these proteins have largely been examined *in vitro*, it remains to be determined if these properties are relevant in a cellular context.

Alternatively, MAPs such as tau, TPX2, and the microtubule stabilizing proteins termed cytoplasmic linker-associated proteins (CLASPs) can also enhance microtubule

nucleation by stabilizing oligomeric tubulin intermediates, suppressing catastrophe events and promoting microtubule lattice formation (Aher et al. 2018; Roostalu, Cade, and Surrey 2015; Wieczorek et al. 2015; Ennulat et al. 1989). Therefore, these MAPs could stimulate microtubule nucleation either independently of or synergistically with the γ-TuRC. Another MAP that likely functions cooperatively with the γ-TuRC and other microtubule nucleation factors like TPX2 is the microtubule polymerase, chTOG (also referred to by the name of its *Xenopus* orthologue, XMAP215). chTOG consists of five tandem TOG domains, each of which interacts with tubulin dimers and promotes microtubule polymerization (Widlund et al. 2011). Several studies have shown that ch-TOG alone can exhibit limited microtubule nucleation activity, but greatly enhances microtubule formation when paired with other nucleating factors (Consolati et al. 2020; B. R. King et al. 2020; Roostalu, Cade, and Surrey 2015; Wieczorek et al. 2015).

An important distinction between these nucleation factors and the γ-TuRC, however, is that only the γ-TuRC could perform templated microtubule nucleation. Templated vs. non-templated microtubule nucleation may have important consequences for the structure and function of the microtubule, such as the number of protofilaments, as described previously, and for the dynamics and stability of the newly nucleated minus-end, as will be discussed in the following section (Brouhard and Rice 2018; Roostalu and Surrey 2017; Chaaban and Brouhard 2017).

1.2.2 Microtubule minus-end capping

While microtubule nucleation is thought to be the primary function of the γ-TuRC, there are additional functions of this complex that play critical roles in microtubule regulation. Specifically, the γ-TuRC can act as a cap at microtubule minus-ends to stabilize them and provide a mechanism to anchor microtubule minus-ends at specific cellular locations (Akhmanova and Kapitein 2022; microtubule anchoring will be discussed in more detail in section 1.2.3). The γ-TuRC can either cap a newly nucleated microtubule, or it can bind to and cap an exposed minus-end generated through a γ-TuRC-independent nucleation factor, or by the severing of a pre-existing microtubule (Fig 1.4; Berman et al. 2023; Wiese and Zheng 2000).

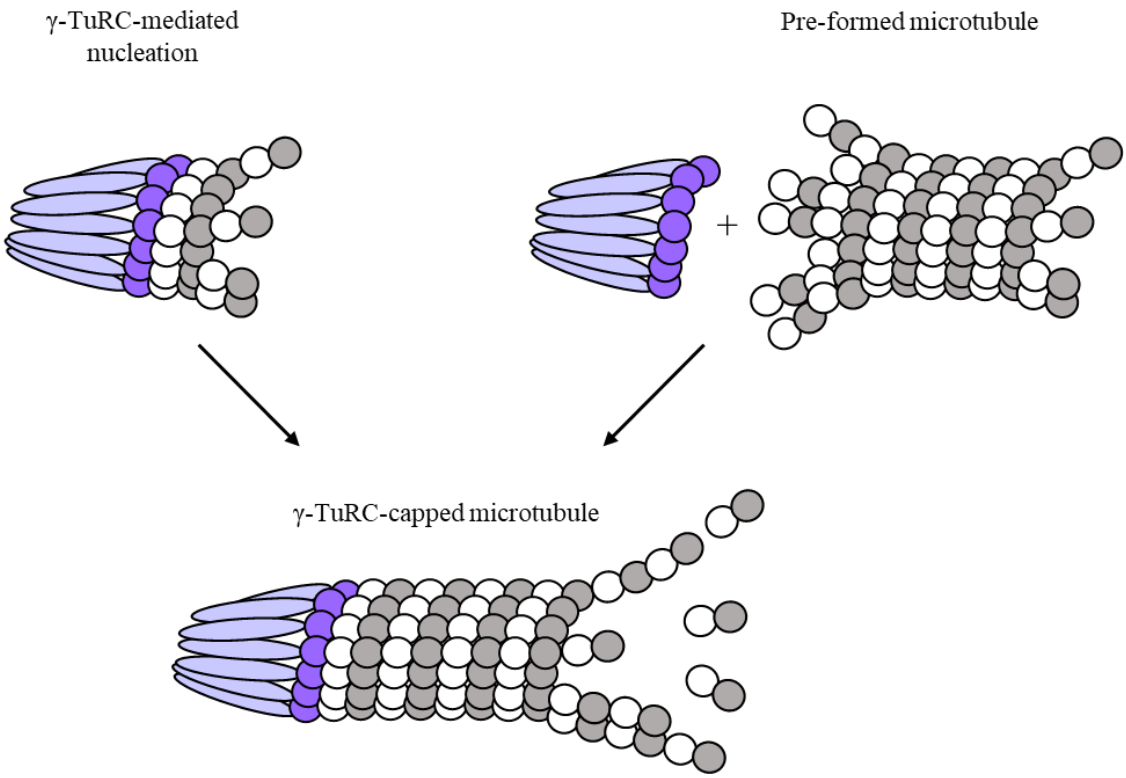

Figure 1.4 Microtubule minus-end capping activity of the γ-TuRC

The γ-TuRC can cap microtubule minus-ends either after a nucleation event, or when it binds to a pre-formed microtubule.

Stabilization of microtubule minus-ends is important to sustain the microtubule by protecting the minus-end from microtubule depolymerases, and from the inherent propensity of microtubules to depolymerize. Due to the GTP-hydrolysis cycle of β-tubulin, microtubules exhibit dynamic instability, the frequent transition between states of growth or shrinkage. As GTP hydrolysis does not happen immediately, there is a higher percentage of GTP-bound tubulin at the ends of microtubules, and a higher percentage of GDP-bound tubulin within the middle of the microtubule polymer. While GTP-bound tubulin has a stabilizing effect on the lattice, GDP-bound tubulin is conformationally strained and is

inherently unstable. Therefore, when the amount of GTP-bound tubulin is decreased, microtubules undergo rapid depolymerization. Polymerization of the microtubule can be reestablished by the reincorporation of GTP-bound tubulin, termed a microtubule rescue event.

New tubulin subunits are quickly added to the microtubule plus-end, resulting in the formation of a "GTP cap," a region with a high number of GTP-bound tubulin that stabilizes the plus-end and prevent depolymerization. In contrast, GTP-bound tubulin is added to the microtubule minus-end more slowly. Therefore, different minus-end interacting proteins act to stabilize it.

In vitro work has shown that γ-TuRCs purified from *Xenopus* egg extracts can bind minus-ends of nucleated or pre-formed microtubules to block further minus-end growth and prevent depolymerization (Wiese and Zheng 2000). Interestingly, these experiments showed that around half of the pre-formed microtubules in a given sample are not capped by the γ-TuRC (Wiese and Zheng 2000). One explanation for this may be that the affinity of the γ-TuRC for a minus-end is relatively low, and therefore binding could not be saturated at the maximum concentration of purified γ-TuRC available. In addition, structural analyses have shown that the protofilaments at the end of the microtubule, and to which the γ-TuRC needs to bind, are flared (Gudimchuk et al. 2020; Chrétien, Fuller, and Karsenti 1995). This arrangement may make it difficult for each γ-tubulin in the γ-TuRC to come in contact with and hold on to the necessary number of α-tubulins at the microtubule minus-end, especially if they exhibit a low binding affinity. For a further discussion on this topic and on the cellular role of γ-TuRC's capping activity, see Chapter 2 of this work.

In addition to the γ-TuRC, other minus-end interacting proteins can bind to and stabilize the minus-end. In contrast to the γ-TuRC, however, these proteins do not bind to the exposed α-tubulins at the microtubule minus-end. A major class of such proteins are calmodulin-regulated spectrin-associated proteins 1 (CAMSAP1), CAMSAP2, and CAMSAP3 which regulate free minus-ends independently of the γ-TuRC (Vineethakumari and Lüders 2022; Akhmanova and Kapitein 2022). CAMSAPs decorate the outer surface of the microtubule minus-end by binding an intradimer site between protofilaments (Fig 1.5). CAMSAPs stabilize and track growing microtubule minus-ends without preventing their polymerization (K. Jiang et al. 2014). Similar to the γ-TuRC, CAMSAP binding to microtubule minus-ends can promote microtubule growth, and provide a mechanism to anchor minus-ends to non-centrosomal sites such as the Golgi apparatus or the cell cortex (Coquand et al. 2021; Wu et al. 2016; Meng et al. 2008). CAMSAPs also play an important role in regulating microtubule minus-ends in differentiated neurons, where predominantly non-centrosomal microtubules are formed (He et al. 2022; Noordstra et al. 2016; Yau et al. 2014).

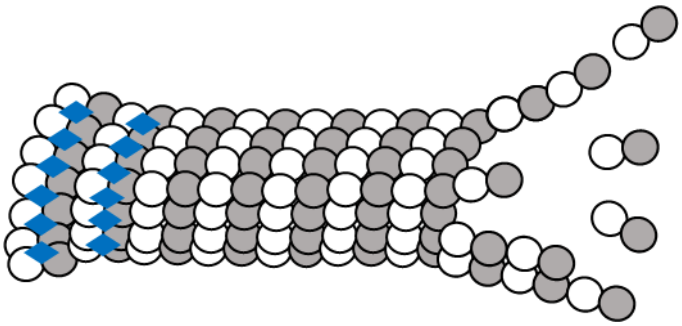

Figure 1.5 CAMSAP binding to microtubule minus-ends

(A) Schematic of CAMSAP binding to the intradimer interface between protofilaments. Adapted from Atherton et al. 2019.

Another minus-end regulating protein is the protein abnormal spindle-like microcephaly associated (ASPM). ASPM has been shown *in vitro* to track growing microtubule minus-ends and, together with the microtubule severing enzyme katanin, limit their polymerization (K. Jiang et al. 2017). In cells, ASPM likely regulates the lengths of microtubule minus-ends at the spindle poles and stabilizes their dynamics in order to maintain poleward microtubule flux (K. Jiang et al. 2017). The microtubule minus-end binding protein NuMA similarly regulates the poleward movement of microtubules by recruiting dynactin and dynein, a minus-end directed microtubule motor (Hueschen et al. 2017; Elting et al. 2014). In summary, the capping activity of the γ-TuRC and the recognition of minus-ends by CAMSAPs, ASPM, and NuMA, can stabilize minus-end dynamics, thus protecting again depolymerization and promoting plus-end directed microtubule growth, and allow for the organization of microtubules in the necessary orientation.

The capping of cytoskeletal polymers is not unique to microtubules. Similar to microtubules, actin filaments are also polar, with a pointed/minus-end and a barbed/plus-end. In contrast to the dynamic instability feature of microtubules, actin polymers exhibit treadmilling, whereby actin monomers are lost from the pointed end and are added to the barbed end (Lappalainen et al. 2022). This generates a steady state pool of polymerizable actin monomers. However, in order for actin filaments to execute cellular functions, such as motility, individual filaments need to be able to polymerize at fast rates that require a higher concentration of polymerizable actin. One way that the cell overcomes this obstacle is by the barbed end capping activity of capping protein (CP; Carlier and Shekhar 2017). CP capping of a fraction of actin filaments restricts their polymerization, thus increasing the steady state concentration of polymerizable actin available and allowing for increased polymerization rates for the uncapped filaments. In contrast, proteins that cap the pointed ends of actin filaments, such as tropomodulin and the Arp2/3 complex, block subunit loss and therefore decrease the available pool of actin monomers (Pollard 2016). While the results of end capping of microtubule and actin filaments differ, they are similar in that, in both cases, capping acts to regulate filament dynamics to be compatible with cellular needs.

1.2.3 Microtubule minus-end localization and anchoring

The γ-TuRC's capping activity not only protects the minus-end and stabilizes microtubule growth, it also provides a molecular handle for the organization of microtubule minus-ends (Akhmanova and Kapitein 2022). The γ-TuRC cap can be recognized by different recruiting factors, allowing for more efficient and controlled microtubule sorting and organization during interphase, mitosis, and in specialized microtubule arrays found in differentiated cells such as neurons.

During both interphase and mitosis, the centrosome acts as the cell's primary MTOC (Sanchez and Feldman 2017). The centrosome is composed of two orthogonally arranged centrioles, cylindrical structures with a core of nine microtubule triplets, and the surrounding proteinaceous matrix called the pericentriolar material (PCM; Fig. 1.6 A). Several PCM components can recruit and tether the γ-TuRC to the centrosome (Akhmanova and Kapitein 2022; Vineethakumari and Lüders 2022). These include CDK5RAP2, which may also play a role in activating the γ-TuRC's nucleation activity, pericentrin, AKAP450, CEP192, NEDD1, and ninein (Gavilan et al. 2018; Choi et al. 2010; Fong et al. 2008; Haren et al. 2006; Lüders, Patel, and Stearns 2006; Delgehyr, Sillibourne, and Bornens 2005; Dictenberg et al. 1998).

While centrosomal microtubules seem to dominate the microtubule arrays in both interphase and mitosis, studies in recent years have shown that centrosomal structures themselves are not essential (Hoffmann 2021). Instead, centrosomes are important for increasing the faithfulness and efficiency of cellular processes such as cell division. Importantly, several cell types lack centrosomes, such as female oocytes and plant cells, or have inactivated centrosomes such as in developed neurons (B. Liu and Lee 2022; Lüders 2021; Dumont and Desai 2012). Cell division and microtubule organization has even been observed in cells where centrosomes were removed, either by laser ablation or chemical methods (Watanabe et al. 2020; Khodjakov et al. 1999). Interestingly, however, the PCM components involved in anchoring the γ-TuRC are still required for acentrosomal microtubule organization, highlighting the importance of this γ-TuRC activity (Watanabe et al. 2020; So et al. 2019).

Interphase and mitotic cells also contain non-centrosomal MTOCs. Namely, the Golgi apparatus serves as a major site for interphase microtubule organization (Fig. 1.6 B). Several centrosomal proteins, such as CDK5RAP2 and AKAP450, can also localize to the Golgi to anchor the γ-TuRC (Fig. 1.6 B; F. Chen et al. 2022; Wu et al. 2016). These proteins can also tether CAMSAP decorated minus-ends at the Golgi (Fig. 1.6 B). More work is necessary to understand why the Golgi anchors both γ-TuRC and CAMSAP-bound minus-ends, and how these populations of microtubules differ from each other.

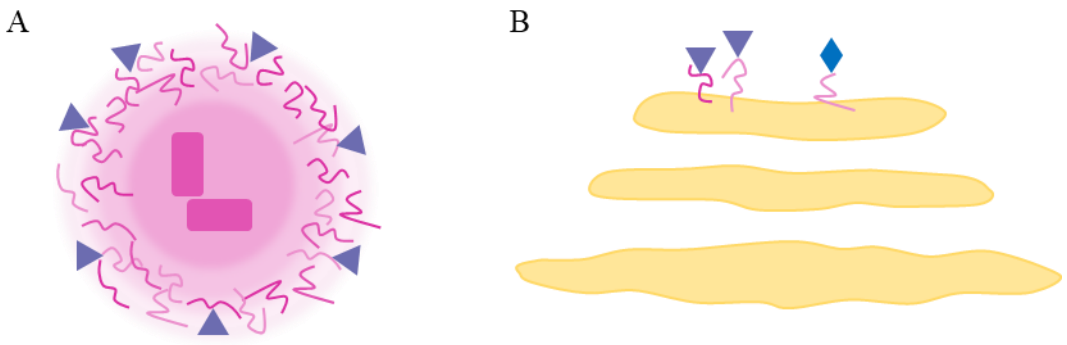

Figure 1.6 Microtubule minus-end anchoring at the centrosome and Golgi

(A) Schematic of the centrosome. Disordered proteins such as CDK5RAP2 occupy the PCM (pink) that surrounds the perpendicularly oriented centrioles (dark pink). PCM proteins can anchor the γ-TuRC (purple) to the centrosome. (B) Schematic of the Golgi apparatus (yellow). Centrosomal proteins can anchor γ-TuRC or CAMSAP (blue) bound microtubule minus-ends. Adapted from Wu and Akhmanova 2017.

In mitosis, non-centrosomal microtubule arrays are key components of the mitotic spindle. Microtubules are nucleated and anchored within the spindle itself and at the chromatin (Fig. 1.7 A; Valdez et al. 2023; Prosser and Pelletier 2017). The octameric augmin complex regulates spindle-mediated microtubule nucleation in order to generate dense and uniformly polar microtubule arrays at either side of the bipolar spindle (Fig. 1.7 B; Zhang et al. 2022; Zupa et al. 2022; David et al. 2019; Verma and Maresca 2019; Goshima et al. 2008). The augmin complex binds to both microtubules and the γ-TuRC, thus allowing for branched microtubule nucleation (Fig. 1.7 B). Other γ-TuRC associated proteins, such as TPX2 and NEDD1, may work together with the augmin complex to regulate spindle microtubule organization (Alfaro-Aco, Thawani, and Petry 2017; Petry et al. 2013; H. Zhu et al. 2008). Depletion of augmin complex components reduces the microtubule spindle mass, highlighting the importance of anchoring the γ-TuRC at the correct cellular locations (David et al. 2019; Goshima et al. 2008; H. Zhu et al. 2008).

Chromatin-mediated microtubule nucleation was discovered several years ago, and countered the conventional "search and capture" model of spindle assembly and chromosome-microtubule attachments (Verma and Maresca 2022; Heald and Khodjakov 2015; Tulu et al. 2006; Heald et al. 1996; Kirschner and Mitchison 1986; Karsenti, Newport, and Kirschner 1984; McGill and Brinkley 1975). According to this model, the polymerization of microtubules from opposite spindle poles would allow for their eventual attachment to kinetochores, followed by faithful chromosome segregation. Chromatin-mediated nucleation proceeds with a reverse order of events; microtubules are nucleated at the chromosomes in a RanGTP-dependent manner, and the microtubule minus-ends are sorted and organized towards the spindle poles (Fig. 1.7 C). This is likely a γ-TuRC-

dependent process, where the γ-TuRC is localized to chromosomes, promotes microtubule formation, and assists in the polarization of minus-ends (Yokoyama et al. 2014; Mishra et al. 2010; Bucciarelli et al. 2009; Ohba et al. 1999; Wilde and Zheng 1999).

While many questions still remain regarding chromatin-mediated microtubule formation, recent studies have provided a model where following microtubule nucleation, either by the γ-TuRC or other nucleation factors such as TPX2, microtubule plus-ends polymerize towards the chromosomes and their minus-ends are directed towards the spindle poles (Lecland and Lüders 2014; Maiato, Rieder, and Khodjakov 2004; Heald et al. 1996; Witt, Ris, and Borisy 1980). This minus-end organization depends on dynein, a minus-end directed motor that can guide the microtubule towards the spindle pole. The association of the γ-TuRC with dynein underscores the importance of the γ-TuRC in the polarized organization of chromatin-derived microtubules (Lecland and Lüders 2014; Young et al. 2000; Heald et al. 1996; Merdes et al. 1996).

However, it may be that not all microtubules are oriented with the minus-ends facing towards spindle poles. Recent work has shown that microtubules form within the fibrous corona, a fibrous meshwork that resides on the outer surface of kinetochores (Wu et al. 2023). This pathway is dependent on LIC1, a light intermediate chain of dynein, pericentrin, and the γ-TuRC. The minus-ends of microtubules nucleated by this pathway are anchored at kinetochores, and their plus-ends extend towards the poles (Fig 1.7 D). This is inconsistent with evidence that all populations of microtubules in the spindle are oriented with their minus-ends towards the poles (Euteneuer and McIntosh 1981). It may be that these reversed polarity microtubules are short-lived, and play a role in orienting and organizing microtubules with the opposite polarity in order to promote robust spindle

assembly and microtubule plus-end attachment to kinetochores, as studies in yeast have suggested (Kitamura et al. 2010). In summary, this pathway adds another element of γ-TuRC-mediated microtubule regulation in microtubule organization.

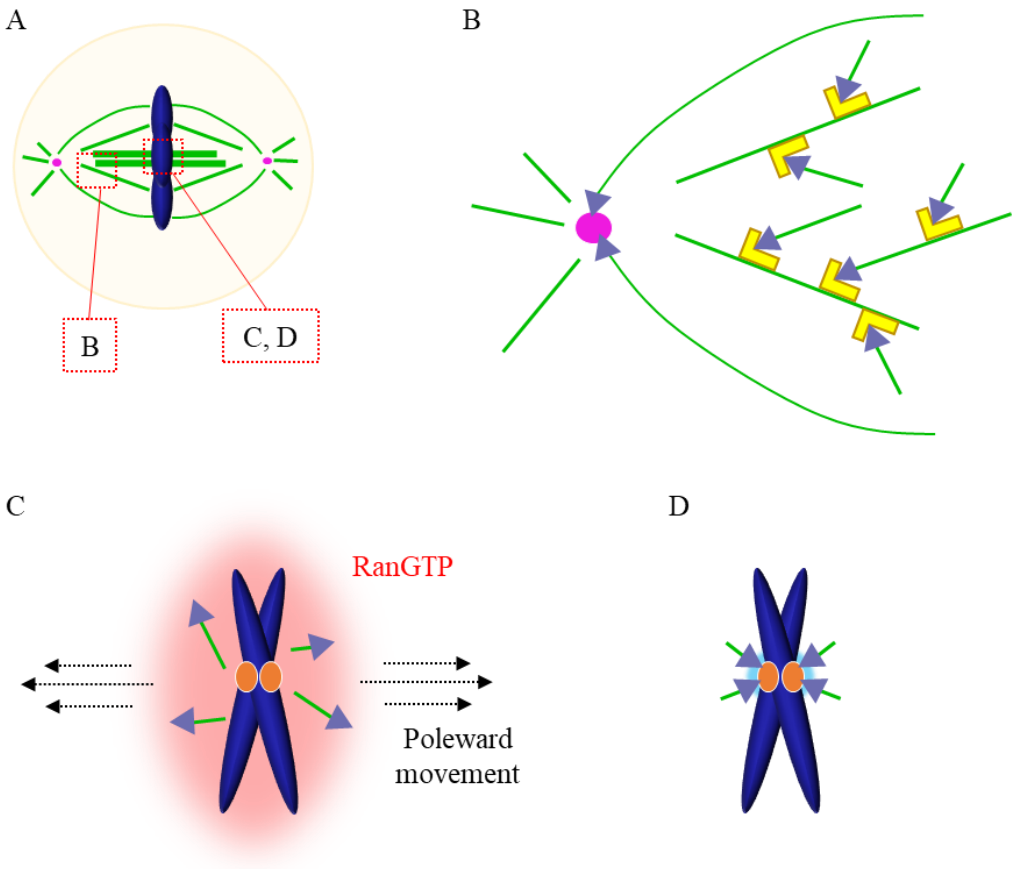

Figure 1.7 Non-centrosomal microtubule nucleation pathways help to form the mitotic spindle

(A) The three major microtubule nucleation pathways during mitosis are (1) centrosomal (centrosomes in pink), (2) branched spindle microtubules, and (3) chromatin-mediated. (B) The augmin complex (yellow) binds to spindle microtubules (green) and the γ-TuRC (purple) to anchor newly nucleated branched spindle microtubules. (C) The RanGTP gradient (red) surrounding mitotic chromosomes (DNA: blue, kinetochores: orange) regulates chromatin-mediated microtubule nucleation. Microtubules are organized and transported towards the opposing spindle poles. (D) Microtubules nucleated within the fibrous corona (blue) of the kinetochores may have opposite polarity relative to other microtubules in the mitotic spindle. Adapted from Wu et al. 2023.

1.3 γ-TuRC proteins in disease

Dysregulation of γ-TuRC proteins has been observed in several diseases, including cancer and neurodevelopmental disorders. This is not surprising, as microtubule targeting agents, which inhibit microtubule dynamics, are commonly used to treat tumors (Akhmanova and Steinmetz 2015). Additionally, mutations in several MAPs, such as CDK5RAP2 and ASPM, have also been shown to lead to neurodevelopmental disorders such as microcephaly (Tungadi et al. 2017; Bond et al. 2005).

In some cases, γ-TuRC proteins may be the drivers of disease onset and progression. Mutations in MZT1 are associated with patients predisposed to sarcomas (Ballinger et al. 2023). Mutations in γ-tubulin, specifically isoform 1 (TUBG1), are associated with lissencephaly and microcephaly (Brock et al. 2018; Bahi-Buisson et al. 2014; Poirier et al. 2013). Additionally, GCP2, GCP4, and GCP5 mutations have been identified in patients with microcephaly and anomalies in brain and eye development (Maver et al. 2019; Mitani et al. 2019; Scheidecker et al. 2015). Errors in GCP6 mRNA processing can lead to decreased GCP6 protein levels, which is also associated with neurological disorders, and can result from the loss of WBP11, a pre-mRNA splicing factor that is required for GCP6 expression (Park et al. 2020).

In other cases, it is unclear if changes in γ-TuRC proteins are the drivers or passengers in disease progression. For example, centrosomal aberrations are common features in several cancer types, and are associated with worse clinical outcomes. One such phenotype may be centrosome amplification, where a cell contains supernumerary centrosomes. γ-Tubulin overexpression is a molecular marker for centrosome amplification, but it remains unclear if this is a cause or result of the extra number of centrosomes in the cell (Piemonte, Anstine, and Keri 2021). This uncertainty is

underscored by the observation that other critical centrosomal proteins, such as pericentrin, centrin, polo-like kinase 4 (PLK4), and cyclin E1 are also overexpressed (Piemonte, Anstine, and Keri 2021). Another common centrosomal aberration is centrosome hypertrophy, or elevated centrosome volumes. This phenotype is often observed in triple-negative breast cancer tumor samples, where increased amounts of γ-tubulin were found to be localized to larger centrosomes (Piemonte, Anstine, and Keri 2021). The overexpression of more minor γ-TuRC proteins has also been found to be a marker of other cancer types, such as MZT2A in non-small cell lung cancer (Wang et al. 2021). NSCLC patients with increased MZT2A expression were found to have more advanced tumors and poorer survival rates.

Mutations in known cancer associated proteins can also affect γ-TuRC functions, leading to disease phenotypes. For example, BRCA1 has been shown to ubiquitinate γ-tubulin and mediate its degradation, thereby limiting γ-TuRC recruitment to the centrosome (Sung and Giannakakou 2014; Sankaran et al. 2005). Mutations in BRCA1 may lead to an excess of the γ-TuRC at the centrosome, resulting in centrosome amplification and/or increased microtubule dynamics (Sung and Giannakakou 2014). γ-Tubulin also associates with other proteins involved in DNA repair in addition to BRCA1, such as Rad51 and ATR, suggesting that its activity with these proteins may not be strictly centrosomal, but that it may also play a nuclear role (B. R. Oakley, Paolillo, and Zheng 2015). In summary, expanding our understanding of the biology of the γ-TuRC may have important implications for investigating the onset of and potential treatments for such diseases.

Chapter 2: A nucleotide-binding-independent role for γ-tubulin in microtubule minus-end capping and cell division

Note to readers: The results discussed below arose from a collaborative effort between myself and several colleagues in the Kapoor Lab and the Chait lab at The Rockefeller University. A closely related version was published in The Journal of Cell Biology (DOI: 10.1083/jcb.202204102). With the permission of Prof. Kapoor, I have included relevant studies done by the Chait lab in the 2.3.2 Results section as they provide important information regarding my studies. Members of the Kapoor lab assisted with some of the experiments shown in the Results sections, but all data and analyses presented are my own.

2.1 Summary

The γ-Tubulin Ring Complex (γ-TuRC) has essential roles in centrosomal and non-centrosomal microtubule organization during vertebrate mitosis. While there have been important advances in understanding γ-TuRC-dependent microtubule nucleation, γ-TuRC capping of microtubule minus-ends remains poorly characterized. Here, we utilized biochemical reconstitutions and cellular assays to examine the human γ-TuRC's capping activity. Single filament assays showed that the γ-TuRC remained associated with a nucleated microtubule for tens of minutes. In contrast, caps at dynamic microtubule minus-ends displayed lifetimes of ~1 minute. Reconstituted γ-TuRCs with nucleotide-binding deficient γ-tubulin (γ-tubulin$^{\Delta GTP}$) formed ring-shaped complexes that did not nucleate microtubules, but capped microtubule minus-ends with lifetimes similar to those measured for wild-type complexes. In dividing cells, microtubule regrowth assays revealed that while knockdown of γ-tubulin suppressed non-centrosomal microtubule formation, add-back of γ-tubulin$^{\Delta GTP}$ could substantially restore this process. Our results suggest that γ-TuRC capping is a nucleotide-binding-independent activity that plays a role in non-centrosomal microtubule organization during cell division.

2.2 Introduction

During mitosis, the formation and organization of non-centrosomal microtubules, such as those generated by chromosome-dependent microtubule nucleation, contribute to the assembly of the bipolar mitotic spindle (Kapoor 2017; Meunier and Vernos 2016; Heald and Khodjakov 2015). Cell biology studies have demonstrated that the γ-TuRC plays a critical role in these pathways (Lüders and Stearns 2007). Depletion of γ-TuRC components in various model systems, including C. elegans, S. cerevisiae, D. melanogaster, and cultured human cells, results in the loss of spindle bipolarity (McKinley and Cheeseman 2017; Ramírez Cota et al. 2017; Mahoney et al. 2006; Hannak et al. 2002; Strome et al. 2001). Moreover, microtubule regrowth assays in cells depleted of γ-TuRC proteins show either complete or significant loss of non-centrosomal microtubule formation, while centrosomal microtubules form, albeit more slowly (Tsuchiya and Goshima 2021; Ramírez Cota et al. 2017; Hannak et al. 2002). While the loss of γ-TuRC-dependent microtubule nucleation could be responsible for these phenotypes, it is possible that other activities of this complex may also be important. Specifically, bulk biochemical assays have suggested that the γ-TuRC acts as a cap to suppress the addition or loss of tubulin subunits at the microtubule minus-end (Wiese and Zheng 2000). Capping by the γ-TuRC can occur following a nucleation event where the γ-TuRC remains associated with the newly nucleated microtubule, or when the γ-TuRC binds to the free minus-end of an existing microtubule (Wiese and Zheng 2000). However, we do not understand the role of γ-TuRC's capping activity in microtubule formation and organization in cells.

Cryo-EM structures of the Xenopus and human γ-TuRC have revealed that the complex is an asymmetric, cone-shaped assembly (Wieczorek, Urnavicius, et al. 2020; Consolati et al. 2020; Peng Liu et al. 2019). The most abundant γ-TuRC component, γ-

tubulin, is positioned at the top of the cone, where it can mediate interactions with α,β-tubulin dimers. The asymmetric cone is composed of seven Y-shaped subunits, four of which are comprised of the evolutionarily conserved γ-tubulin small complex (γ-TuSC) proteins γ-tubulin, GCP2 and 3, and three γ-TuSC-like Y-shaped subunits, consisting of γ-tubulin bound to GCP4, 5 or 6 (Kollman et al. 2010; Murphy et al. 2001; Oegema et al. 1999). Across the interior the cone resides a luminal bridge, which is composed of the N-terminal domains of GCP6 and GCP3 associated with actin and MZT1 proteins, while MZT2 interacts with the outer face of the cone (Würtz et al. 2022; Wieczorek, Huang, et al. 2020). These findings from structural studies, along with additional biochemical data, have facilitated analyses of recombinant γ-TuRC and the basis of the γ-TuRC's asymmetric organization (Würtz et al. 2021a; Wieczorek et al. 2021; Zimmermann et al. 2020). Reconstitution studies thus far have predominantly focused on the γ-TuRC's nucleation activity (Würtz et al. 2021a; Wieczorek et al. 2021; Zimmermann et al. 2020), which is retained in a partial γ-TuRC complex lacking the luminal bridge (γ-TuRC$^{\Delta LB}$; Wieczorek et al. 2021). Additionally, GTP binding by γ-tubulin has been found to be important for γ-TuRC-mediated microtubule nucleation (Wieczorek et al. 2021; Gombos et al. 2013). A point mutation in γ-tubulin's nucleotide binding pocket (N229A), which reduces the yeast γ-tubulin's affinity for nucleotide by ~3 orders of magnitude, compromised microtubule nucleation activity in yeast γ-TuSCs and the partial human complex γ-TuRC$^{\Delta LB}$ (Wieczorek et al. 2021; Gombos et al. 2013). However, the dependence of the γ-TuRC's microtubule capping activity on nucleotide binding by γ-tubulin is not known.

Here, we examine the microtubule minus-end capping activity of the γ-TuRC. We find that the association of γ-TuRCs with microtubule minus-ends following a nucleation

event persists over tens of minutes, while caps at dynamic minus-ends have lifetimes of ~1 minute. Nucleotide-binding-deficient γ-TuRC capped dynamic microtubules at similar lifetimes, despite its compromised nucleation activity. Microtubule regrowth assays in mitotic cells revealed that non-centrosomal microtubule formation, which was suppressed in γ-tubulin knockdown cells, is observed in cells expressing nucleotide-binding deficient γ-tubulin. Together, our results suggest that γ-TuRC capping is nucleotide-binding-independent and contributes to non-centrosomal microtubule formation and organization during cell division.

2.3 Results

2.3.1 γ-TuRC$^{\gamma\text{-Tub-WT}}$ caps nucleated and pre-formed microtubules, and suppresses microtubule minus-end dynamics

To examine the association of the γ-TuRC with microtubule minus-ends, recombinant γ-TuRC$^{\gamma\text{-Tub-WT}}$ containing green fluorescent protein (GFP)-tagged MZT2 was purified, as described previously (Wieczorek et al. 2021). We first used this complex to perform nucleation assays and characterized the association of the γ-TuRC at the minus-end of newly formed microtubules (Fig. 2.1 A). Nucleation of microtubules from a single surface-bound γ-TuRC$^{\gamma\text{-Tub-WT}}$ was monitored for up to 30 minutes, after which photobleaching of the γ-TuRC$^{\gamma\text{-Tub-WT}}$ or overcrowding of the microtubules that formed limited our analyses. For the majority of nucleation events (~88%; n=76 total events from N=3 independent experiments), the γ-TuRC remained associated with the microtubule for several minutes (range: 7.0-29.8 minutes; Fig. 2.1 B and C) and was not observed to dissociate over the course of experiment, consistent with previous qualitative analyses (Consolati et al. 2020).

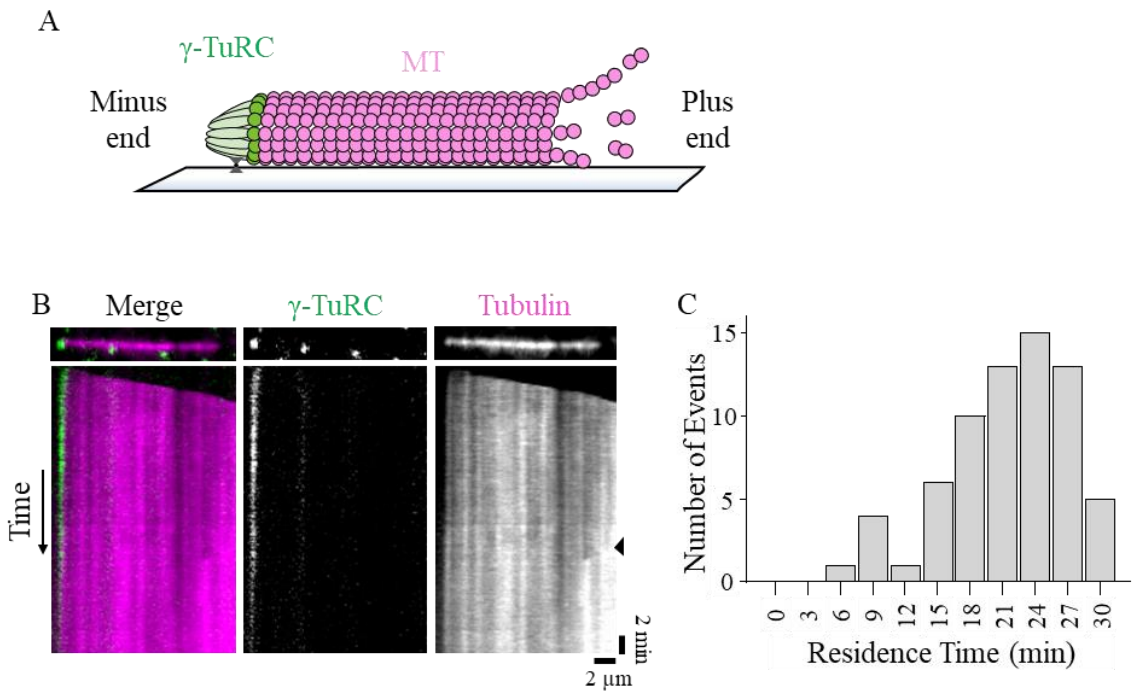

Figure 2.1 Recombinant γ-TuRC$^{γ\text{-}Tub\text{-}WT}$ caps nucleated microtubules

(A) Schematic of the TIRF-based assay to analyze microtubules nucleated by recombinant γ-TuRC. Surface immobilized GFP-tagged γ-TuRC (green) and polymerized tubulin (pink), are shown. (B) Image and kymograph of a microtubule nucleation event from γ-TuRC$^{γ\text{-}Tub\text{-}WT}$. Two-color overlay of tubulin (magenta) and γ-TuRC$^{γ\text{-}Tub\text{–}WT}$ (green), and single channel images are shown. Black triangle (right kymograph) marks signal from the appearance of another polymerizing microtubule nucleated nearby. (C) Frequency distribution of the residence times of γ-TuRC$^{γ\text{-}Tub\text{-}WT}$ at microtubule minus-ends after a nucleation event. Bin size=3 minutes, n=67 total events, N=3 independent experiments. These experiments were performed with M. Wieczorek (Kapoor lab).

Next, we established a TIRF-based assay to examine the capping of taxol-stabilized microtubules by γ-TuRC$^{\gamma\text{-Tub-WT}}$. Taxol-stabilized microtubules were attached to passivated coverslips to which the plus-end directed kinesin-1 fragment (residues 1-560, K560) was adsorbed, and their motility in the presence of MgATP (100 μM) was used to determine microtubule polarity and to exclude any non-specifically coverslip-attached γ-TuRC (Fig. 2.2 A). Following incubation with γ-TuRC$^{\gamma\text{-Tub-WT}}$ (50 pM), we observed 23 ± 7% (n= 1,770 microtubules from N=3 independent experiments) of the taxol-stabilized minus-ends to be capped (Fig. 2.2 B and C), consistent with previous work (Zheng et al. 1995). We next performed this assay using GMPCPP-stabilized microtubules, and found that 25 ± 3% (n= 2,326 microtubules from N=3 independent experiments) of the minus-ends were capped (Fig. 2.2 B and C). Interestingly, taxol- and GMPCPP-stabilized microtubules have been shown to predominantly have 13 or 14 protofilaments, respectively (A. Rai et al. 2021; Ginsburg et al. 2017). As the γ-TuRC similarly capped taxol- and GMPCPP-stabilized microtubules, our data suggests that changes in protofilament number (13 vs. 14) do not substantially affect the capping activity of the γ-TuRC under our experimental conditions. Further, the γ-TuRC cap often persisted at stable microtubule minus-ends for >2 minutes, although this could not be measured quantitatively due to the motility of the microtubules in this assay.

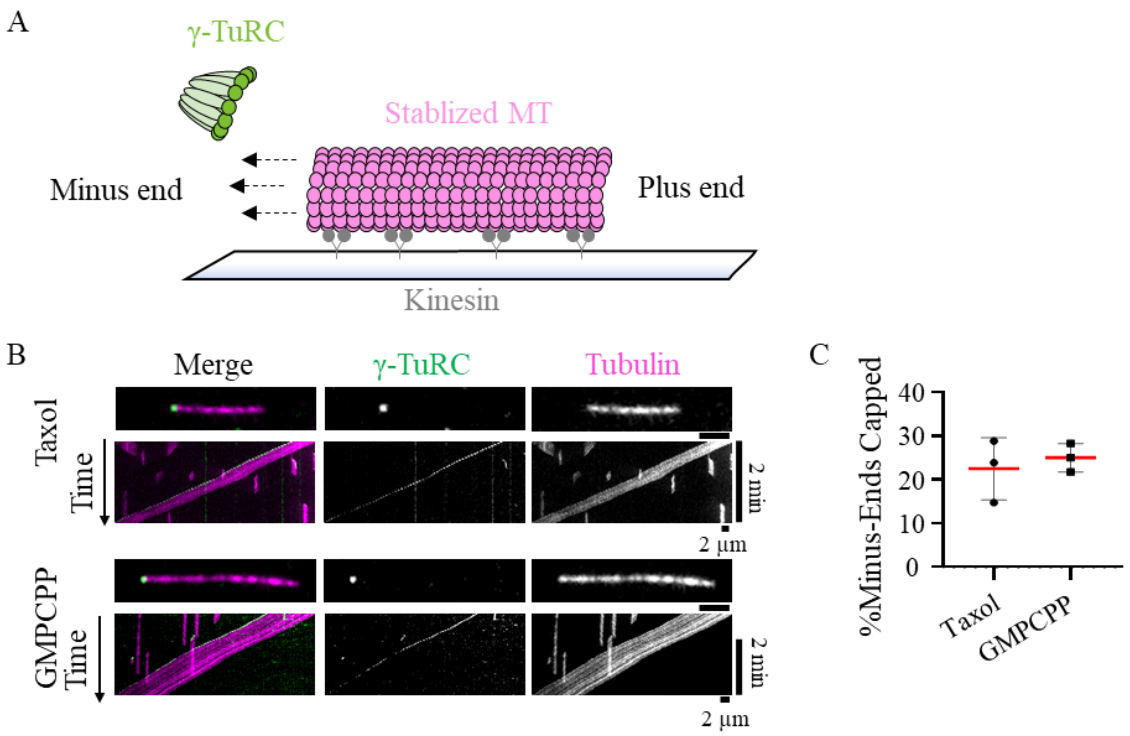

Figure 2.2 Recombinant γ-TuRC$^{γ\text{-}Tub\text{-}WT}$ caps stabilized microtubule minus-ends

(A) Schematic of the assay to analyze GFP-tagged γ-TuRC (green) capping of stabilized microtubules (pink) bound to surface-immobilized kinesin motor domains (non-fluorescent). Arrows indicate the directional movement of microtubules in the presence of MgATP (100 µM). (B) Images and kymographs of γ-TuRC$^{γ\text{-}Tub\text{–}WT}$ capping taxol- or GMPCPP- stabilized microtubules. Two-color overlay of tubulin (magenta) and γ-TuRC$^{γ\text{-}Tub\text{–}WT}$ (green), and single channel images are shown. (C) Quantification of the percentage of taxol- or GMPCPP-stabilized microtubule minus-ends capped by γ-TuRC$^{γ\text{-}Tub\text{-}WT}$. Mean (red line) and error (standard deviation) are shown. Taxol: n=1,770 events from N=3 independent experiments. GMPCPP: n=2,326 events from N=3 independent experiments. These assays were performed with recombinant γ-TuRC$^{γ\text{-}Tub\text{–}WT}$ purified by M. Wieczorek and A. Aher (Kapoor lab).

We next examined the interactions of GFP-tagged γ-TuRCs with dynamic microtubules (Fig. 2.3 A). Surface-bound, GMPCPP-stabilized microtubule "seeds" were incubated with γ-TuRC (10-30 pM) and soluble tubulin (15 µM). Both microtubule ends were observed to grow as "dim" extensions from a"bright" seed, with the minus-ends being identified as the slower polymerizing extensions (Walker et al. 1988). Puncta of γ-TuRC$^{\gamma\text{-Tub-WT}}$ were found to bind dynamic microtubule minus-ends over the course of the experiment (total time: 10 minutes, imaging interval: 3 seconds; Fig. 2.3 B and C). Kymographs of single filaments showed dynamic minus-ends, and binding of the γ-TuRC$^{\gamma\text{-Tub-WT}}$ suppressed growth and shrinkage (Fig. 2.3 B and C). For the majority (~83%, n=89 total events from N=3 independent experiments) of these events, the γ-TuRC$^{\gamma\text{-Tub-WT}}$ was found to associate and then dissociate from the minus-end (Fig. 2.3 B). Dissociation of the γ-TuRC$^{\gamma\text{-Tub-WT}}$ was followed by the resumption of minus-end dynamics (Fig. 2.3 B). An exponential fit of the cumulative frequency plot for these events provided a mean residence time (τ) of 0.80 ± 0.20 minutes (95% C.I. Fig. 2.3 D). In the remaining capping events (~17%), the γ-TuRC bound to a minus-end, but did not dissociate during the course of the experiment (10 minutes; Fig. 2.3 C). We repeated our experiments for longer periods of time (total time: 30 minutes, interval: 10 seconds) and found that, again, the majority of events (~83%) showed both binding and dissociation of the γ-TuRC, and an exponential fit of the cumulative frequency of the residence times for theses events provided a mean residence time (τ) of 1.30 ± 0.30 minutes (95% C.I., Fig. 2.3 E). Furthermore, γ-TuRC dissociation from the minus-end was not observed during the course of this experiment (30 minutes) for a fraction of the events (~17%, n=134 total events from N=2 independent experiments). As the full binding and unbinding cycle was not observed, these events were

not included in the mean residence time calculation (see methods). The apparent residence time for all events (black bars: both association and dissociation observed; gray bars: association, but no dissociation observed) from the longer imaging experiments are shown using a frequency distribution plot (Fig. 2.3 F).

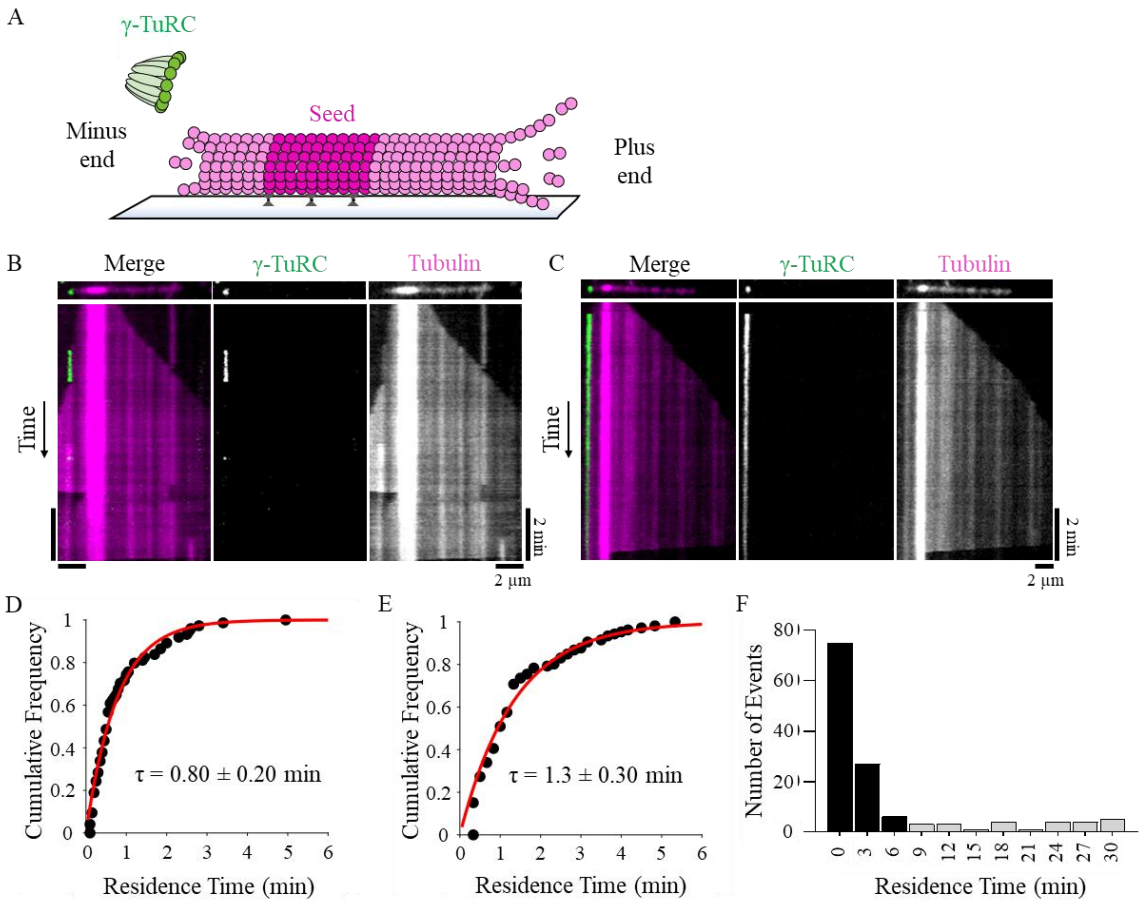

Figure 2.3 Recombinant γ-TuRC$^{\gamma\text{-Tub-WT}}$ caps dynamic microtubule minus-ends

(A) Schematic of the assay to analyze recombinant γ-TuRC binding to dynamic microtubules. Biotinylated 'bright' GMPCPP seed (magenta, 12.5% X-rhodamine-tubulin), polymerizing 'dim' (pink, 2.5% X-rhodamine-tubulin) minus- and plus-end extensions, and GFP-tagged γ-TuRCs (green) are shown. (B and C) Images and kymographs of γ-TuRC$^{\gamma\text{-Tub–WT}}$ capping events on dynamic microtubules. Two-color overlay of tubulin (magenta) and γ-TuRC$^{\gamma\text{-Tub–WT}}$ (green), and single channel images are shown. (D and E) Cumulative frequency of the residence times of γ-TuRC$^{\gamma\text{-Tub-WT}}$ capping events where association and dissociation of the cap were observed from short (10 minute; D) or long (30 minute; E) imaging experiments, fitted to a single exponential (red line) with indicated mean residence time, τ. Error=95% C.I. D: n=74 events (83% of total events), N=3 independent experiments. E: n=107 events (83% of total events) from N=3 independent experiments. (F) Frequency distribution of γ-TuRC$^{\gamma\text{-Tub-WT}}$ residence times from longer imaging experiments (30 minutes). Events where γ-TuRC$^{\gamma\text{-Tub-WT}}$ dissociation from minus-ends is observed (black bars) and where γ-TuRC$^{\gamma\text{-Tub-WT}}$ remains associated with minus-ends throughout the course of imaging (gray bars) are plotted. Bin size=3 minutes. n=134 total events from N=2 independent experiments. Scale bars: distance (horizontal)=2 μm, time (vertical)=2 minutes. These experiments were performed with M. Wieczorek (Kapoor lab)

Taken together, our findings indicate that γ-TuRC capping suppresses dynamics at microtubule minus-ends. The γ-TuRC binds a nucleated microtubule for tens of minutes or a stabilized pre-formed microtubule for 2 or more minutes, and caps a dynamic microtubule minus-ends with lifetimes of ~1 minute.

2.3.2 Nucleotide-binding deficient γ-tubulin incorporates into native-like γ-TuRCs that cannot nucleate microtubules

Next, we examined the role of GTP-binding to γ-tubulin within the context of the γ-TuRC holocomplex. To this end, we purified recombinant γ-TuRC$^{\gamma\text{-TubΔGTP}}$, a complex that incorporates γ-tubulin with an N229A point mutation. While the homologous mutation has been shown to reduce GTP binding to yeast γ-tubulin (Gombos et al. 2013), its effect on human γ-tubulin has not yet been characterized. To analyze this, we also expressed and purified recombinant WT and N229A-γ-tubulin (Fig. 2.4 A). Native mass spectrometry indicated that WT γ-tubulin could bind nucleotide. By contrast, GTP binding to N229A-γ-tubulin was suppressed (Fig. 2.4 B and C).

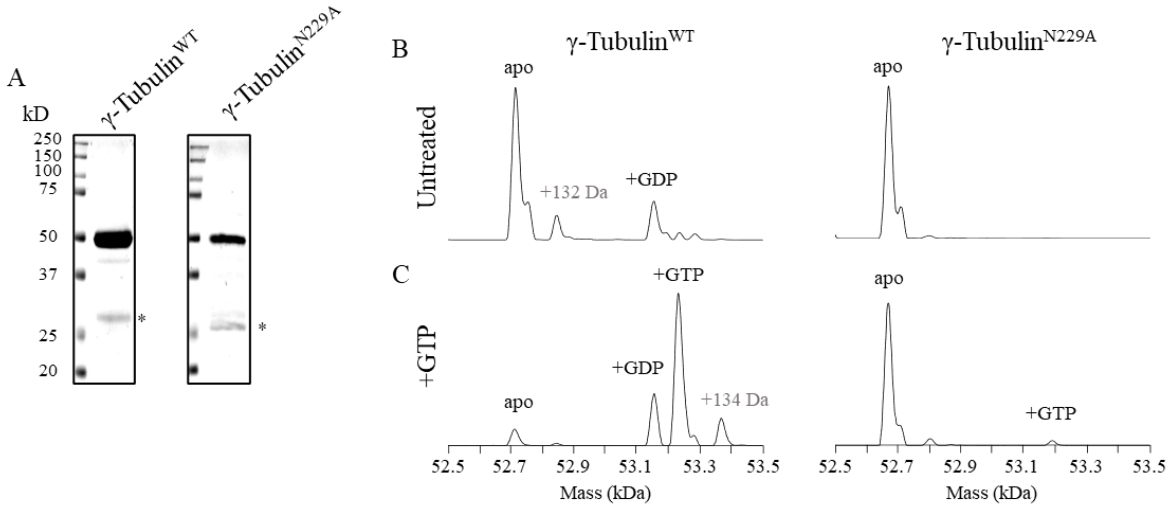

Figure 2.4 Native mass spectrometry analysis of γ-tubulin^{N229A}

(A) SDS-PAGE analysis (Coomasie) of recombinant, purified γ-tubulin^{WT} (left) and γ-tubulin^{N229A} (right) after gel filtration. Asterisk indicates a contaminant at ~25kDa. (B and C) Native mass spectrometry analysis of γ-tubulin^{WT} and γ-tubulin^{N229A} before (B) and after (C) incubation with MgGTP. Native mass spectrometry experiments were performed and analyzed by P. D. Olinares (Chait lab).

We characterized the γ-TuRC$^{γ\text{-}TubΔGTP}$ in four ways. First, sucrose gradient centrifugation indicated that the mutant γ-tubulin is incorporated into a complex that migrates to ~35% sucrose, a percentage comparable to what we have observed for recombinant WT and native complexes (Fig. 2.5 A; Wieczorek, Urnavicius, et al. 2020; Wieczorek et al. 2021). Second, mass spectrometry analysis confirmed the presence of all 10 overexpressed γ-TuRC proteins (Fig. 2.5 B). Third, we used negative stain electron microscopy to characterize the overall structure of the complex. The γ-TuRC$^{γ\text{-}TubΔGTP}$ appeared as asymmetric cones in negative-stain EM micrographs (Fig. 2.5 C). Reference-

free 2D classification provided a dataset with different views of the complex, including some where individual spokes were discernible (Fig. 2.5 D). Particles corresponding to these 2D classes were then used to produce a 3D reconstruction of the complex, which revealed 14-spoke γ-TuRCs with a "seam" between the first and last spokes, and a density in the lumen of the cone (Fig. 2.5 E). This low-resolution structure is consistent with recently published high-resolution cryo-EM structures of the human and Xenopus γ-TuRCs (Consolati et al. 2020; Wieczorek, Urnavicius, et al. 2020; Peng Liu et al. 2019). Correspondingly, a model of the native human γ-TuRC could be rigid body–fitted into the γ-TuRC$^{\gamma\text{-TubΔGTP}}$ density (Protein Data Bank accession nos. 6V6S, 6X0U, and 6X0V; Wieczorek, Urnavicius, et al. 2020; Wieczorek, Huang, et al. 2020; Fig. 2.5 F). Fourth, we examined the microtubule nucleation activity of the γ-TuRC$^{\gamma\text{-TubΔGTP}}$ and found that microtubules were rarely observed in the γ-TuRC$^{\gamma\text{-TubΔGTP}}$ sample in the course of the experiment (30min). The few microtubules observed did not originate from GFP puncta. By contrast, the γ-TuRC$^{\gamma\text{-Tub-WT}}$ sample revealed several GFP-puncta-associated microtubules within minutes (Fig. 2.5 G and H).

A

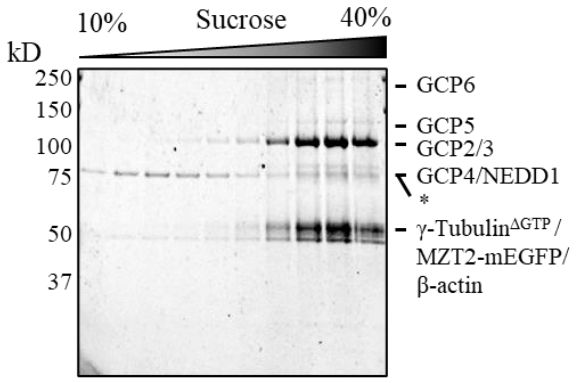

B

Protein	Coverage (%)	Unique /Total
γ-Tubulin	80.49	10/49
GCP2	81.49	64/115
GCP3	79.71	52/113
GCP4	61.77	44/44
GCP5	49.22	56/56
GCP6	39.14	74/74
NEDD1	79.70	63/68
MZT1	98.78	8/8
MZT2A	86.08	17/17
Actin	41.60	2/16

C

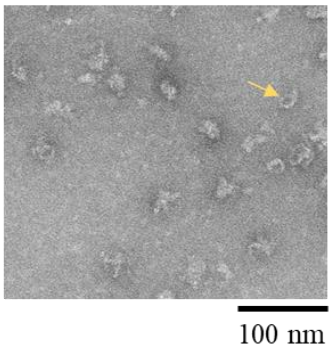

D

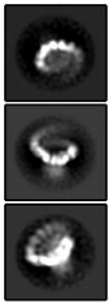

E

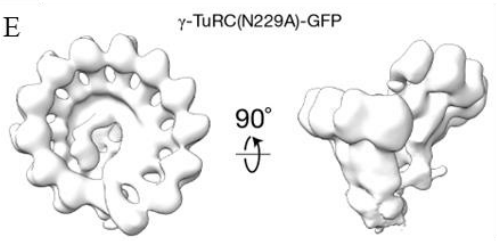

F

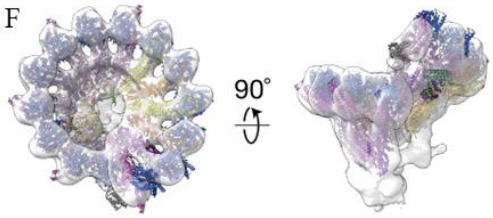

G

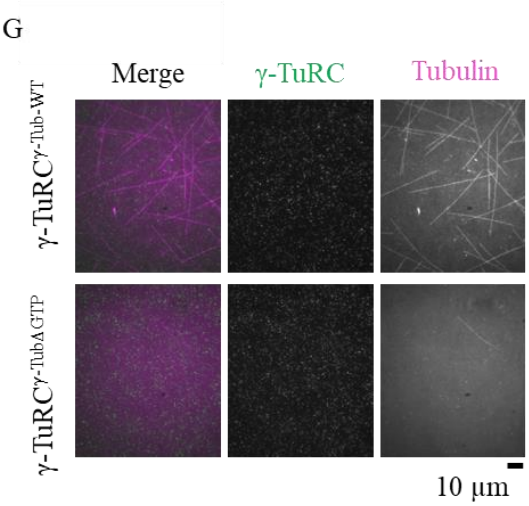

H

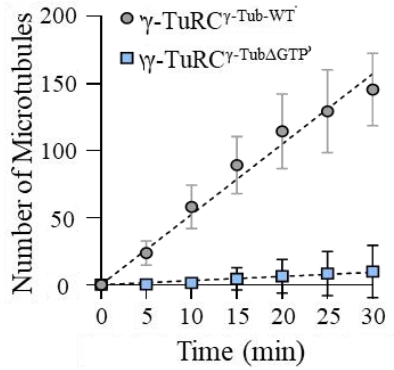

Figure 2.5 Recombinant γ-TuRC$^{\gamma\text{-Tub}\Delta GTP}$ assembles into a 14-spoke assembly and cannot nucleate microtubules

(A) SDS-PAGE analysis (Coomasie) of γ-TuRC$^{\gamma\text{-Tub}\Delta GTP}$ after sucrose gradient centrifugation and fractionation. The percentage (W/V) of sucrose is indicated at the top. Asterisk (*) indicates a 70kD contaminant with a sedimentation peak at a lower sucrose percentage than the γ-TuRC$^{\gamma\text{-Tub}\Delta GTP}$ components. (B) γ-TuRC proteins identified in liquid chromatography-mass spectrometry analysis of the γ-TuRC$^{\gamma\text{-Tub}\Delta GTP}$ complex. Coverage represents the percentage of identified protein sequences. "Unique/Total" designates the ratio of unique and total peptides identified. (C) Transmission EM micrograph of negatively stained γ-TuRC$^{\gamma\text{-Tub}\Delta GTP}$. Scale bar=100 nm. (D) 2D averages showing three orientations of γ-TuRC$^{\gamma\text{-Tub}\Delta GTP}$ particles. Scale bar=20 nm. (E) Two views of a 3D reconstruction of γ-TuRC$^{\gamma\text{-Tub}\Delta GTP}$. (F) Rigid body fit of the native human γ-TuRC model in the γ-TuRC$^{\gamma\text{-Tub}\Delta GTP}$ density map (Protein Data Bank accession nos. 6V6S, 6X0U, and 6X0V). The fitting was performed by M Wieczorek (Kapoor lab). (G) Images of nucleation assays in the presence of γ-TuRC$^{\gamma\text{-Tub-WT}}$ (top) or γ-TuRC$^{\gamma\text{-Tub}\Delta GTP}$ (bottom). Two-color overlay of tubulin (magenta) and γ-TuRC$^{\gamma\text{-Tub}\Delta GTP}$ (green), and single channel images are shown. Scale bar=10μm. (H) Quantification of the number of microtubules at the indicated time points for γ-TuRC$^{\gamma\text{-Tub-WT}}$ or γ-TuRC$^{\gamma\text{-Tub}\Delta GTP}$ microtubule nucleation assays. Mean (symbols) and error (standard deviation) are shown. Data were fitted using a linear regression (dashed lines). n=4 replicates from N=2 independent experiments.

Together, these data indicate that the N229A mutation in γ-tubulin suppresses the microtubule nucleation activity of the γ-TuRC holocomplex, but does not substantially alter the overall structural organization of the complex Additional studies will be needed to determine the high-resolution structure of the γ-TuRC$^{\gamma\text{-TubΔGTP}}$ and analyze why this complex cannot nucleate microtubules.

2.3.3. γ-TuRC$^{\gamma\text{-TubΔGTP}}$ caps stable and dynamic microtubule minus-ends

We next examined microtubule capping by γ-TuRC$^{\gamma\text{-TubΔGTP}}$ and first focused on stabilized microtubules. Under assay conditions similar to those used to examine the γ-TuRC$^{\gamma\text{-Tub-WT}}$ (Fig. 2.2 A), puncta of γ-TuRC$^{\gamma\text{-TubΔGTP}}$ (50 pM) were observed to bind the minus-ends of taxol- and GMPCPP-stabilized microtubules (Fig. 2.6A). The percentage of capped minus-ends was 18 ± 3% (n= 1,503 microtubules from N= 3 independent experiments) for taxol- stabilized microtubules, and 21 ± 4% (n= 1,634 microtubules from N= 4 independent experiments) for GMPCPP-stabilized microtubules (Fig. 2.6 A and B). Qualitatively, the γ-TuRC$^{\gamma\text{-TubΔGTP}}$ cap at most stable microtubule minus-ends lasted for at least two minutes, as observed for γ-TuRC$^{\gamma\text{-Tub-WT}}$ in this assay.

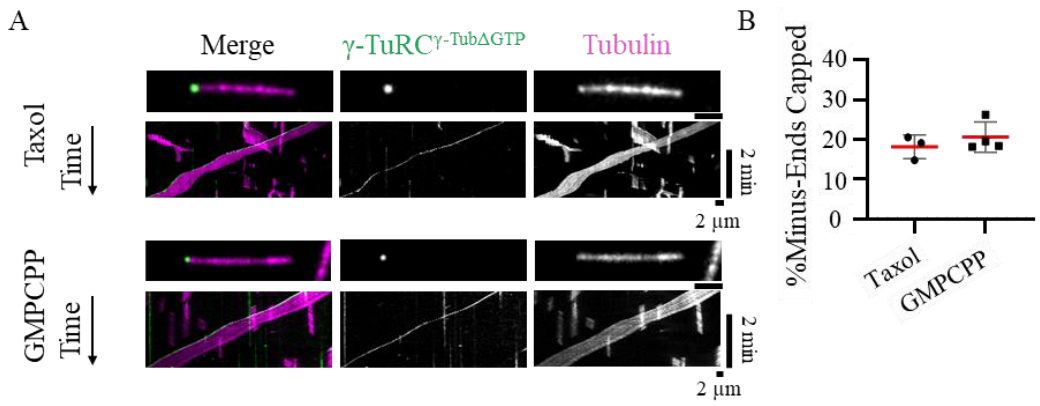

Figure 2.6 Recombinant γ-TuRC$^{γ\text{-}TubΔGTP}$ caps stable microtubule minus-ends

(A) Images and kymographs of γ-TuRC$^{γ\text{-}TubΔGTP}$ capping taxol- or GMPCPP- stabilized microtubules bound to surface immobilized kinesin motor domains. Two-color overlay of tubulin (magenta) and γ-TuRC$^{γ\text{-}Tub–WT}$ (green), and single channel images are shown. (B) Quantification of the percentage of taxol- or GMPCPP-stabilized microtubule minus-ends capped by γ-TuRC$^{γ\text{-}TubΔGTP.}$ Mean (red line) and error (standard deviation) are shown. Taxol: n=1,503 events from N=3 independent experiments. GMPCPP: n=1,634 events from N=4 independent experiments.

We next analyzed the capping of dynamic microtubules by γ-TuRC$^{γ\text{-}TubΔGTP}$. Puncta of γ-TuRC$^{γ\text{-}TubΔGTP}$ (10-30 pM) were observed to bind the minus-ends of dynamic microtubules (Fig. 3C and D). The capping activity of the γ-TuRC$^{γ\text{-}TubΔGTP}$ was qualitatively similar to that of the γ-TuRC$^{γ\text{-}Tub\text{-}WT}$. Binding of γ-TuRC$^{γ\text{-}TubΔGTP}$ suppressed microtubule dynamics at minus-ends (Fig. 3C and D), and minus-end growth/shrinkage resumed following γ-TuRC$^{γ\text{-}TubΔGTP}$ dissociation (Fig. 3C). Notably, we observed that in the majority of events (~81%, n=105 total events from N=3 independent experiments), the

γ-TuRC$^{\gamma\text{-TubΔGTP}}$ associated with and then dissociated from the minus-end, similar to the experiments performed with γ-TuRC$^{\gamma\text{-Tub-WT}}$. The cumulative frequency distribution of these events provided a mean residence time of 1.1 ± 0.25 minutes (95% C.I.; time interval: 3 seconds, total time: 10 minutes; Fig. 3E). The remaining events (~19%) did not show γ-TuRC$^{\gamma\text{-TubΔGTP}}$ dissociation throughout the course of the experiment (10 minutes). Longer image acquisition conditions (frame interval: 10 seconds, total time: 30 minutes), showed a similar distribution of events. The majority of events (~77%) showed both binding and dissociation of the γ-TuRC$^{\gamma\text{-TubΔGTP}}$ with a mean residence time of 1.80 ± 0.40 minutes (95% C.I., Fig. 3F and G, black bars), while a smaller percentage of events (~23%, n=111 event from N=2 independent experiments) did not show dissociation of the γ-TuRC$^{\gamma\text{-TubΔGTP}}$ (Fig. 3G, gray bars).

We further compared the γ-TuRC$^{\gamma\text{-TubΔGTP}}$ and γ-TuRC$^{\gamma\text{-Tub-WT}}$ capping activities by measuring the landing rate, referring to the number of capping events divided by the concentration of the γ-TuRC, the time duration of the experiment, and the number of dynamic microtubules. For the γ-TuRC$^{\gamma\text{-Tub-WT}}$, the average landing rate was 17.5 ± 7.8 μM^{-1} sec^{-1} $minus\text{-}end^{-1}$ (n=10 measurements from N=3 independent experiments, Fig. S1E). The average landing rate for the γ-TuRC$^{\gamma\text{-TubΔGTP}}$ was 15.9 ± 7.0 μM^{-1} sec^{-1} $minus\text{-}end^{-1}$ (n= 10 measurements from N=3 independent experiments, Fig. S1E), which was not significantly different from the γ-TuRC$^{\gamma\text{-Tub-WT}}$ landing rate (unpaired two-tailed Student's t test, p=0.65). Overall, these data suggest that capping of stabilized and dynamic microtubule ends by γ-TuRC does not depend on GTP binding by γ-tubulin.

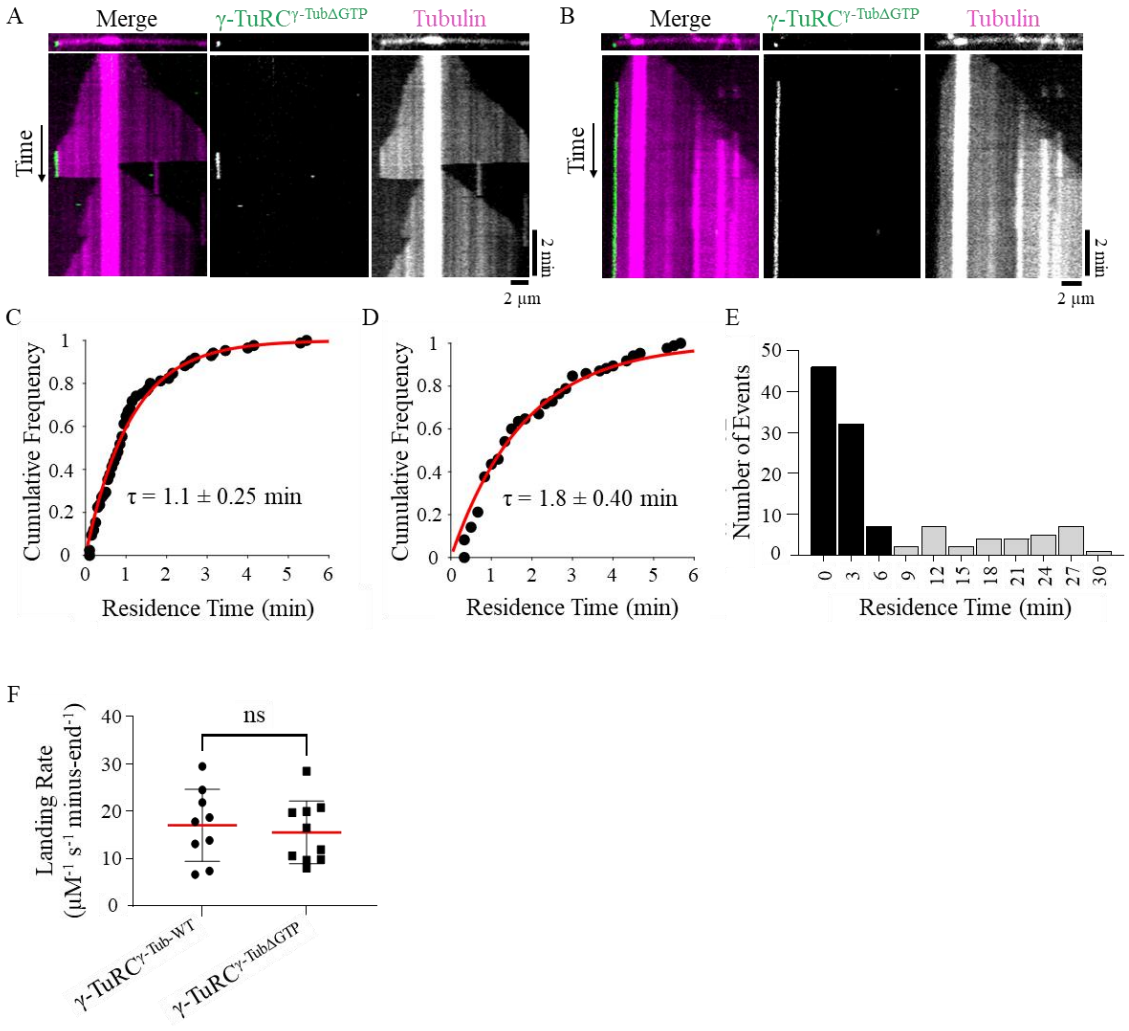
A
Merge
γ-TuRC^γ-TubΔGTP
Tubulin
Time
2 min
2 µm
B
Merge
γ-TuRC^γ-TubΔGTP
Tubulin
Time
2 min
2 µm
C
Cumulative Frequency
τ = 1.1 ± 0.25 min
Residence Time (min)
D
Cumulative Frequency
τ = 1.8 ± 0.40 min
Residence Time (min)
E
Number of Events
Residence Time (min)
F
Landing Rate (µM⁻¹ s⁻¹ minus-end⁻¹)
ns
γ-TuRC^γ-Tub-WT
γ-TuRC^γ-TubΔGTP

Figure 2.7 Recombinant γ-TuRC$^{γ\text{-}TubΔGTP}$ caps dynamic microtubule minus-ends

(A and B) Images and kymographs of γ-TuRC$^{γ\text{-}TubΔGTP}$ capping events on dynamic microtubules. Two-color overlay of tubulin (magenta) and γ-TuRC$^{γ\text{-}TubΔGTP}$ (green), and single channel images are shown. (C and D) Cumulative frequency of the residence times of γ-TuRC$^{γ\text{-}TubΔGTP}$ capping events where association and dissociation of the cap were observed from under short (10 minute; C) or long (30 minute; D) imaging experiments fitted to a single exponential (red line) with indicated mean residence time, τ. Error=95% C.I. 10 minutes: n=85 total events (81% of total) from N=3 independent experiments. 30 minutes: n=85 events (77% of total) from N=2 independent experiments. (E) Frequency distribution of γ-TuRC$^{γ\text{-}Tub\text{-}WT}$ residence times from longer imaging experiments (30 minutes). Events where γ-TuRC$^{γ\text{-}TubΔGTP}$ dissociation is observed (black bars) and where γ-TuRC$^{γ\text{-}TubΔGTP}$ minus-end association persisted (gray bars) are plotted. Bin size=3 minutes. n=111 total events from N=2 independent experiments. Scale bars: distance (horizontal)=2 μm, time (vertical)=2 minutes. (F) Landing rates= number of capping events/[(μM γ-TuRC)*(experiment duration in seconds)*(number of total minus-ends)] of γ-TuRC$^{γ\text{-}Tub\text{-}WT}$ or γ-TuRC$^{γ\text{-}TubΔGTP}$ under short (10 minute) experiment conditions. Mean (red line) and error (standard deviation) are shown. γ-TuRC$^{γ\text{-}Tub\text{-}WT}$, n=9 measurements, γ-TuRC$^{γ\text{-}TubΔGTP}$, n=10 measurements, from N=3 independent experiments. ns=not significant, unpaired two-sided Student's t test, p=0.65. These experiments were performed with M. Wieczorek (Kapoor lab).

2.3.4. Non-centrosomal microtubules form in the presence of γ-tubulin$^{\Delta GTP}$

While γ-tubulin depletion results in mild phenotypes during interphase, γ-tubulin has been shown to play a key role in regulating mitotic progression and spindle assembly (Tsuchiya and Goshima 2021; Hutchins et al. 2010; Lüders, Patel, and Stearns 2006; Hannak et al. 2002; Strome et al. 2001). Yet, it is unknown if the γ-TuRC's capping activity contributes to these processes. Therefore, we next examined the role of nucleotide-binding deficient γ-tubulin in dividing cells. We first generated a cell line with inducible expression of shRNA to γ-tubulin (hereafter, γ-tubulin^{KD}). Relative to uninduced control cells (mitotic index: 6 ± 1%, n = 3,653 total cells, from N = 3 independent experiments), γ-tubulin knockdown resulted in an increase in the mitotic index (21 ± 5%, n = 4,800 total cells from N = 3 independent experiments) and an increase in cells displaying misaligned chromosomes and poorly separated spindle poles (hereafter, disrupted spindles; 75 ± 7%, n = 1,009 total cells from N = 3 independent experiments; control cells: 8 ± 1%, n = 205 total cells, from N = 3 independent experiments; Fig. 2.8 A-C). These phenotypes are consistent with prior work (Choi et al. 2010; Haren et al. 2006). While western blot analysis showed that residual amounts of endogenous γ-tubulin remained in whole cell lysates (~25%, Fig. 2.8 D and E), γ-tubulin puncta were not observed by immunofluorescence, consistent with the loss of γ-tubulin in mitotic cells with disrupted spindles (Fig. 2.8 C).

We next used the γ-tubulin^{KD} cell line to generate "addback" cell lines which upon treatment with doxycycline, expressed both shRNA and RNAi-resistant C-terminally GFP-tagged WT or GTP-binding deficient N229A-γ-tubulin (hereafter, γ-tubulin^{WT+KD} and γ-tubulin$^{\Delta GTP+KD}$). In these cell lines, the levels of γ-tubulin^{WT}-GFP and γ-tubulin$^{\Delta GTP}$-GFP were similar to levels of endogenous γ-tubulin in control cells and the knockdown efficiencies were comparable to that of γ-tubulin^{KD} (Fig. 2.8 D and E). Importantly, γ-

tubulin$^{\Delta GTP+KD}$ cells displayed a ~4-fold increase in the mitotic index (26 ± 8%, n=2,801 total cells from N=3 independent experiments) relative to untreated controls, and an increase in the fraction of cells with disrupted spindles (81 ± 14%, n=741 total cells from N=3 independent experiments; Fig. 2.8 A, B, F). In contrast, the γ-tubulin^{WT+KD} cells had a mitotic index (9 ± 1%, n= 2,923 total cells from N= 3 independent experiments) and fractions of disrupted spindles (24 ± 7%, n=253 from N=3 independent experiments) comparable to uninduced controls (Fig. 2.8 A, B, F). These phenotypes were dependent on depletion of endogenous γ-tubulin, as a cell line expressing γ-tubulin$^{\Delta GTP}$-GFP, but not the shRNA, did not display mitotic defects (mitotic index= 7 ± 1%, n=2,457 total cells and disrupted spindles=10 ± 5%, n=187 total cells from N=3 independent experiments; Fig 2.8 A, B, F). Importantly, both γ-tubulin$^{\Delta GTP}$-GFP and γ-tubulin^{WT}-GFP localized to centrosomes (Fig. 2.8 F), and sucrose gradients of cell lysates showed a peak for γ-tubulin at ~30% sucrose (Fig 2.8 I), consistent with incorporation of γ-tubulin$^{\Delta GTP}$-GFP and γ-tubulin^{WT}-GFP into the γ-TuRC complexes (Tsuchiya and Goshima 2021; Haren et al. 2020).

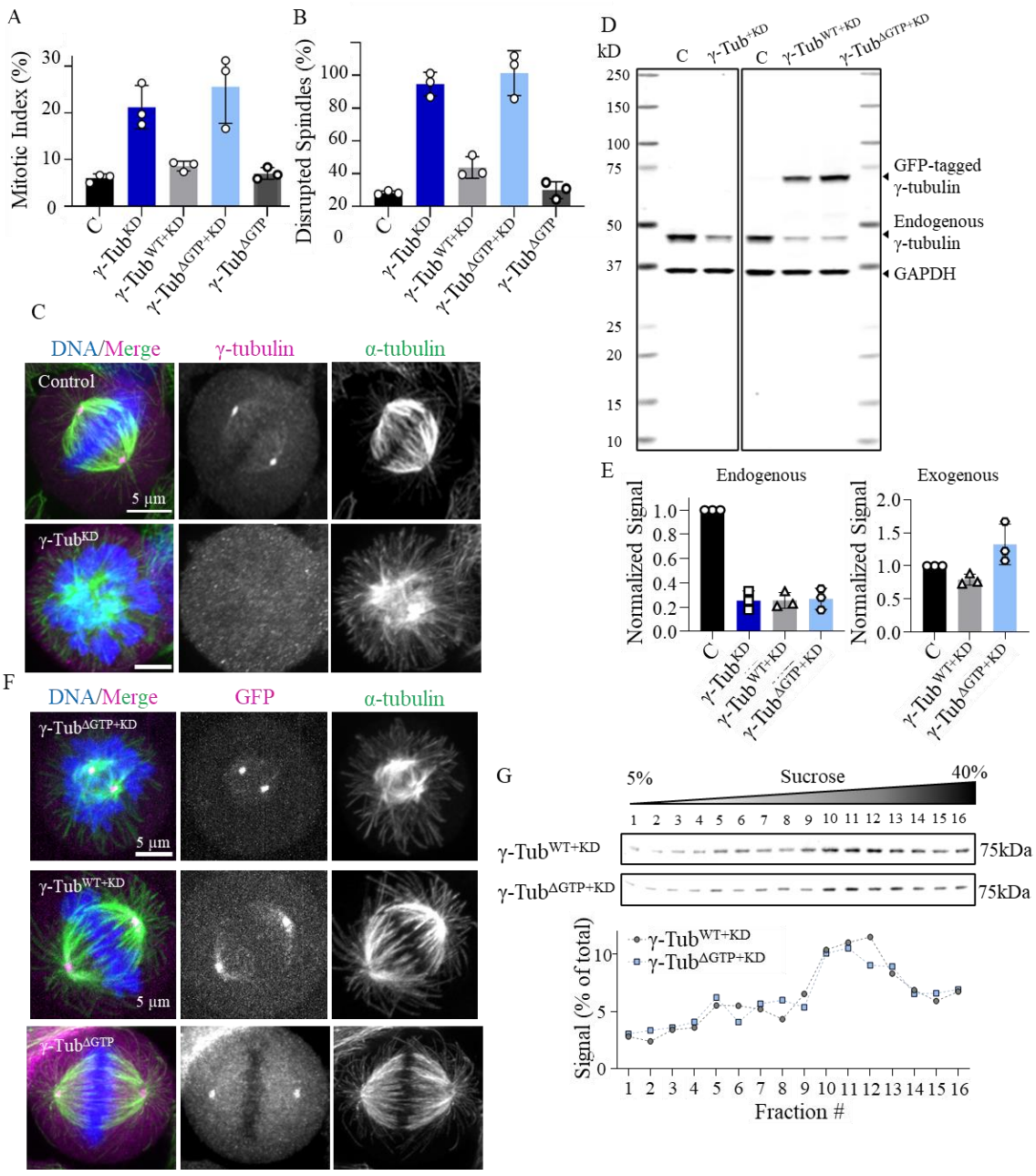
A
Mitotic Index (%)
30
20
10
0
C
γ-Tub^KD
γ-Tub^WT+KD
γ-Tub^ΔGTP+KD
γ-Tub^ΔGTP
B
Disrupted Spindles (%)
100
80
60
40
20
0
C
γ-Tub^KD
γ-Tub^WT+KD
γ-Tub^ΔGTP+KD
γ-Tub^ΔGTP
C
DNA/Merge
γ-tubulin
α-tubulin
Control
5 μm
γ-Tub^KD
D
kD
C
γ-Tub^KD
C
γ-Tub^WT+KD
γ-Tub^ΔGTP+KD
250
150
100
75
50
37
25
20
15
10
GFP-tagged γ-tubulin
Endogenous γ-tubulin
GAPDH
E
Endogenous
Exogenous
Normalized Signal
1.0
0.8
0.6
0.4
0.2
0.0
2.0
1.5
1.0
0.5
0.0
C
γ-Tub^KD
γ-Tub^WT+KD
γ-Tub^ΔGTP+KD
F
DNA/Merge
GFP
α-tubulin
γ-Tub^ΔGTP+KD
5 μm
γ-Tub^WT+KD
5 μm
γ-Tub^ΔGTP
G
5%
Sucrose
40%
1 2 3 4 5 6 7 8 9 10 11 12 13 14 15 16
γ-Tub^WT+KD
75kDa
γ-Tub^ΔGTP+KD
75kDa
γ-Tub^WT+KD
γ-Tub^ΔGTP+KD
Signal (% of total)
10
5
0
1 2 3 4 5 6 7 8 9 10 11 12 13 14 15 16
Fraction #

Figure 2.8 γ-tubulin$^{\Delta GTP+KD}$ cells form disrupted spindles

(A) Analysis of the mean mitotic index. n=>2,000 cells per condition from N=3 independent experiments. (B) The mean percentage of mitotic cells that displayed disrupted spindles. n=>200 cells per condition from N=3 independent experiments. (C) Images of fixed mitotic uninduced control and γ-tubulin^{KD} cells. Single-channel images (maximum-intensity projections) and overlays show γ-tubulin (magenta), α-tubulin (green), and DNA (blue). (D) Western blot analysis of cell lysates. Bands corresponding to the expected molecular weights of GFP-tagged γ-tubulin, endogenous γ-tubulin, and GAPDH are indicated, along with the corresponding molecular weight standard. (E) Quantification of endogenously and exogenously expressed γ-tubulin levels in these cell lines determined by western blotting, relative to loading control (GAPDH). The signal relative to control is plotted. Mean and error (standard deviation) are shown. N=3 independent experiments. (F) Images of fixed γ-tubulin$^{\Delta GTP+KD}$, γ-tubulin^{WT+KD}, and γ-tubulin$^{\Delta GTP}$ cells. Single-channel images (maximum-intensity projections) and overlays show GFP (native signal; magenta), α-tubulin (green), and DNA (blue). (G) Analysis of whole cell lysates from γ-tubulin^{WT+KD} and γ-tubulin$^{\Delta GTP+KD}$ cell lines using sucrose gradient centrifugation. Western blot of γ-tubulin (top) and quantification of the percentage of γ-tubulin antibody signal within each sucrose gradient fraction (bottom) are shown.

We next performed a microtubule regrowth assay to examine how nucleotide-binding deficient γ-tubulin affected cellular microtubule formation (Fig. 2.9 A). In the different cell lines, at the earliest time points of regrowth (2 minutes), microtubules grew predominantly from two sites with similar fluorescence intensities, consistent with growth from centrosomes (Fig. 2.9 B-E). At later time points (5 minutes), several additional microtubule foci were observed in control and γ-tubulin^{WT+KD} cells (80 ± 11% and 90 ± 11% of cells, n=67 and 50 total cells from N=3 independent experiments, respectively; Fig. 2.9 D and F). In the case of the γ-tubulin^{KD} cells, few additional microtubule foci formed at later time points (5 minutes; 27 ± 12% of cells; n=79 total cells from N=3 independent experiments, Fig. 2.9 D and F-G). These findings are consistent with previous studies (Ramírez Cota et al. 2017; Lüders, Patel, and Stearns 2006). Importantly, γ-tubulin$^{\Delta GTP+KD}$ cells showed several foci at non-centrosomal sites at these later time points (88 ± 4%, n=95 total cells from N=4 independent experiments; Fig. 2.9 D, F, H). Together, these data suggest that addback of γ-tubulin$^{\Delta GTP}$-GFP allows for microtubule formation at non-centrosomal sites.

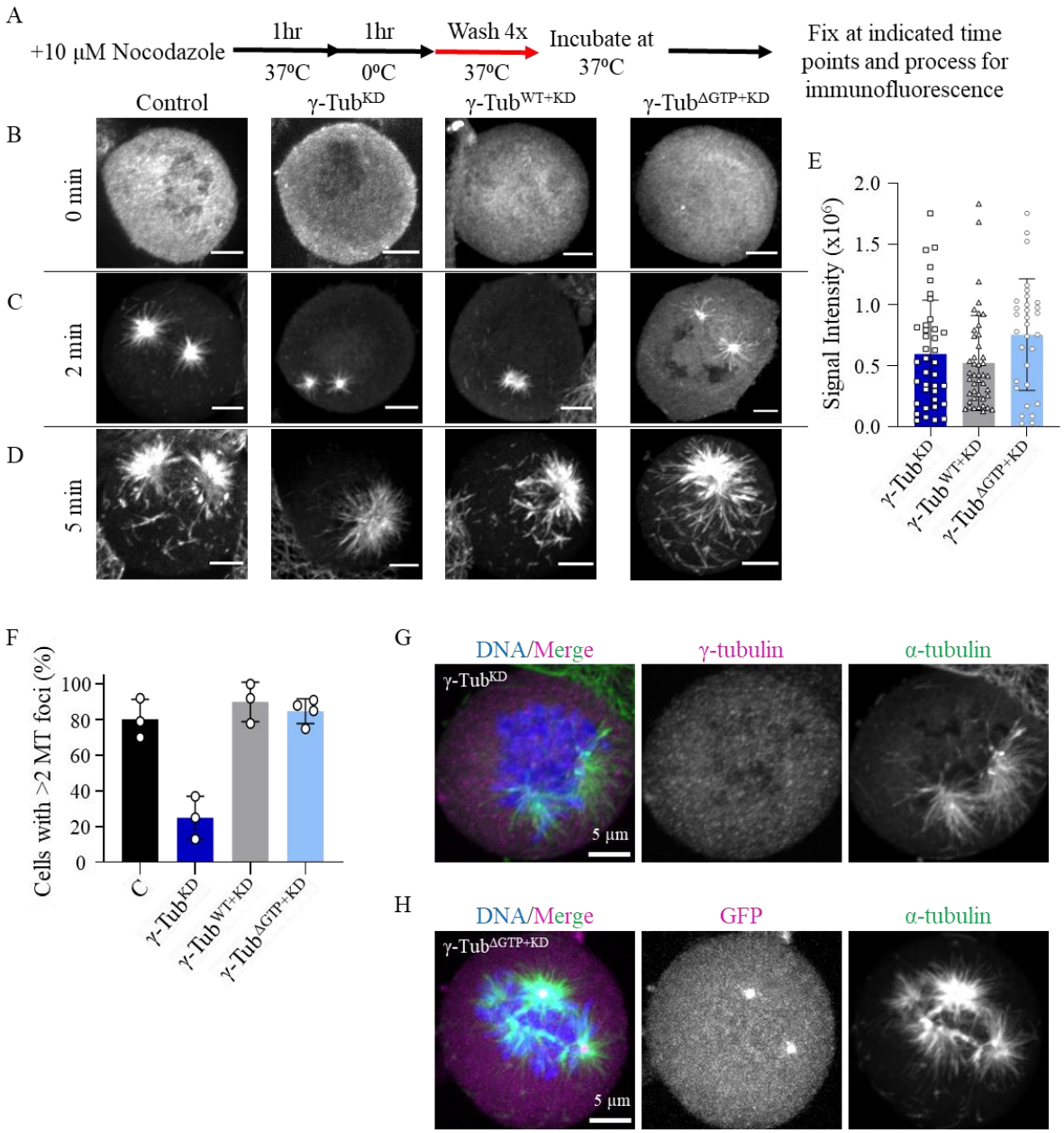
A
+10 µM Nocodazole
1hr
37ºC
1hr
0ºC
Wash 4x
37ºC
Incubate at
37ºC
Fix at indicated time points and process for immunofluorescence
Control
γ-Tub^KD
γ-Tub^WT+KD
γ-Tub^ΔGTP+KD
B
0 min
C
2 min
D
5 min
E
Signal Intensity (x10^6)
2.0
1.5
1.0
0.5
0.0
γ-Tub^KD
γ-Tub^WT+KD
γ-Tub^ΔGTP+KD
F
Cells with >2 MT foci (%)
100
80
60
40
20
0
C
γ-Tub^KD
γ-Tub^WT+KD
γ-Tub^ΔGTP+KD
G
DNA/Merge
γ-tubulin
α-tubulin
γ-Tub^KD
5 µm
H
DNA/Merge
GFP
α-tubulin
γ-Tub^ΔGTP+KD
5 µm

Figure 2.9 γ-tubulin$^{\Delta GTP+KD}$ cells display non-centrosomal microtubule formation

(A) Schematic of fixed cell microtubule regrowth assay. Cells were fixed at the indicated time points and processed for immunofluorescence (B-D) Images of fixed mitotic cells at 0 (B), 2 (C), and 5 (D) minutes post-nocodazole washout. Single-channel images (maximum-intensity projections) of α-tubulin are shown. (E) Quantification of the mean microtubules fluorescent signal at 2 minutes post-nocodazole washout in the indicated cell lines. n= >30 cells per condition from N=3 independent experiments. (F) Quantification of the mean percentage of mitotic cells that display >2 microtubule foci at 5 minutes post-nocodazole washout. n=>45 cells per condition from N≥ 3 independent experiments. (G and H) Images of fixed mitotic γ-tubulin^{KD} and γ-tubulin$^{\Delta GTP+KD}$ cells 5 minutes post-nocodazole washout. Single-channel images (maximum-intensity projections) and overlays show γ-tubulin (immunofluorescence; G) or GFP (native signal; H; magenta), α-tubulin (green), and DNA (blue). Scale bars=5 μm. Error bars= standard deviation (E and F).

2.3.5. Microtubule regrowth assays in live cells show non-centrosomal microtubule foci formation and coalescence

We next repeated the microtubule regrowth assay in live cells to further characterize the course of microtubule foci formation and to exclude the possibility that the multiple sites of microtubule growth stemmed from the fragmentation of one or two sites of growth (Fig. 2.10 A). In order to avoid further modification of the γ-tubulin cell lines, we utilized the microtubule stain SiR-Tubulin (Lukinavičius et al. 2014). We found that microtubule foci became visible at 5-10 minutes following the exchange to warm media (Fig. 2.10A-F). This delay relative to the fixed cell assay may be, in part, due to dim SiR-Tubulin labeling of newly formed microtubules (David et al. 2019). Additionally, Z-stacks were acquired as the microtubule foci were dynamic within the cell cytoplasm. The number of Z-planes was limited in order to minimize phototoxicity; consequently, one of the two centrosomes, identified as bright GFP puncta in cells expressing GFP-tagged γ-tubulin, was sometimes outside of the Z-planes acquired at certain time points (Fig. 2.10 D).

In γ-tubulin^{KD} cells, SiR-Tubulin-labeled microtubules appeared at predominantly two foci, consistent with our fixed cell experiments (Fig. 2.10 B). In contrast, cells expressing addback of γ-tubulin^{WT}-GFP displayed several microtubule foci throughout the cytoplasm (Fig. 2.10 C and D). Non-centrosomal sites could be discerned, as the centrosomes were marked by bright GFP puncta (Fig. 2.10 D). As in our fixed cell analysis, γ-tubulin$^{\Delta GTP+KD}$ also displayed several microtubule foci at sites other than the centrosomes (Fig. 2.10 E and F). In γ-tubulin^{KD} cells, the number of microtubule foci ranged from 1-4 at 10 minutes (total mean= 2 ± 1, n=18 total cells from N=2 independent experiments; Fig. 2.10 G), as quantified using the methods depicted in figure 2.11. In contrast, the number of foci in γ-tubulin^{WT+KD} cells ranged from 3-10 (total mean=7 ± 2, n=13 total cells from

N=3 independent experiments; Fig. 2.10 G and 2.11), and in γ-tubulin$^{\Delta GTP+KD}$ cells from 2-9 (total mean=6 ± 2, n=23 total cells from N=3 independent experiments; 2.10 G and 2.11. In both γ-tubulin^{WT+KD} and γ-tubulin$^{\Delta GTP+KD}$ cells, centrosomal and non-centrosomal foci grew brighter as time progressed. As the signal intensity of these foci increased, they also began to coalesce (Fig. 2.10 C-F). Together, these data suggest that addback of nucleotide-binding deficient γ-tubulin, in dividing cells lacking endogenous γ-tubulin, leads to microtubule foci formation at non-centrosomal sites.

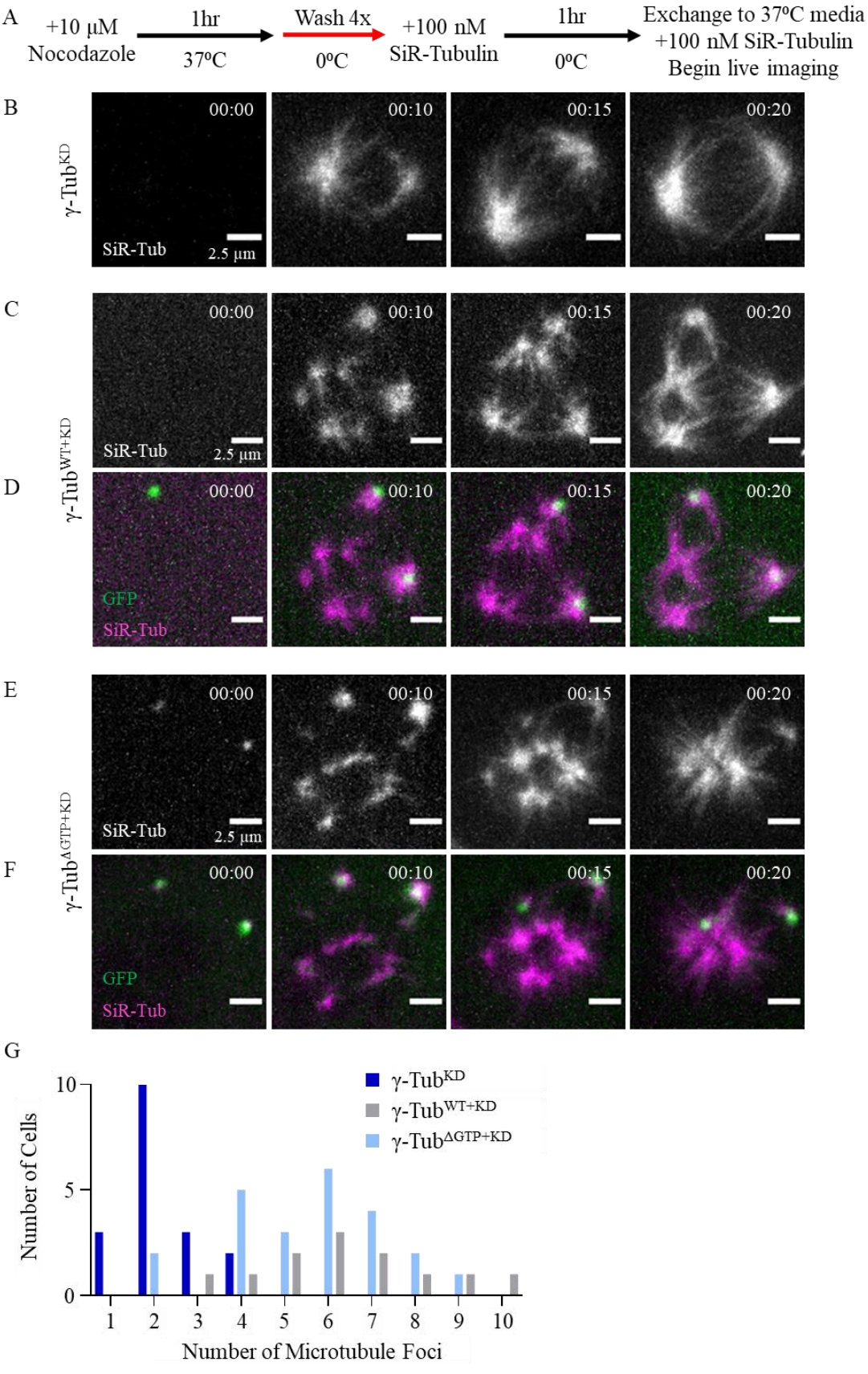
A
+10 µM Nocodazole
1hr
37ºC
Wash 4x
0ºC
+100 nM SiR-Tubulin
1hr
0ºC
Exchange to 37ºC media
+100 nM SiR-Tubulin
Begin live imaging
B
γ-Tub^KD
C
γ-Tub^WT+KD
D
γ-Tub^WT+KD
E
γ-Tub^ΔGTP+KD
F
γ-Tub^ΔGTP+KD
00:00
00:10
00:15
00:20
SiR-Tub
2.5 µm
GFP
SiR-Tub
G
γ-Tub^KD
γ-Tub^WT+KD
γ-Tub^ΔGTP+KD
Number of Cells
Number of Microtubule Foci
0
5
10
1
2
3
4
5
6
7
8
9
10

Figure 2.10 Microtubule foci formation and coalescence in live γ-tubulin$^{\Delta GTP+KD}$ cells

(A) Schematic of the live cell microtubule regrowth assay. (B-F) Live imaging of microtubule regrowth assay by spinning disc confocal microscopy in γ-tubulin^{KD} (B; no GFP signal), γ-tubulin^{WT+KD} (C and D), and γ-tubulin$^{\Delta GTP+KD}$ (E and F) cells. Maximum-intensity projections at individual time points are shown. Timestamps= hh:mm. Single-channel images (B, C, E) show SiR-Tubulin-labeled microtubules. Overlays (D and F) show GFP-tagged γ-tubulin (green) and SiR-Tubulin-labeled microtubules (magenta). Scale bar=2.5 μm. (G) Quantification of the number of microtubule foci in γ-tubulin^{KD} (dark blue bars, n=18 total cells from N=2 independent experiments), γ-tubulin^{WT+KD} (gray bars, n=13 total cells from N=3 independent experiments), and γ-tubulin$^{\Delta GTP+KD}$ (light blue bars, n=23 total cells from N=3 independent experiments) cells.

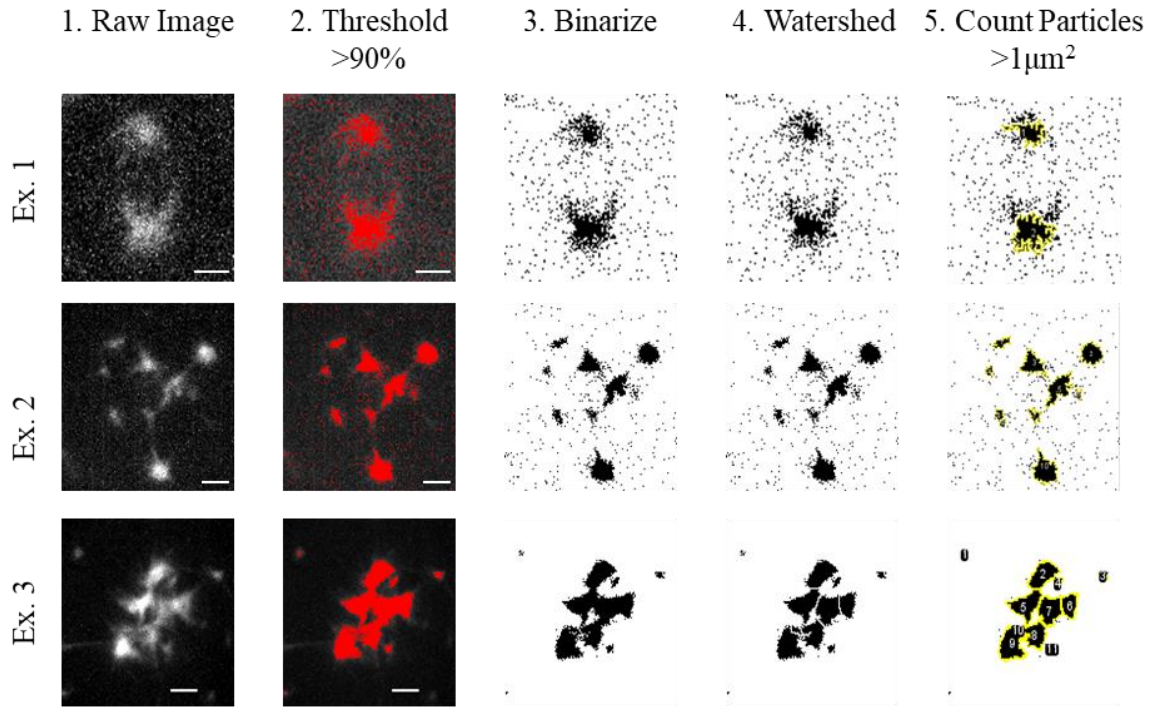

Figure 2.11 Analysis of live cell microtubule regrowth assays

Examples demonstrating the workflow for counting the number of microtubule foci. 1. The raw images were compiled as maximum intensity projections. 2. A signal intensity threshold of >90% was applied. 3. The image was binarized. 4. The signal was segmented using the Watershed plugin in FIJI. 5. Any particles greater than 1 µm2 were counted using the Analyze Particles tool in FIJI. Example 1 illustrates this workflow in a γ-tubulin^{KD} cell. Examples 2 and 3 illustrate this workflow in γ-tubulin^{WT+KD} and γ-tubulin$^{\Delta GTP+KD}$ cells where the foci were either small and dispersed (Example 2), or large and clustered together (Example 3). Scale bar=2.5 µm.

2.4 Discussion

In summary, our studies characterize the γ-TuRC's capping activity in biochemical assays and cellular contexts. In light of our in vitro findings that the γ-TuRC$^{\gamma\text{-TubΔGTP}}$ does not nucleate microtubules, but can cap microtubule minus-ends, we propose that nucleotide-binding deficient γ-tubulin promotes the formation of non-centrosomal microtubules in dividing cells through its capping activity. These microtubules are likely nucleated through pathways within the spindle or at kinetochores that may involve proteins such as TPX2 and CLASP1, which have been implicated to nucleate non-centrosomal microtubules during mitosis in the absence of γ-tubulin (Renda et al. 2022; Tsuchiya and Goshima 2021; Gruss et al. 2002).

We suggest a model where γ-TuRC's capping activity can suppress minus-end dynamics and mediate transport and organization within the bipolar spindle (Fig. 2.12). Interestingly, the turnover of individual non-centrosomal spindle microtubules has been found to be on a similar 1 minute time scale as our measured residence times for γ-TuRC capping of dynamic microtubules (Needleman et al. 2009). Additionally, fluorescently tagged γ-tubulin molecules have been found to interact transiently within the spindle, and to traverse the length of the half spindle (5-10 μm) within ~2 minutes (Lecland and Lüders 2014; Hallen et al. 2008). Furthermore, the γ-TuRC has been shown to interact with dynein, a minus-end directed motor protein that contributes to the organization of microtubules at the spindle poles, whose motility in the spindle is on the order of 2-6 μm per minute (Lecland and Lüders 2014; Young et al. 2000; Heald et al. 1996; Merdes et al. 1996). This model is consistent with our observation that the microtubule foci in γ-tubulin$^{\Delta\text{GTP+KD}}$ cells coalesce over time, which is likely to be a dynein-dependent process (Tulu et al. 2006; Heald et al. 1996).

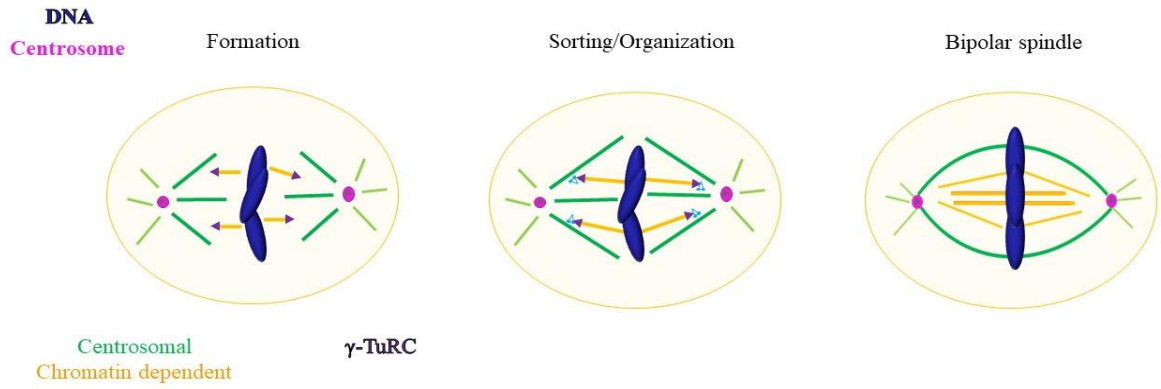

Figure 2.12 Model of the role of the γ-TuRC's capping activity during bipolar spindle formation

Schematic showing the proposed model for the mitotic role of γ-TuRC's capping activity during non-centrosomal microtubule formation. The γ-TuRC cap at newly forming microtubule minus-ends would protect and stabilize these microtubules, and allow for attachment of factors such as motor proteins which would sort and organize these microtubules into the requisite bipolar architecture.

Dissociation of the γ-TuRC from microtubule minus-ends would allow for regulation of microtubule turnover, resumed minus-end dynamics, or the binding of other minus-end associated proteins (Martin and Akhmanova 2018). Interestingly, we and others have found that centrosomal microtubule formation is not as severely affected by the loss of γ-TuRC components (Ramírez Cota et al. 2017; Lüders, Patel, and Stearns 2006; Hannak et al. 2002). This may be partially due to the localization of other minus-end capping proteins such as ASPM and NuMA at spindle poles, or of centriolar and pericentriolar matrix proteins which can mediate different mechanisms of spindle formation (Watanabe

et al. 2020; Baumgart et al. 2019; Woodruff et al. 2017; K. Jiang et al. 2017; Gaglio, Saredi, and Compton 1995).

Our findings that the lifetimes and nucleotide-dependencies differ between γ-TuRC capping of dynamic minus-ends and nucleation of new microtubules suggest that the type of contacts that are formed between γ-tubulin and α,β-tubulin are different during these types of events. As the reported structures of γ-tubulin do not reveal major conformational changes upon different nucleotide-bound states (Rice, Montabana, and Agard 2008; Aldaz et al. 2005), it remains unclear how nucleotide-binding by γ-tubulin can impact γ-TuRC activities. Nonetheless, regulation of γ-tubulin's nucleotide binding state may allow for modulation between long and short capping lifetimes. Interestingly, a recently identified phosphorylation site within the nucleotide-binding pocket of yeast γ-tubulin likely interferes with nucleotide binding, suggesting a potential regulatory mechanism (Brilot et al. 2021). Together, our results suggest a role for the γ-TuRC's capping activity in mitotic spindle assembly, and may have implications for the formation and organization of microtubules in other contexts, such as in non-centrosomal microtubule organizing centers in differentiated cells (Sanchez and Feldman 2017).

Chapter 3: Studies towards further characterization of the γ-TuRC and its cellular activities

Note to readers: The mass spectrometry results discussed below arose from a collaborative effort between myself and Dr. Wenzhu Zhang in the lab of Prof. Brian Chait lab at The Rockefeller University. I have included relevant studies done by Dr. Zhang in the 3.3 Results section as they provide important information regarding my studies. All other data and analyses presented are my own.

3.1 Introduction

Microtubule formation is regulated by a complex containing the tubulin isoform γ-tubulin, referred to as the γ-tubulin ring complex (γ-TuRC). The γ-TuRC allows for cellular control over microtubule polymerization, depolymerization, and localization through its major microtubule-related activities, namely templated nucleation of microtubules, capping of newly nucleated microtubules or of exposed microtubule minus-ends, and anchoring microtubule minus-ends at specific cellular locations, such as at the centrosomes, Golgi, or kinetochores, by interacting with different binding partners (Berman et al. 2023; Wu et al. 2023; Gavilan et al. 2018; Wu et al. 2016; Fong et al. 2008; Efimov et al. 2007; Zimmerman et al. 2004; Wiese and Zheng 2000; Dictenberg et al. 1998; Zheng et al. 1995). The γ-TuRC is an asymmetric, ring-shaped complex composed of seven pairs of γ-tubulin complex proteins (GCPs), of which there are GCP2-6, each respectively bound to γ-tubulin, and in the interior of the ring the N-termini of GCP3 and GCP6 interact with MOZART1 (MZT1) and actin, composing what is referred to as the luminal bridge (Würtz et al. 2022; Wieczorek, Urnavicius, et al. 2020; Wieczorek, Huang, et al. 2020; Consolati et al. 2020; Peng Liu et al. 2019). The complex also contains multiple copies of MOZART2 (MZT2), which binds the exterior of the complex and may play a regulatory role (Würtz et al. 2022; Tovey et al. 2018; Wieczorek, Huang, et al. 2020; Huang et al. 2020; Teixido-Travesa et al. 2010). In *Saccharomyces cerevisiae*, which lack GCP4-6, the

yeast homologs of GCP2 and GCP3, Spc97 and Spc98, respectively, assemble into γ-tubulin small complexes (γ-TuSCs; Oegema et al. 1999). Oligomerization of γ-TuSCs into rings has been observed, promoted by an interacting protein, Spc110 (Kollman et al. 2010). Previous evidence has suggested that these γ-TuSC oligomers are not as active compared to vertebrate γ-TuRCs (Kollman et al. 2010; Gunawardane et al. 2000; Oegema et al. 1999). However, it remains unclear how the complete γ-TuRC structure contributes to its different cellular activities, and if these activities can be performed by partial γ-tubulin-containing complexes.

Similar to γ-TuSC oligomerization, it has been proposed that the γ-TuRC assembles in a modular fashion (Würtz et al. 2022; Haren et al. 2020). Importantly, GCP6, the largest and most diverse of the GCPs, has been shown to act as the scaffolding molecule in this assembly. Cellular γ-TuRCs isolated under varying salt conditions or recombinant γ-TuRC assembly intermediate complexes show that GCP6 maintains a minimal subcomplex with GCP4, and GCP4/5 and GCP2/3 subunits oligomerize onto the GCP4/6 pair until a complete γ-TuRC is formed (Würtz et al. 2022; Haren et al. 2020). Structural data suggests that GCP6 can stabilize the additional GCP subunits through the key contacts it makes throughout the γ-TuRC. GCP6's extended N-terminal domain spans the interior of the ring complex, making contact with GCP2/3 subunits on the opposite half of the ring through what is termed the "belt" domain, and with the components of the luminal bridge through the pair of N-terminal helical domains (NHDs; Wieczorek, Huang, et al. 2020). Truncations of the belt or N-terminal domains have been shown to compromise the structural integrity of the γ-TuRC (Würtz et al. 2022; Haren et al. 2020). However, there is

conflicting evidence on the exact defects that these truncations impart on the γ-TuRC's structure and cellular activities.

One study characterizing the N-terminal 56 residues of GCP6, which compose the first of the pair of NHDs, found that this truncation results in the loss of the actin molecule from the luminal bridge, while the remaining luminal bridge components remain intact (Würtz et al. 2022). *In vitro* microtubule nucleation experiments showed that the nucleation activity of γ-TuRCs incorporating this truncated GCP6 is comparable to WT γ-TuRCs, however cells expressing this GCP6 truncation showed an increase in the length of mitotic progression, and a slight (~10%) decrease in the number of cells with aligned chromosomes (Würtz et al. 2022). However, these changes are not as pronounced relative to further truncations of the N-terminus of GCP6, which cause major structural changes in the γ-TuRC as observed by sucrose gradient sedimentation (Haren et al. 2020). Additionally, it is unclear how N-terminal truncations to GCP6 specifically affect each of the complex's cellular activities, namely nucleation, capping, and anchoring of microtubules.

Changes to the γ-TuRC's structure may alter binding domains where interacting partners may associate to modulate the γ-TuRC's localization and function. Partial γ-tubulin-containing complexes may include a different stoichiometry of GCPs, as evidenced by the finding that the GCP4/6 scaffolding pair can oligomerize with only GCP2/3 subunits, even in the absence of a GCP4/5 subunit (Haren et al. 2020). Therefore, it would be useful to establish methods to examine the γ-TuRC's interacting partners and stoichiometric composition and compare these results to those of partial γ-tubulin-containing complexes. The human γ-TuRC composition and interactome have been previously characterized using mass spectrometry (Wieczorek, Urnavicius, et al. 2020;

Consolati et al. 2020; Teixido-Travesa et al. 2010; Hutchins et al. 2010; Murphy et al. 2001). A recent work studying affinity purified γ-TuRCs from *Xenopus laevis* meiotic egg extracts used label-free quantitation (LFQ) mass spectrometry in addition to cryo-EM to characterize the stoichiometry of each subunit (Peng Liu et al. 2019). Using LFQ mass spectrometry when examining γ-TuRC interacting proteins may be beneficial, as this would indicate whether the identified proteins are interacting with complete γ-TuRCs, or with partial complexes that may be composed of only specific components that are over-represented in the sample being analyzed.

Here, we performed two separate studies towards further characterizing the γ-TuRC's cellular activities. First, we performed a single-step affinity-purification of GFP-tagged γ-tubulin from an asynchronous HeLa cell line. We made efforts towards examining the stoichiometry of core γ-TuRC components using LFQ mass spectrometry. In addition, we identified several potential interactors that co-purified with GFP-tagged γ-tubulin. Future experiments will be necessary to validate and elucidate the interaction of these proteins with γ-tubulin alone, or with the γ-TuRC. Second, we expressed N-terminal truncations of GCP6 in HeLa TREx cells depleted of endogenous GCP6 protein by shRNA, in order to determine how the overall composition and function of the γ-TuRC is affected. Fixed and live-cell microscopy experiments show that a partial γ-tubulin-containing complex composed of GCP6 lacking its NHD and belt domains localizes to interphase, but not mitotic, centrosomes. These experiments lay the foundation for future examination of how the γ-TuRC's structure, composition, and interactors affect its cellular activities.

3.2 Results

3.2.1. Quantitative mass spectrometry analysis of affinity-purified γ-tubulin

To examine the composition of cellular γ-TuRCs, we performed affinity purification followed by quantitative mass spectrometry (Fig. 3.1 A, see methods). For these assays, we used a cell line harboring inducible expression of RNAi-resistant, GFP-tagged γ-tubulin, as well as shRNA targeting endogenous γ-tubulin, as described previously (see Chapter 2). First, cells were grown asynchronously in the presence of doxycycline for 72hrs, after which the cells were harvested and flash frozen as small pellets according to published protocols (LaCava, Jiang, and Rout 2016). Typically, we collected 5g of cell pellets from 1L of adherent cell culture. Next, the cells were disrupted using cryomilling until a fine cell powder was obtained. The cell powder was lysed, and the clarified lysate was incubated with GFP-nanobody conjugated dynabeads. The captured protein was eluted under denaturing conditions (Fig. 3.1 B). The presence of γ-tubulin and several GCPs in the eluate was confirmed via western blot (Fig. 3.1 B and C). Next, the eluted sample was electrophoresed briefly to obtain a single gel plug of the sample (LaCava, Jiang, and Rout 2016). The gel plug was crushed into small pieces, which were then subjected to trypsinization. After proteolysis, the peptides were extracted and analyzed by quantitative mass spectrometry (performed by Dr. Wenzhu Zhang).

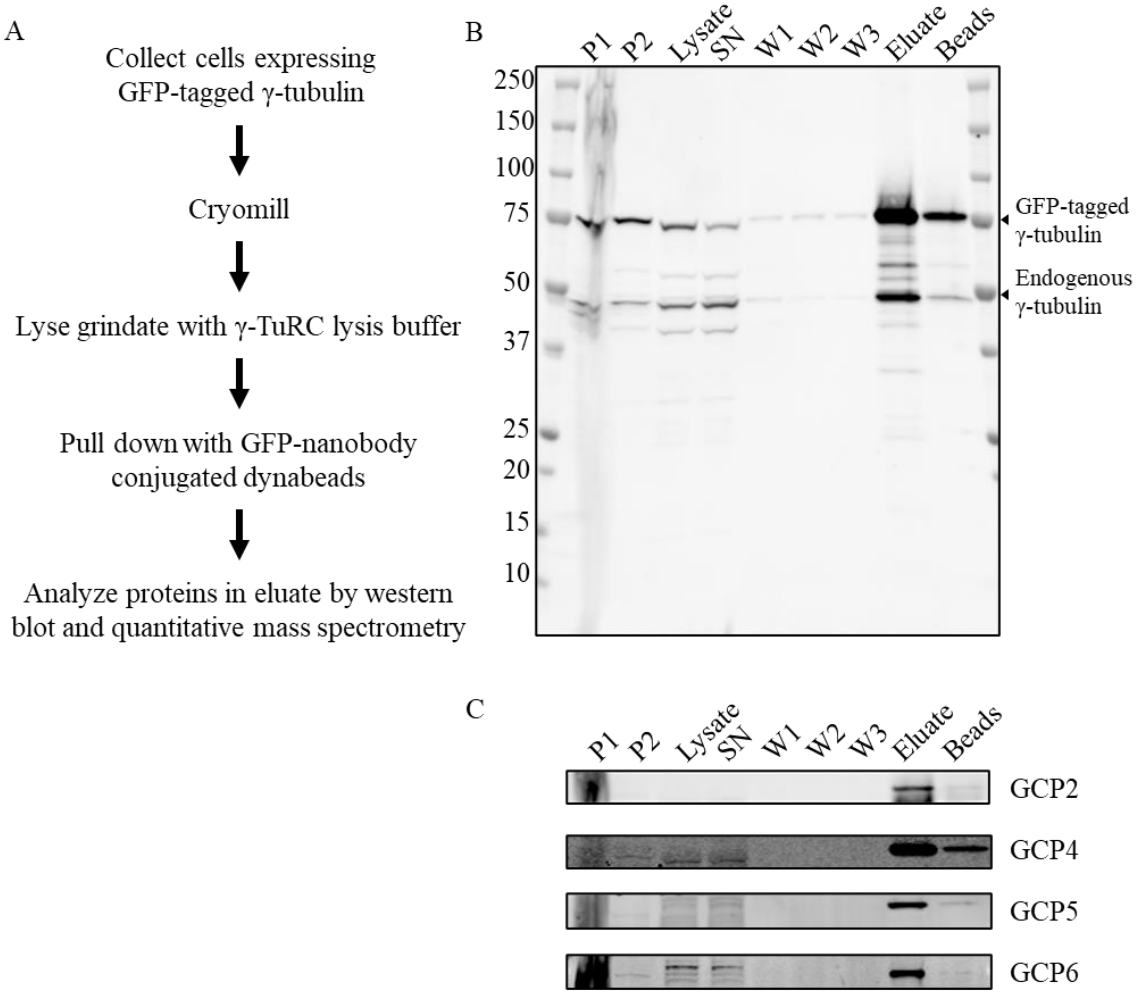

Figure 3.1 Affinity purification of GFP-tagged γ-tubulin

(A) Workflow for affinity purification of GFP-tagged γ-TuRC expressed in HeLa TREx cells. (B) Western blot analysis of samples from each step of the affinity purification protocol, probed with an antibody targeting γ-tubulin. Bands corresponding to GFP-tagged γ-tubulin and endogenous γ-tubulin are indicated. (C) Western blot analysis of samples from each step of the affinity purification protocol, probed with antibodies targeting γ-TuRC components, as indicated.

We performed LFQ mass spectrometry analysis towards characterizing the stoichiometric abundance of individual γ-TuRC components (Table 3.1). We compared the experimental stoichiometries with the expected abundance of each γ-TuRC component based on the known composition of the γ-TuRC (Würtz et al. 2022; Wieczorek, Urnavicius, et al. 2020; Wieczorek, Huang, et al. 2020). The values were derived from four replicates. In one replicate, the cells were treated with nocodazole in order to depolymerize microtubules to account for proteins that may be purified with γ-tubulin indirectly through an interaction with microtubules.

A ~2-fold excess of γ-tubulin was detected in our eluted sample as compared to the known stoichiometry of γ-tubulin in the γ-TuRC (Table 3.1). This may be expected, since γ-tubulin was the target protein in the purification, and as γ-tubulin was overexpressed in these cells. However, more work will be necessary to confirm this hypothesis. Other γ-TuRC components, namely GCP2, GCP3, GCP5, and GCP6, were identified to be present at similar values as the expected stoichiometries. In contrast, however, we quantified a ~4-fold excess of the component GCP4 (Table 3.1). This is consistent with the observation that there is an excess of GCP4 in the HeLa TREx cell line, but it has been proposed that the excess GCP4 protein is not incorporated into the γ-TuRC as it sediments at a lower sucrose density than the remaining γ-TuRC components (Haren et al. 2020; Farache et al. 2016). Future biochemical, structural, and cellular experiments will be necessary to determine if this is the case. Additionally, it would be interesting to examine if GCP4 is expressed in excess of the other γ-TuRC components because it plays a cellular role independent of the complex's major activities. While substoichiometric amounts of MZT1 and MZT2B were quantified, this may reflect the difficulties in identifying these

microproteins (each is expected to be <10kDa). Additionally, the exact stoichiometry of MOZART proteins within the native γ-TuRC complex remains unclear (Würtz et al. 2022; Wieczorek, Huang, et al. 2020), and the stoichiometry of these proteins may be variable depending on the cellular context (Huang et al. 2020; Tovey et al. 2018; Teixido-Travesa et al. 2010).

Table 3.1. LFQ mass spectrometry analysis of γ-TuRC components

Table 3.1 includes data presented in Table 3.2. Listed proteins were identified by affinity purification of GFP-tagged γ-tubulin expressed in HeLa TREx cells. Data is summarized from across 4 replicates. W. Zhang (Chait lab) performed and analyzed these mass spectrometry experiments.

Protein	**Expected abundance**	**Relative abundance (Mean ± SD)**
γ-Tubulin	14	25.23 ± 7.45
GCP2	5	5.69 ± 0.61
GCP3	5	4.52 ± 0.60
GCP4	2	4.59 ± 1.13
GCP5	1	0.68 ± 0.30
GCP6	1	1.11 ± 0.54
MZT1	7 (Würtz et al. 2022)	0.065 ± 0.029
MZT2	>5 (?; TBD)	0.58 ± 0.40

Through our mass spectrometry analysis, we also identified proteins that were isolated with γ-tubulin but are not known components of the γ-TuRC. These are listed in Table 3.2. Some of these proteins, such as LGALS3BP, RuvBL1/2, and the TCP-1 family of proteins are known interactors of the γ-TuRC (Zimmermann et al. 2020; P. Liu, Choi, and Qi 2014; Teixido-Travesa et al. 2010; Brown et al. 1996), while others, such as UBR5 and VCP, have not been previously characterized as γ-tubulin or γ-TuRC interactors but have been suggested to play a role in microtubule regulation (summarized in Table 3.2). More data will be necessary to determine if and how these proteins interact with γ-tubulin, and/or with the γ-TuRC.

Table 3.2 Mass spectrometry analysis of γ-tubulin interacting proteins

The following proteins were identified as interactors of GFP-tagged γ-tubulin following affinity purification. Identified proteins are organized based on their known interactions with I.) the γ-TuRC and the cytoskeleton, II.) their role in protein homeostasis or cell cycle regulation, III.) their localization at the endoplasmic reticulum, golgi, or mitochondria, or IV.) their role in genome maintenance. The protein name, E-value, protein coverage, and the number of unique vs. total peptides are listed. The reported values are from a single replicate. Information regarding the cellular role of the proteins and relevance of the listed proteins to the γ-TuRC, microtubules, or mitosis, is included. The proteins listed were identified in all 4 replicates unless otherwise indicated. W. Zhang (Chait lab) performed the mass spectrometry experiments, and W. Zhang and I analyzed the results together.

Protein	E-Value (log(e))	Cover-age (%)	Peptides (Unique/Total)	Notes and citations
I. γ-TuRC and Cytoskeleton				
γ-Tubulin	-1009.6	91	68/367	γ-TuRC
GCP2	-756.5	74	56/186	γ-TuRC
GCP3	-626.5	72	48/152	γ-TuRC
GCP4	-476.4	81	35/138	γ-TuRC
GCP5	-108	17	10/19	γ-TuRC
GCP6	-218.8	21	21/28	γ-TuRC
MZT2B	-85.7	65	5/22	γ-TuRC
MZT2A	-56.9	27	2/4	γ-TuRC
MZT1	-30.3	70	2/7	γ-TuRC
NME7	-26	12	3/4	A component of the γ-TuRC. Shows autophosphorylation activity that may regulate γ-TuRC functions (P. Liu, Choi, and Qi 2014).
LGALS3BP	-94.9	30	8/14	Role in cell-cell matrix interaction and cell migration. Identified in other γ-TuRC interaction studies, but γ-TuRC related role has not yet been identified (Hutchins et al. 2010; Teixido-Travesa et al. 2010).
RuvBL1	-262.2	64	19/57	AAA ATPase protein chaperone in complex with RuvBL2. Has been implicated in γ-TuRC assembly (Zimmermann et al. 2020). Shown to localize to mitotic centrosomes and play a role in microtubule formation (Fielding et al. 2008; Ducat et al. 2008).
RuvBL2	-266.4	54	22/57	See RuvBL1
β-Actin	-425.2	5	1/17	Recently identified as an integral component of the γ-TuRC (Wieczorek, Urnavicius, et al. 2020; Peng Liu et al. 2019).

γ-Actin	-443	74	27/161	Actin isoform
TCP-1	-468.8	80	32/135	TCP-1 protein chaperone. Participates in the protein folding of α. β, and γ-tubulin. May modulate γ-TuRC assembly and function (Brown et al. 1996; Melki et al. 1993).
CCT2	-471.7	69	31/143	See TCP-1
CCT3	-450.3	74	35/110	See TCP-1
CCT4	-361.2	57	26/90	See TCP-1
CCT5	-394.9	68	31/114	See TCP-1
CCT6A	-372.4	81	31/100	See TCP-1
CCT7	-391.8	69	30/112	See TCP-1
CCT8	-438.5	65	32/109	See TCP-1
MAP7	-305	77	26/73	Microtubule binding protein that enhances the activity of kinesin-1 (Hooikaas et al. 2019).
MAP7D3	-49	9	5/6	Acts redundantly with MAP7 (Hooikaas et al. 2019). *2/4 replicates
NuMA1	-141.9	9	13/14	Microtubule minus-end organizing protein, important for spindle pole formation (Akhmanova and Hoogenraad 2015).
α4A-Tubulin	-334.6	16	4/8	Tubulin
α1B-Tubulin	-346.6	88	26/102	Tubulin
α1C-Tubulin	-265.8	4	1/2	Tubulin
α3E-Tubulin	-227.7	5	1/5	Tubulin
β-Tubulin	-484.4	100	35/198	Tubulin
β3-Tubulin	-304.2	9	3/4	Tubulin
β4B-Tubulin	-477	27	5/29	Tubulin
β6-Tubulin	-226.5	5	1/2	Tubulin
DYNC1H1	-55.2	44	5/7	Dynein heavy chain component of the dynein complex (Reck-Peterson et al. 2018).
DYNLL1	-26.8	60	2/3	Dynein light chain component of the dynein complex (Reck-Peterson et al. 2018).

KIF1C	-42.6	6	5/5	Member of the Kinesin-3 family (Miki, Okada, and Hirokawa 2005). *In 3/4 replicates
KIF20A	-17.4	3	2/3	Member of the Kinesin-6 family. Reported to bind to a RabGTPase and to be involved in cytokinesis (Miki, Okada, and Hirokawa 2005). *In 3/4 replicates
KIF5B	-4.2	2	1/1	Member of the conventional Kinesin-1 family (Miki, Okada, and Hirokawa 2005). *In 3/4 replicates
CEP170	-185.5	54	15/24	A centrosomal protein. Anchors microtubules at the centrosomes (Paz and Lüders 2017).
CEP350	-11.5	1	2/2	A centrosomal protein. Anchors microtubules at the centrosomes (Yan, Habedanck, and Nigg 2006). *In 3/4 replicates
KIAA1967 (aka DBC1, CCAR2)	-388.2	60	30/68	Interacts with centrosomal proteins (Hutchins et al. 2010). May regulate Sirtuins, which play a role in tubulin deacetylation (Nagai et al. 2013).
Plectin	-760.5	19	67/97	Links intermediate filaments with microtubules (Fuchs and Karakesisoglou 2001).
Vimentin	-483.9	83	38/150	Intermediate filaments
Annexin A2	-196.7	55	15/34	Implicated in cortical actin remodeling. Involved in the early stages of cytokinesis and assembly of the acto-myosin ring (Benaud et al. 2015).
Desmoplakin	-175.8	10	19/21	Cytoskeleton. Plays a role in non-centrosomal organization of microtubules in differentiated cells (Lechler and Fuchs 2007).

II. Cell Cycle and Protein Homeostasis				
VCP (aka P97, cdc48)	-217	33	19/36	Master regulator of protein turnover. Plays a role in ciliogenesis (Raman et al. 2015). Regulates localization of Aurora A at centrosomes (Kress et al. 2012) and Aurora B at mitotic chromosomes (Dobrynin et al. 2011). Cells with siRNA targeting VCP show disrupted mitotic spindles (Wojcik, Yano, and DeMartino 2004).
LAP1	-18	3	2/2	Encoded by the *TOR1AIP1* gene. Integral membrane protein of the inner nuclear membrane. Associates with lamin A/C and lamin B1 in the nuclear lamina. Interacts with and activates the AAA-ATPase torsinA (Shin and Worman 2022).
UBR5	-1715	72	122/383	Degrades BuGZ, assisting metaphase-to-anaphase transition (H. Jiang et al. 2015). Promotes ciliogenesis by ubiquitination of the centrosomal and ciliary protein CSPP1 and regulating its cytoplasmic organization (Shearer et al. 2018).
MISP	-215.4	47	17/31	Substrate of PLK1. Plays a role in spindle orientation (M. Zhu et al. 2013).
Ran	-14.5	15	2/2	Nuclear GTPase that regulates chromatin-mediated microtubule nucleation during mitosis. Its GTP-bound form is concentrated around chromosomes during mitosis (Prosser and Pelletier 2017).

RanBP2	-210.7	9	19/23	Component of the Ran signaling pathway that is recruited to kinetochores (Cheeseman and Desai 2008). Phosphorylated by Aurora A, B and PLK1 (Kettenbach et al., n.d.).
RanGAP1	-76.6	17	6/7	Stimulate the GTPase activity of Ran. associates with the spindle and is localized away from the chromosomes (Matunis, Coutavas, and Blobel 1996; Prosser and Pelletier 2017).
CDK1	-21.2	11	3/3	Phosphorylates chromosome passenger complex (CPC) proteins (Lampson and Cheeseman 2011). Also phosphorylates NEDD1 to regulate branched spindle microtubule nucleation (Johmura et al. 2011).
AMBRA1	-199.1	33	17/22	Master regulator of the G1 to S phase transition and genomic integrity via the Cyclin D pathway (Maiani et al. 2021). Tethered to the cytoskeleton via dynein (Di Bartolomeo et al. 2010).
MTA2	-43.4	25	4/4	Part of the metastatic tumor antigen (MTA) family of chromatin modifiers. Part of the nucleosome remodeling and histone deacetylation (NuRD) complex. Shown to localize to the centrosome by interacting with pericentrin (Sillibourne et al. 2007). *In 3/4 replicates

RhoGEF17	-167.3	13	15/19	Identified as an essential mitotic gene in the MitoCheck RNAi screen (Neumann et al. 2010). Targets Mps1 to mitotic kinetochores and regulates SAC functions (Isokane et al. 2016).
RICTOR	-68.5	7	8/10	Regulatory subunit of mTOR complex 2 (Oh and Jacinto 2011).
III. ER, golgi, or mitochondria associated				
CKAP4	-13.5	4	2/2	Anchors the ER to the microtubule cytoskeleton (Klopfenstein, Kappeler, and Hauri 1998).
TECR	-150.9	61	14/33	ER-associated
COPA	-116.8	13	12/14	ER and golgi-associated
DPM1	-109.7	45	10/19	ER-associated
RCN1	-110.9	51	9/19	ER-associated
RCN2	-95.6	40	7/12	ER-associated
Calnexin	-95.4	28	9/12	ER-associated
HSPA8	-480.1	80	36/131	heat shock protein
HSPD1	-323.1	64	25/61	heat shock protein
HSP90AB1	-252.1	45	22/50	heat shock protein
HSPA1A	-241.1	37	13/34	heat shock protein
HSPA9	-230.1	39	18/25	heat shock protein
HSP90AA1	-212.4	16	9/13	heat shock protein
HSPA5	-203.8	34	15/30	heat shock protein
HSP90B1	-149.8	24	13/26	heat shock protein
HSPB1	-139.9	85	10/40	heat shock protein
DNAJA1	-90.5	35	7/15	HSP70 co-chaperone
CPS1	-843.1	66	63/196	mitochondrial
ATAD3A	-461.6	69	34/172	mitochondrial
ATAD3B	-361.1	23	9/28	mitochondrial
SLC25A4	-377.6	17	4/8	mitochondrial
SLC25A3	-287.9	72	23/70	mitochondrial
SLC25A5	-429.7	88	35/123	mitochondrial
SLC25A6	-395	44	12/35	mitochondrial
ATP5A1	-308.7	57	24/67	mitochondrial
ATP5B	-125.5	32	12/25	mitochondrial
ATP5C1	-112.9	58	11/34	mitochondrial

GOT2	-197.3	42	16/34	mitochondrial
LRPPRC	-168.7	15	16/25	mitochondrial
MRPS34	-153.7	70	13/46	mitochondrial
SHMT2	-144.6	42	13/19	mitochondrial
DNAJA3	-119.9	40	10/24	mitochondrial
IV. Genome Maintenance				
MATR3	-330.1	56	26/75	DNA maintenance
AKAP8	-186.7	54	15/24	DNA maintenance
DDB1	-127.4	18	12/18	DNA maintenance
HNRNPM	-925.6	89	65/576	RNA maintenance
INTS6	-413.9	51	33/62	RNA maintenance
DDX41	-332.9	53	28/56	RNA helicase
HELZ	-263.6	20	24/31	RNA helicase
RBM14	-250.1	68	21/43	RNA binding protein
HNRNPU	-244.4	42	21/41	RNA maintenance
HNRNPH1	-243.7	62	16/63	RNA maintenance
DDX5	-206	44	16/41	RNA helicase
PRPF8	-179.7	10	17/20	RNA maintenance
HNRNPF	-170.5	37	10/24	RNA maintenance
DHX9	-155.3	16	14/25	RNA helicase
DDX21	-111.8	24	11/18	RNA helicase. May play a role in chromatin maintenance in mitosis (De Wever et al. 2012).
HNRNPK	-92.1	30	9/12	RNA maintenance
ZNF318	-660.5	40	55/99	Gene expression
PRRC2B	-594.8	44	47/84	Gene expression
GIGYF2	-367.6	47	28/53	Gene expression
PUF60	-284.5	63	21/64	Gene expression
RPL4	-255.2	60	21/54	Gene expression
SF3B2	-248.4	41	21/45	Gene expression
RPS3	-209.3	83	18/58	Gene expression
EEF1A1	-199.6	76	17/46	Transcription factor
EEF2	-182.3	24	17/30	Transcription factor
TRIM28	-169.8	44	14/26	Gene expression. Interacts with the NDC80 complex (Hutchins et al. 2010).
RPS5	-167.4	65	12/69	Gene expression
RPLP0	-165	60	13/28	Gene expression

RPS4X	-141.1	64	13/27	Gene expression
YBX1	-128.1	82	9/13	Gene expression
RPL6	-114.4	54	10/26	Gene expression
RPL7	-102.4	60	11/24	Gene expression

Optimization of the affinity-purification methods may result in more direct identification of relevant interactors. Additionally, synchronizing the cell cycle before harvesting may improve the detection of low-abundance interactions. Future work will be needed to determine if these protein interactors play roles in microtubule formation, cytoskeletal regulation, or largely within cell division.

3.2.2 N-terminal truncations of GCP6 result in partial γ-tubulin-containing complexes

Separately, we sought to examine how changes to the overall γ-TuRC structure may affect the cellular functions of the complex. To this end, we focused on the γ-TuRC component GCP6, as this component has been identified to serve as the scaffolding unit of the complex around which the other GCP proteins can bind and assemble into larger ring-shaped structures (Haren et al. 2020). GCP6 is the largest and most divergent of the GCPs in terms of its structure (Wieczorek, Urnavicius, et al. 2020; Wieczorek, Huang, et al. 2020; Murphy et al. 2001; Gunawardane et al. 2000). While it contains the GRIP1 and GRIP2 domains that typify the GCP family of proteins, it also contains an extended insert (residues ~608-1474) whose role is not well understood (Haren et al. 2020; Wieczorek, Urnavicius, et al. 2020; Murphy et al. 2001). Additionally, the N-terminal residues (~1-351) preceding the GRIP1 domain contains two N-terminal domains that extend through the lumen of the γ-TuRC, and make key contacts throughout the interior of the complex (Wieczorek, Huang,

et al. 2020). First, residues ~1-120 form two helical domains (hereafter referred to as the NHD) which bind MZT1 and contact the actin molecule within the luminal bridge (Figure 3.2 A-C). Second, residues ~120-250 form an α-helix termed the GCP6 "belt" that contacts the luminal surface of the GCP2 and 3 molecules residing at positions 3-6 (Fig. 3.2A-C).

Previous work suggests that these domains maintain the structural integrity of the ring-shaped complex (Würtz et al. 2022; Haren et al. 2020). Thus, truncating the NHD or the belt domains of GCP6 would lead to the loss of key contacts within the γ-TuRC and result in partial complexes. Based on known structural and biochemical data, we hypothesized that truncating the NHD of GCP6 (residues 1-120; hereafter referred to as ΔNHD) would result in the removal of the luminal bridge, leading to the loss of γ-TuRC subunits 1, 2, 13, and 14 which come in contact with it (Fig. 3.2 D). Further truncating the N-terminus of GCP6 to remove both the NHD and the belt domains (residues 1-250; hereafter referred to as ΔN-Belt) would remove the key contacts maintaining the structural stability of γ-TuRC subunits 3, 4, 5, and 6, possibly resulting in a further reduced partial γ-tubulin-containing complex (Fig. 3.2 E). Interestingly, the core γ-TuRC subunits 7-12, composed of an oligomer of GCP2-GCP3-GCP4-GCP5-GCP4-GCP6, have been observed to be the most stable γ-TuRC assembly intermediate (Würtz et al. 2022; Haren et al. 2020).

To test this, we aimed to express these GCP6 truncations in cells. First, we established a cell line which, upon doxycycline induction, expressed shRNA targeting endogenous GCP6 (Fig 3.2 F, hereafter shGCP6). Next, a construct with doxycycline-inducible expression of C-terminally GFP-tagged GCP6 was introduced to the shGCP6 cell line. Three cell lines were generated, each expressing either WT, ΔNHD, or ΔN-Belt constructs of GFP-tagged GCP6 (hereafter $GCP6^{FL}$, $GCP6^{\Delta NHD}$, and $GCP6^{\Delta N\text{-}Belt}$,

respectively; Fig. 3.2 F). Western blot analysis showed a slight downward shift in the signal for GCP6 in each of these cell lines, consistent with a decrease in GCP6 molecular weight (Fig. 3.2 F). In order to examine the approximate size of the γ-tubulin-containing complexes in these cell lines, we incubated cell lysates from each of these cell lines with beads conjugated to GFP-nanobody and performed an affinity purification. The eluted samples were analyzed using sucrose gradient sedimentation, followed by western blot. In the $GCP6^{FL}$ cell line, the peak signal for γ-tubulin was observed at fraction 8 (Fig. 3.2 F and G). In contrast, in the $GCP6^{\Delta NHD}$ and $GCP6^{\Delta N\text{-}Belt}$ cell lines, the peak signal for γ-tubulin was observed at fraction 6 and 4, respectively, consistent with the incorporation of γ-tubulin into smaller partial complexes (Fig. 3.2 F and G). Together, these data indicate that truncations of the NHD and belt domains of GCP6 result in partial γ-tubulin-containing complexes in cells, as has been observed previously (Würtz et al. 2022; Haren et al. 2020).

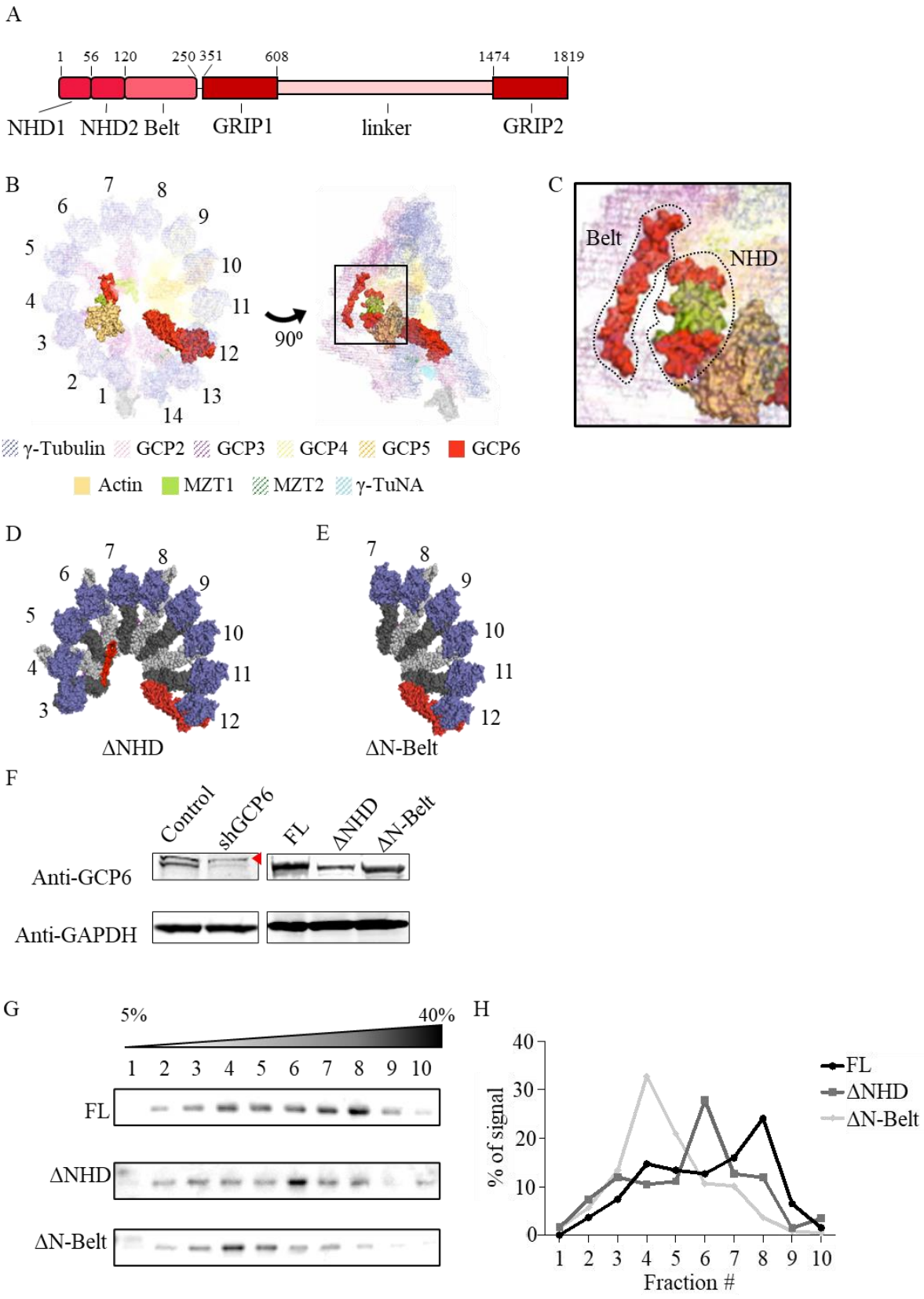
A
1 56 120 250 351 608 1474 1819
NHD1 NHD2 Belt GRIP1 linker GRIP2
B
90º
γ-Tubulin GCP2 GCP3 GCP4 GCP5 GCP6
Actin MZT1 MZT2 γ-TuNA
C
Belt
NHD
D
ΔNHD
E
ΔN-Belt
F
Control shGCP6 FL ΔNHD ΔN-Belt
Anti-GCP6
Anti-GAPDH
G
5% 40%
1 2 3 4 5 6 7 8 9 10
FL
ΔNHD
ΔN-Belt
H
% of signal
Fraction #
FL
ΔNHD
ΔN-Belt

Figure 3.2 N-terminal truncations of GCP6 result in partial γ-tubulin-containing complexes

(A) Schematic of the domain architecture of GCP6, with key residues indicated. (B) A 3D reconstruction of the native γ-TuRC shown in two different views with the position of each GCP subunit indicated, adapted from Wieczorek, Urnavicius, et al. 2020. All components besides for GCP6 are shown with a mesh overlay to highlight the extension of GCP6 (solid red) through the complex. The dashed box surrounds the NHD and belt domains of GCP6. (C) A zoomed in view of the NHD and belt domains of GCP6 and their contacts within the lumen of the γ-TuRC. (D and E) Hypothesized architectures of the ΔNHD and ΔN-Belt complexes with the truncated versions of GCP6 (red). The other GCP subunits are shown in gray-scale as the identity of the subunits at the indicated positions may vary from those in the native architectures. (F) Western blot analysis of cell lysates. Bands corresponding to GCP6 and GAPDH are indicated. A non-specific band recognized by the antibody targeting GCP6 is indicated (red arrow). (G) Analysis of GFP-nanobody affinity purified samples for $GCP6^{FL}$, $GCP6^{\Delta NHD}$, and $GCP6^{\Delta N\text{-}Belt}$ cell lines using sucrose gradient centrifugation. Western blot probing for γ-tubulin is shown. (H) Quantification of the γ-tubulin signal in each sucrose gradient fraction (%signal= signal in individual fraction/ sum of the signal in all ten fractions).

3.2.3 GCP6$^{\Delta NHD}$ cells from bipolar spindles, but spindles in GCP6$^{\Delta N\text{-}Belt}$ cells are disrupted

We next examined how the cellular expression of NHD and N-Belt truncated GCP6 constructs, in addition to depletion of endogenous GCP6 via shRNA, affects the mitotic phenotype. We found that compared to the mitotic index of uninduced control cells (5 ± 2%, n=2,884 total cells, from N=3 independent experiments; Fig. 3.3 A), the mitotic index was increased in shGCP6 cells (15 ± 5%, n=290 total cells, from N=2 independent experiments; Fig 3.3 A), indicating that loss of GCP6 causes mitotic arrest, as reported previously (Haren et al. 2020; Ramírez Cota et al. 2017; Bahtz et al. 2012). Furthermore, mitotic cells with GCP6 knockdown displayed a higher percentage of disrupted spindles (78 ± 13%, n=60 total cells, from N=3 independent experiments; Fig. 3.3 B and C), as compared to uninduced controls (6 ± 1%, n=32 total cells, from N=2 independent experiments; Fig 3.3 B and C). Consistently, GCP6^{FL} cells showed a reduced mitotic index (3%, n=2,171 total cells, from N=2 independent experiments; Fig. 3.3 A) and rescue of spindle bipolarity (19 ± 5% of n=49 total cells were disrupted, from N=3 independent experiments; Fig. 3.3 B and C). The GCP6$^{\Delta NHD}$ cell line also displayed a low mitotic index (4%, n=1932 total cells from N=2 independent experiments) and formed bipolar spindles (19 ± 6% of n=45 total cells were disrupted, from N=2 independent experiments), despite these cells harboring an incomplete γ-TuRC. This is in contrast to a recently published study which observed an increase in mitotic defects in a cell line expressing GCP6 truncated of the first of the two NHDs (Würtz et al. 2022). More detailed experimental characterization of the GCP6$^{\Delta NHD}$ cell line will be necessary reveal any subtle phenotypes.

However, GCP6$^{\Delta N\text{-}Belt}$ cells appeared similar to the shGCP6 cell line, with an increased mitotic index (16 ± 1%, n=935 total cells, from N=3 independent experiments;

Fig. 3.3 A) and a high percentage of cells displaying disrupted mitotic spindles (81 ± 1%, n=46 total cells, from N=3 independent experiments; Fig. 3.3 B and C), suggesting that the partial γ-tubulin-containing complex in these cells is not sufficient for sustaining bipolar spindle formation. Furthermore, centrosomal γ-tubulin signal was visible in the $GCP6^{FL}$ and $GCP6^{\Delta NHD}$ cell lines but was not observed in $GCP6^{\Delta N\text{-}Belt}$ mitotic cells (Fig. 3.3 C). Imaging of live cells showed that the GFP signal of the GCP6 constructs was also localized to mitotic centrosomes in the $GCP6^{FL}$ and $GCP6^{\Delta NHD}$ cell lines, but not in $GCP6^{\Delta N\text{-}Belt}$ cells (Fig. 3.3 D).

Overall, these data suggest that a minimal γ-tubulin-containing complex is required for cells to assemble microtubules into the bipolar spindle, localize γ-tubulin and related proteins to the centrosomes, and progress through cell division. While the partial γ-tubulin-containing complex present in $GCP6^{\Delta NHD}$ cells is seemingly sufficient for these processes, the smaller partial complex assembled in $GCP6^{\Delta N\text{-}Belt}$ cells is not.

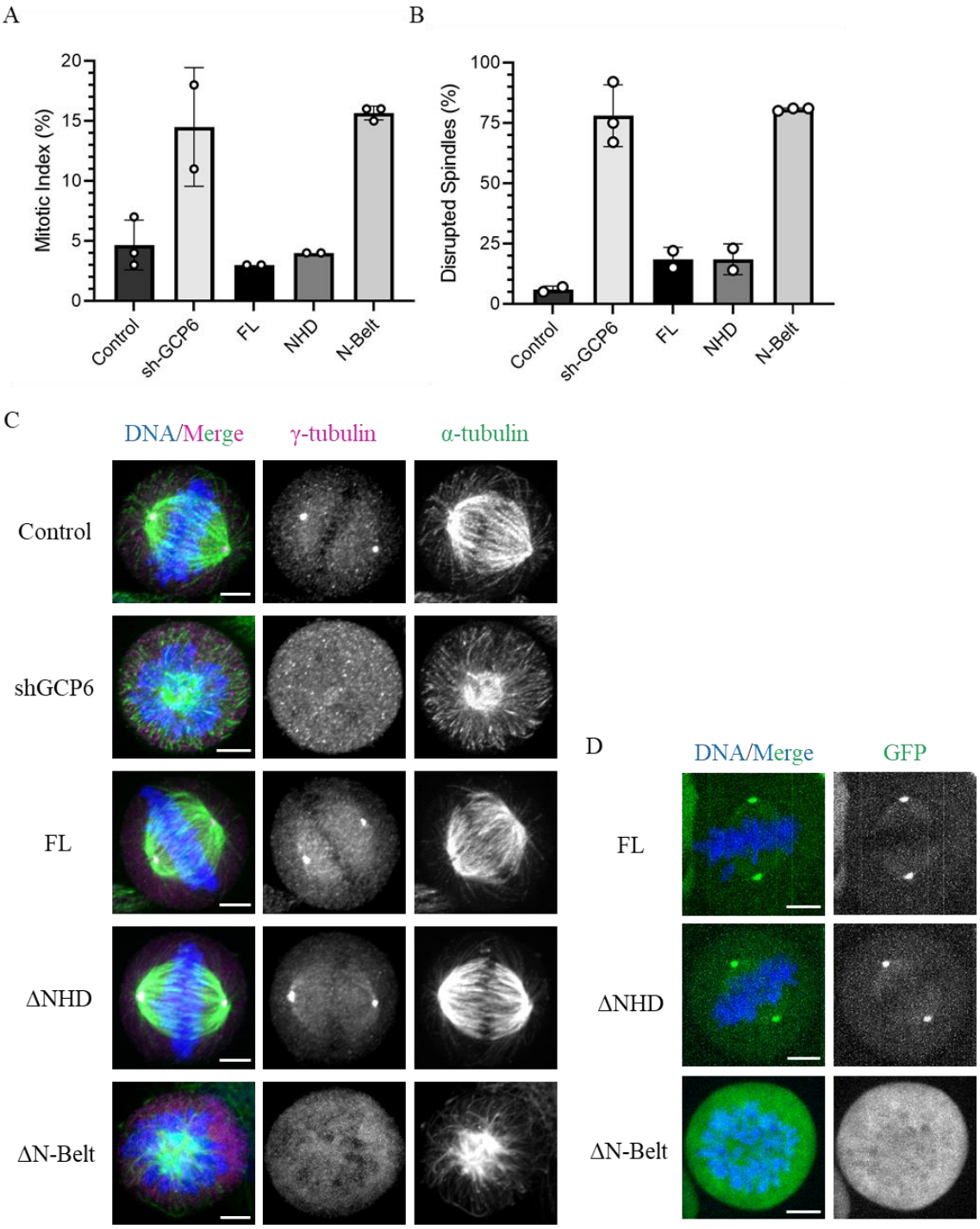
A
Mitotic Index (%)
20
15
10
5
0
Control
sh-GCP6
FL
NHD
N-Belt
B
Disrupted Spindles (%)
100
75
50
25
0
Control
sh-GCP6
FL
NHD
N-Belt
C
DNA/Merge
γ-tubulin
α-tubulin
Control
shGCP6
FL
ΔNHD
ΔN-Belt
D
DNA/Merge
GFP
FL
ΔNHD
ΔN-Belt

Figure 3.3 GCP6$^{\Delta NHD}$ cells form bipolar mitotic spindles, while GCP6$^{\Delta N\text{-}Belt}$ cells form disrupted spindles and are arrested in mitosis

(A) Analysis of the mean mitotic index. n=>300 cells per condition from N=2-3 independent experiments. (B) The mean percentage of mitotic cells that displayed disrupted spindles. n=>30 cells per condition from N=2-3 independent experiments. (C) Images of fixed mitotic uninduced control, shGCP, GCP6^{FL}, GCP6$^{\Delta NHD}$, and GCP6$^{\Delta N\text{-}Belt}$ cells. Single-channel images (maximum-intensity projections) and overlays show γ-tubulin (magenta), α-tubulin (green), and DNA (blue). (D) images of live mitotic GCP6^{FL}, GCP6$^{\Delta NHD}$, and GCP6$^{\Delta N\text{-}Belt}$ cells. Single-channel images (maximum-intensity projections) and overlays show GFP (green), and DNA (blue).

3.2.4 GCP6$^{\Delta N\text{-}Belt}$ cells show interphase γ-tubulin and GCP6 localization, which is lost upon entry into mitosis

While we did not observe γ-tubulin signal at the centrosomes in mitotic GCP6$^{\Delta N\text{-}Belt}$ cells, γ-tubulin signal remained at the centrosomes of interphase GCP6$^{\Delta N\text{-}Belt}$ cells (Fig. 3.4 A). In contrast, shGCP6 cells did not show centrosomal localization of γ-tubulin (Fig. 3.4 A). To further investigate this, we performed live cell imaging to assess the centrosomal localization of GFP-tagged GCP6-ΔN-Belt. Similar to the γ-tubulin signal, GFP signal was observed at interphase centrosomes (Fig. 3.4 B and C), but not in mitotic cells as shown previously (Fig. 3.3 D).

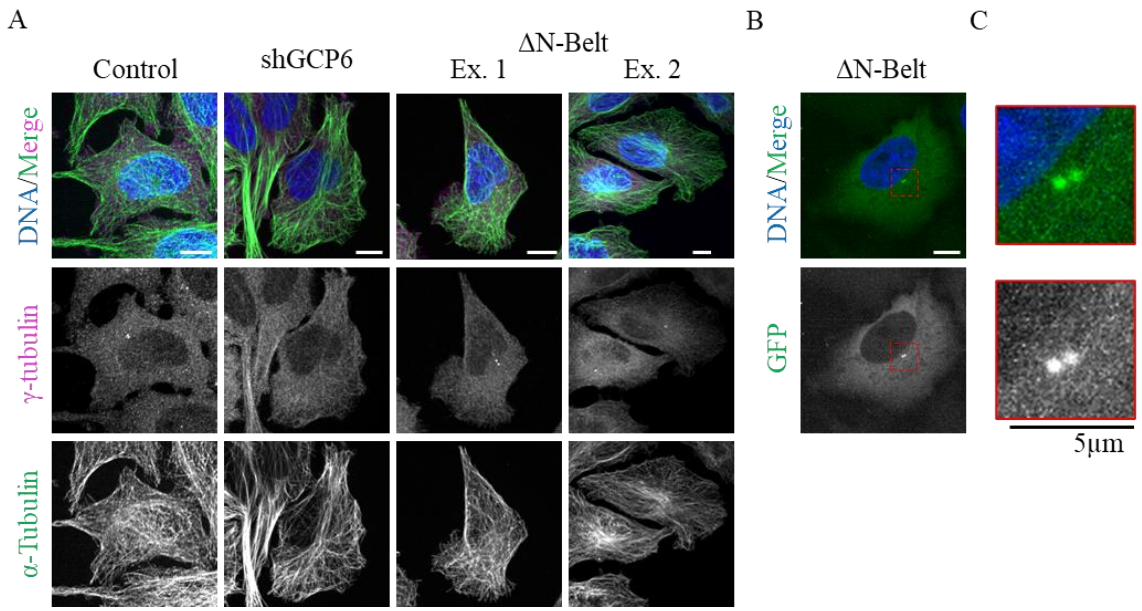

Figure 3.4 γ-tubulin localizes to interphase centrosomes in GCP6$^{\Delta N\text{-}Belt}$ cells, but not shGCP6 cells

(A) Images of fixed interphase uninduced control, shGCP, and GCP6$^{\Delta N\text{-}Belt}$ cells. Single-channel images (maximum-intensity projections) and overlays show γ-tubulin (magenta), α-tubulin (green), and DNA (blue). (B) Images of live interphase GCP6$^{\Delta N\text{-}Belt}$ cells. Single-channel images (maximum-intensity projections) and overlays show GFP (green), and DNA (blue). (C) Zoom-in view of centrosome localized GFP signal shown in B. Single-channel images (maximum-intensity projections) and overlays show GFP (green), and DNA (blue).

We next asked how the centrosomal GFP signal changes as GCP6$^{\Delta N\text{-Belt}}$ cells transition from interphase to mitosis. We performed live cell imaging of GCP6^{FL} or GCP6$^{\Delta N\text{-Belt}}$ cells and tracked the centrosomal GFP signal in prophase cells as they transitioned to metaphase. In GCP6^{FL} cells, the GFP signal was observed to accumulate at the centrosomes which at first appeared in close proximity to each other (Fig. 3.5 A). As time progressed, the centrosomes moved further from each other, and were ultimately positioned at opposite poles of the cell while the DNA congressed at the metaphase plate (Fig. 3.5 A). In GCP6$^{\Delta N\text{-Belt}}$ cells, the GFP signal was initially observed at the centrosomes, which like the initial time points in GCP6^{FL} cells, were in close proximity to each other (Fig. 3.5 B). As the cell progressed into mitosis, however, the centrosomes were not able to separate from each other, and eventually the GFP signal decreased until it was no longer detected. The DNA remained disorganized, and the cell remained in mitotic arrest throughout the course of the experiment (>1 hour) (Fig. 3.5 B).

Together, these data suggest that GCP6-ΔN-Belt can be localized to interphase, but not mitotic, centrosomes. As γ-tubulin localized to interphase centrosomes in the presence of GCP6-ΔN-Belt, but not in the absence of GCP6, as in the shGCP6 condition, these data are consistent with GCP6-ΔN-Belt forming a γ-tubulin-containing complex that may have interphase-specific functions that are lost upon cellular entry into mitosis.

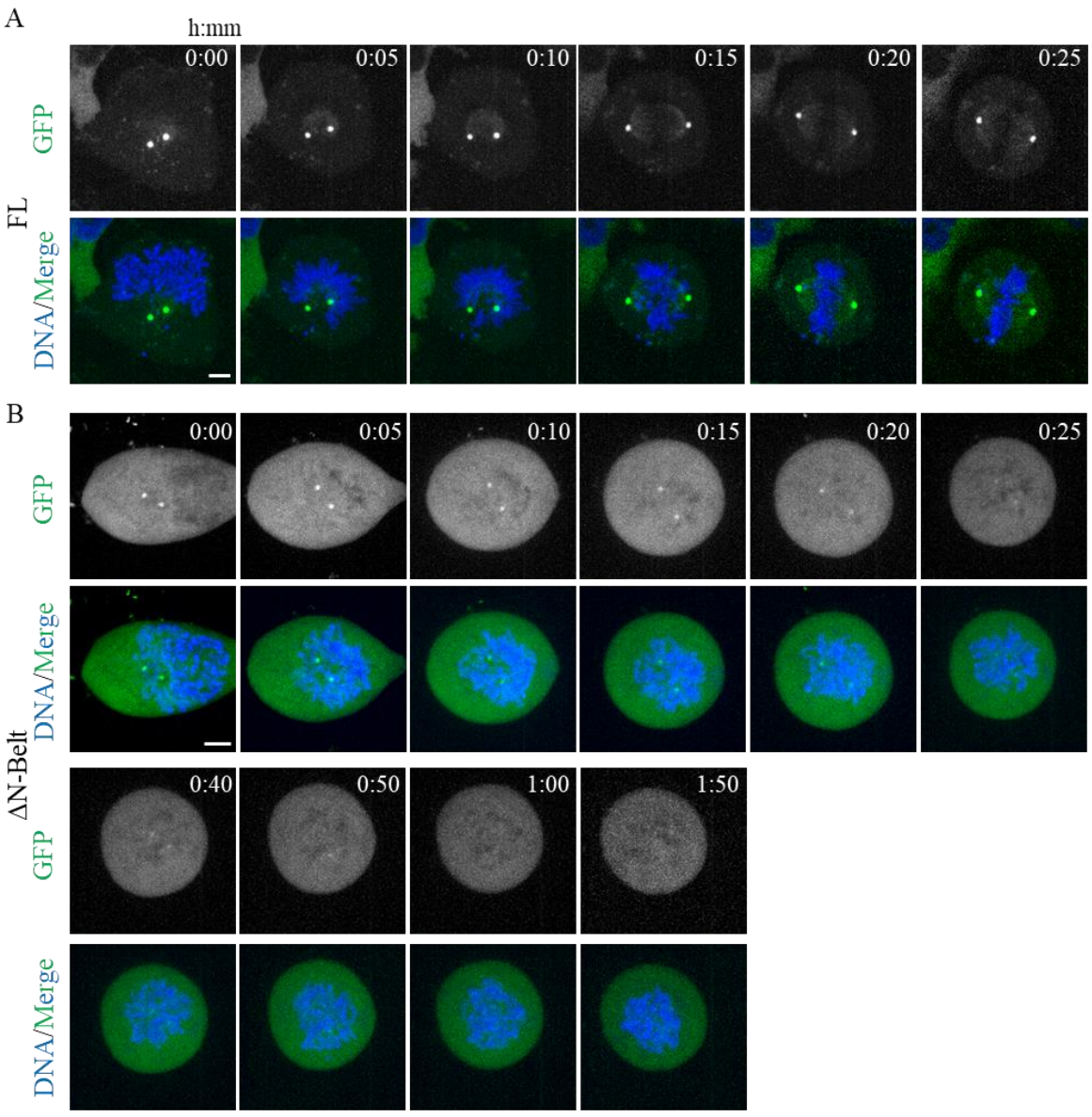

Figure 3.5 GFP-tagged GCP6-ΔN-Belt is lost from centrosomes as the cell transitions from interphase into mitosis

(A and B) Time-lapse images of live interphase $GCP6^{FL}$ (A) and $GCP6^{\Delta N\text{-}Belt}$ (B) cells. Single-channel images (maximum-intensity projections) and overlays show GFP (green), and DNA (blue). Scale bar = 5µm. Time stamps = h:mm.

3.3 Discussion

Our mass spectrometry experiments lay the foundations for characterizing several known and potentially new γ-TuRC interactors that play a role in different biological processes including cytoskeletal dynamics, cell division, protein homeostasis, and gene expression. There are several known γ-TuRC interacting proteins that are missing from our results, such as Nedd1 and Augmin complex proteins, which have been identified in other works (Teixido-Travesa et al. 2010). This may be a result of differences in the affinity purification methods. Furthermore, cell synchronization may increase the abundance of certain cell cycle specific γ-TuRC interactors which remained minimal in our asynchronous samples.

Characterization of the γ-TuRC's composition and interactors would enable the analysis of how these aspects change in response to modifications in the γ-TuRC's structure. Here, we found that truncating specific N-terminal domains of GCP6 results in partial γ-tubulin-containing complexes. Guided by the structure of the native human γ-TuRC, which contains 14 γ-tubulin/GCP heterodimers, and our sucrose gradient centrifugation analysis, we hypothesize that these partial complexes have 10 γ-tubulin/GCP heterodimers in GCP6$^{\Delta NHD}$ cells, and 6 γ-tubulin/GCP heterodimers in GCP6$^{\Delta N\text{-}Belt}$ cells. Future work utilizing LFQ mass spectrometry and structural methods will determine the components of these partial complexes and their relative stoichiometries. Additional mass spectrometry and cellular analyses will allow for the examination of which γ-TuRC interacting proteins can no longer bind to these partial complexes, and how this may affect the γ-TuRC's activities.

In light of our cell biology studies, we suggest that the partial γ-tubulin-containing complex in the GCP6$^{\Delta N\text{-}Belt}$ cell line maintains an interaction interface needed for

localization of the γ-TuRC to interphase centrosomes, but not to mitotic centrosomes (Fig. 3.6). Given that the identity and/or structural conformation of GCP proteins in this partial complex may differ from those in the native γ-TuRC, it may be that these interacting sites are not translatable to the native cellular context. However, it would be interesting to test whether the native γ-TuRC is localized to interphase and mitotic centrosomes by different interacting partners.

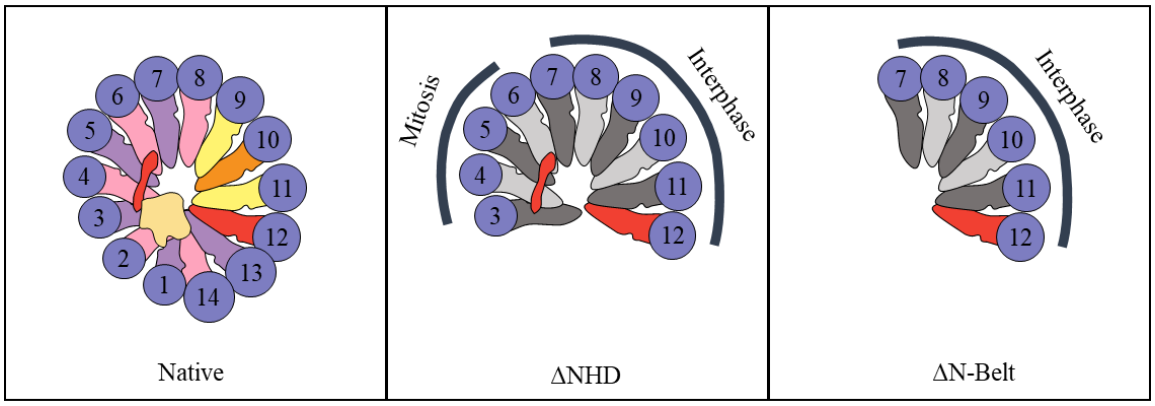

Figure 3.6 Proposed modular binding interfaces regulating cell cycle dependent

Schematic showing the proposed γ-TuRC binding interfaces that can associate with different interacting proteins during interphase or mitosis. The GCP6$^{\Delta NHD}$-containing complex would maintain both interphase and mitotic interfaces, while the GCP6$^{\Delta N\text{-}Belt}$-containing complex would maintain only the interphase binding interface.

Several different centrosomal proteins have been suggested to bind and localize the γ-TuRC (Akhmanova and Kapitein 2022). The observation that the γ-TuRC concentration at the centrosome increases during the transition from interphase to mitosis may indicate that a mitosis specific factor recruits the γ-TuRC (Haren, Stearns, and Lüders 2009;

Khodjakov and Rieder 1999). Furthermore, the centrosome's pericentriolar matrix composition changes during the interphase to mitosis transition (Woodruff, Wueseke, and Hyman 2014). This further indicates that a cell cycle specific factor may regulate γ-TuRC localization, and that different factors may bind to unique γ-TuRC interfaces.

Chapter 4: Outlook and Future Directions

4.1 Summary

Microtubule dynamics are essential to mitosis. In addition to the growth and shrinkage of microtubules, their formation is another key property that needs to be regulated in order for cell division to proceed. In this work, I discuss how different activities of the γ-TuRC, specifically, nucleation, capping, and anchoring, play a role in microtubule formation and mitotic spindle assembly. First, I show that the γ-TuRC's capping activity can be distinct from its nucleation activity, as γ-TuRC's comprised of GTP-binding deficient γ-tubulin could cap, but not nucleate, microtubules. Further, microtubule regrowth assays in HeLa cells expressing this mutant suggest that the γ-TuRC's capping activity, independent of its nucleation activity, can promote microtubule formation at non-centrosomal sites. Second, I characterize the γ-TuRC's potential interacting proteins, and examine how cell cycle specific interactions may differ in partial γ-tubulin-containing complexes. Expression of N-terminally truncated GCP6 lacking the NHD and "belt" domains, which are critical for maintaining the structural integrity of the ring complex, results in interphase specific centrosomal localization of γ-tubulin and the truncated GCP6, while both are lost from mitotic centrosomes. This data suggests that different interfaces of the γ-TuRC maintain cell cycle specific interactions. Here, I discuss remaining open questions and potential future directions that could further enhance our understanding of this important cellular complex.

4.2 Distinguishing between the γ-TuRC's nucleation and capping activities

Microtubule formation can be facilitated by several different cellular factors, as discussed in the introduction to this chapter. What differentiates the γ-TuRC from these other factors? The data discussed in chapter 2 of this work suggest that the combination of the γ-TuRC's templated nucleation and minus-end capping activities imparts unique properties to the newly formed microtubules that other microtubule formation pathways cannot provide. In both γ-tubulin^{KD} or γ-tubulin$^{\Delta GTP+KD}$ cell lines, separated bipolar spindles could not be formed, consistent with some property of the microtubules in these cells being functionally different from the microtubules in wild-type cells. This suggests that microtubules nucleated by the γ-TuRC adopt certain properties that are necessary for bipolarization. More work will be necessary to uncover what these properties are.

In light of our *in vitro* data that γ-TuRC composed of GTP-binding deficient γ-tubulin cannot nucleate microtubules, the rescue of non-centrosomal microtubule formation in mitotic γ-tubulin$^{\Delta GTP+KD}$ cells suggests that γ-TuRC-independent microtubule nucleation pathways are active. However, as non-centrosomal microtubule formation is limited in γ-tubulin^{KD} cells, our data suggests that even these γ-TuRC-independent microtubule nucleation pathways rely on the γ-TuRC's capping activity in order for microtubule growth to be sustained. Below are 3 hypotheses as to why this may be:

1. Microtubules nucleated by γ-TuRC-independent pathways exhibit growth/shrinkage dynamics at both the plus and minus-ends and are therefore prone to complete disassembly. Minus-end capping by the γ-TuRC restricts microtubule dynamics at this end, thereby strengthening the stability of the microtubule polymer as a whole. This is consistent with recent work which suggests that microtubule fragility at the minus-end can affect the dynamics of the plus-end (A. Rai et al. 2021).

2. Uncapped microtubule minus-ends are vulnerable to microtubule depolymerases, and therefore may be depolymerized before they have the chance to be visualized. Minus-end capping by the γ-TuRC could sustain the growth of microtubule polymers by preventing depolymerases such as Kif2A and MCAK from accessing the minus-end, as shown recently (Henkin et al. 2023).

3. By capping the microtubule minus-end, the γ-TuRC also serves as a handle to localize the microtubule to specific sites. γ-TuRC-independent nucleation pathways may not be able to be specifically localized in this way, and therefore may remain dispersed in the absence of γ-TuRC's capping activity, resulting in the loss of substantiated microtubule foci.

Additional work will be necessary to examine these possibilities and elucidate the mechanisms by which the γ-TuRC's capping activity promotes microtubule formation.

4.3 The structure of the capped minus-end

It would be interesting to examine the high-resolution structure of the γ-TuRC-capped microtubule minus-end. While this has been observed at low resolution using negative stain electron microscopy, it remains unclear how exactly the γ-tubulin molecules in the γ-TuRC interact with the α-tubulins at the microtubule minus-end (Würtz et al. 2021b; Kollman et al. 2010; Keating and Borisy 2000; Wiese and Zheng 2000; Zheng et al. 1995). In addition, differentiating between the structure of a capped, γ-TuRC-nucleated minus-end and a γ-TuRC-capped, independently formed microtubule may have important implications for understanding this interaction. It may be that after a nucleation event, all of the γ-tubulin molecules are engaged with the α-tubulins of each protofilament, whereas in a capped, pre-formed microtubule, only a subset of the α-tubulins are engaged (Fig. 4 A

and B). This is consistent with a recent study which suggests that the mechanism by which a microtubule is nucleated may affect the strength of γ-TuRC binding to the minus-end (D. Rai et al. 2022). Furthermore, there may be structural differences between a nucleation-competent γ-TuRC, and a γ-TuRC that is only capping a minus-end, which may shed light on the mechanisms mediating these interactions.

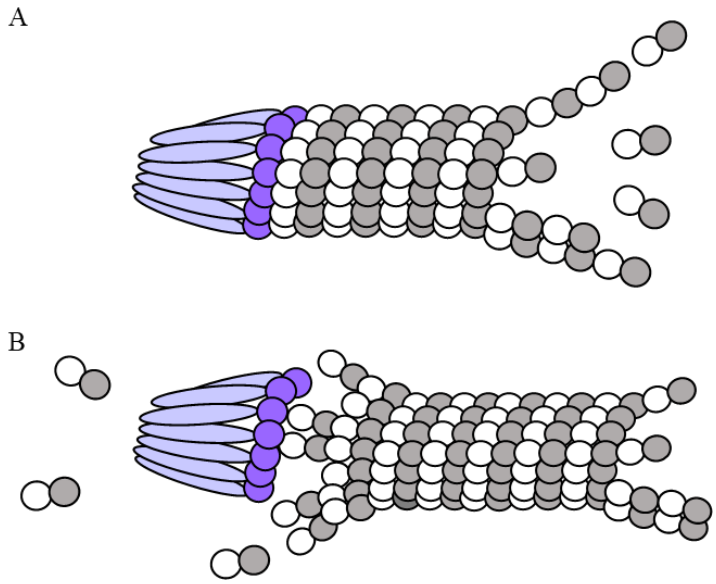

Figure 4.1 The γ-TuRC cap at nucleated or pre-formed minus-ends

(A and B) Schematic of the hypothesized interaction between the γ-TuRC and the microtubule minus-end in a γ-TuRC-nucleated (A) or a pre-formed (B) microtubule. In a nucleated microtubule, all of the protofilaments can be engaged by the γ-TuRC, whereas in the pre-formed microtubule, the flaring of the protofilaments at the minus-end may result in only a subset of them being engaged.

4.4 Generating a γ-TuRC that nucleates, but does not cap, microtubules

To further characterize the functional differences between the nucleation and capping activities of the γ-TuRC, it would be interesting to generate a complex that retains its nucleation activity, but can no longer cap microtubules. This is conceptually difficult, as, in theory, the interactions necessary for the γ-TuRC to bind tubulin dimers and nucleate a microtubule are related to, if not the same as, the interactions that mediate the continued binding of the γ-TuRC at the minus-end as a cap. Given the GTP-dependency of the γ-TuRC's nucleation activity, however, one hypothesis is that a γ-tubulin mutant which can bind, but not hydrolyze GTP, would be captured in a "nucleation on" state.

GTP-hydrolysis deficient mutants have been identified for α,β-tubulin dimers. However, these are not translatable to γ-tubulin, as the catalytically active residue resides in α-tubulin, which induces the hydrolysis of the GTP molecule being held by β-tubulin during polymerization (Manka and Moores 2018; Anders and Botstein 2001). However, a genetic screen in yeast γ-tubulin identified mutations which maintains its affinity for GTP, while markedly enhancing the K_d for GDP (Gombos et al. 2013). One of these mutations, D68N in human γ-tubulin (D70N in yeast), is of particular interest due its homology to the catalytic D67 residue in the GTP-binding pocket of Ras-GTPases. In both cases, the aspartate residue is important for coordinating the magnesium ion in the GTP-binding pocket (Gombos et al. 2013; Goldberg 1998). Biochemical and cellular experiments incorporating a D68 γ-tubulin mutant may reveal new insights into how GTP hydrolysis regulates the γ-TuRC's different activities.

4.5 Relationship between the γ-TuRC's architecture and its cellular functions

In chapter 3 of this work, I discussed how the loss of particular binding interfaces on the γ-TuRC may affect its minus-end anchoring activity. This phenotype was pronounced in GCP6$^{\Delta N\text{-}Belt}$ cells, which expressed the smallest partial γ-tubulin-containing complex, while no obvious interphase or mitotic phenotype was observed in GCP6$^{\Delta NHD}$ cells, which express the relatively "medium" sized partial γ-tubulin-containing complex. It would be interesting to further investigate the binding interfaces on the native γ-TuRC and examine how the γ-TuRC's interactome changes when these interfaces are perturbed.

While no general mitotic spindle defects were observed in GCP6$^{\Delta NHD}$ cells, there may still be subtle changes to the activity of the partial γ-tubulin-containing complex in this cell line relative to the native complex. We hypothesize that the GCP6$^{\Delta NHD}$ truncation results in the loss of GCP6 contacts with the luminal bridge components, ultimately leading to the dissociation of 4 γ-tubulin-GCP dimer "spokes" from the ring complex (see Figure 3.6). This complex may be functionally similar to a previously characterized recombinant complex lacking the luminal bridge, termed the γ-TuRC$^{\Delta LB}$ (Wieczorek et al. 2021). Characterization of the γ-TuRC$^{\Delta LB}$ showed that this complex could nucleate microtubules with a similar efficiency as the wild-type recombinant complex (Wieczorek et al. 2021). However, it has not yet been tested whether this partial complex caps or anchors microtubule minus-ends as effectively as the full ring complex. For instance, the strength of the interaction of the partial complex may be weaker than the full complex, since fewer microtubule protofilaments can be engaged. Furthermore, it may only stabilize a portion of the minus-end, allowing continued growth/shrinkage dynamics at the exposed protofilaments, and leaving those protofilaments vulnerable to microtubule depolymerases. This question is particularly interesting, as the evolution of the 14-membered γ-TuRC in

higher organisms from the 2-membered γ-TuSC in budding yeast suggests a biological advantage to the formation of a complete ring complex (Peng Liu et al. 2021; Kollman et al. 2011). What this advantage is, and how different regions of the γ-TuRC's architecture contribute to it, remains to be elucidated.

Materials and Methods

Plasmids

The following plasmids were used in this study.

pACEBac1-γ-Tubulin-TEV-HIS6 (Wieczorek et al. 2021).

pACEBac1-γ-Tubulin$^{\Delta GTP}$-TEV-HIS6 (Wieczorek et al. 2021).

pACEBac1-γ-TuSC (Wieczorek et al. 2021).

pACEBac1-γ-TuRC-GFP (Wieczorek et al. 2021).

pACEBac1-γ-TuSC$^{\gamma\text{-tub}\Delta GTP}$ (Wieczorek et al. 2021).

pACEBac1-γ-TuRC$^{\gamma\text{-tub}\Delta GTP}$ was generated by replacing the wild-type γ-tubulin in pACEBac1-γ-TuRC-GFP with N229A-γ-tubulin.

pMal-C2-TEV protease (pRK793; Addgene plasmid 8827; Kapust et al. 2001)

pET17b-K560 (gift from R.D. Vale)

pET21-PelB-GFP nanobody clone LaG16 (gift from M. Rout, Fridy et al. 2014).

pSuperior.retro.puro-sh-γ-Tubulin was generated with the target sequence 5'-A**G**GA**G**GACATGTT**C**AA**G**GA-3' (Choi et al. 2010; Lüders, Patel, and Stearns 2006) according to the manufacturer's protocol (OligoEngine).

pSuperior.retro.puro-sh-GCP6 was generated with the target sequence 5'-AAACG**A**GA**C**TACTT**C**CT**T**A-3' (Ramírez Cota et al. 2017) according to the manufacturer's protocol (OligoEngine).

pCDNA5/FRT/TO-γ-tubulin$^{WT\text{-}RNAi\text{-}resistant}$-GFP was generated by inserting the cDNA for γ-tubulin into the vector using restriction enzymes. 4 silent mutations were introduced into the shRNA target sequence using site-directed mutagenesis by PCR (NCBI reference sequence NC_000017.11): G2228A, C2231T, C2237T, G2240A, noted as bold letters in the sh-RNA target sequence above. To account for any non-specific mutations that may have occurred in the vector backbone, the sequence-confirmed gene was excised by restriction enzymes, and re-ligated into the cut original vector.

pCDNA5/FRT/TO-γ-tubulin$^{\Delta GTP\text{-}RNAi\text{-}resistant}$-GFP was generated by site directed mutagenesis of the WT plasmid. After confirmation of mutagenesis by sequencing, the gene was excised by restriction enzymes and re-ligated into the cut original vector.

pCDNA5/FRT/TO-GCP6$^{FL\text{-}RNAi\text{-}resistant}$-prescission-GFP was generated by inserting the cDNA for GCP6 into the vector using restriction enzymes. The Q5 site directed mutagenesis kit (NEB, E0552S) was used to introduce the following 4 silent mutations into the sh-RNA target sequence (NCBI reference sequence NC_000022.11): A954T, C957T, C963T, T966A, noted as bold letters in the sh-RNA target sequence above. To account for any non-specific mutations that may have occurred in the vector backbone, the sequence-confirmed gene was excised by restriction enzymes, and re-ligated into the cut original vector.

pCDNA5/FRT/TO-GCP6$^{\Delta NHD\text{-}RNAi\text{-}resistant}$-prescission-GFP and pCDNA5/FRT/TO-GCP6$^{\Delta N\text{-}Belt\text{-}RNAi\text{-}resistant}$-prescission-GFP were generated by truncating amino acids 1-120 or 1-250, respectively, using the Q5 site directed mutagenesis kit with the FL RNAi-resistant construct as the template. To account for any non-specific mutations that may have occurred in the vector backbone, the sequence-confirmed gene was excised by restriction enzymes, and re-ligated into the cut original vector.

Antibodies

The following primary and secondary antibodies were purchased from commercial sources, with their application and working concentrations indicated in parentheses.

Anti- γ-tubulin: Millipore Sigma, GTU-88 (western blot: 1:000; immunofluorescence: 1:500). Anti-γ-tubulin: Millipore Sigma, T5192 (immunofluorescence, 1: 250).

Anti-GCP2: Santa Cruz, SC-390116 (western blot, 1:100).

Anti-GCP4: GeneTrex, GTX115949 (western blot, 1:1000).

Anti-GCP5: BioWorld, I779 (western blot, 1:250).

Anti-GCP6: Abcam, AB95172 (western blot, 1:1000).

Anti-GAPDH: ProteinTech, 1E6D9 (western blot, 1:1000).

Anti-α-tubulin: Invitrogen, clone YL1/2 (immunofluorescence: 1:500).

FITC-conjugated Anti-β-tubulin: Sigma, F2043 (immunofluorescence, 1:1000).

Goat anti-Rat Alexa Fluor 594: Invitrogen, A-11007 (immunofluorescence, 1:1000).

Donkey anti-Rabbit Texas Red: Jackson Immunoresearch, 711-075-152 (immunofluorescence, 1:500).

Goat anti-Mouse Alexa Fluor 488: Invitrogen, A-11001 (immunofluorescence, 1:500).

Janelia Fluor 646-Hoechst: Janelia Materials (immunofluorescence, 1:1000).

Goat polyclonal anti-Mouse IRDye 680RD: LI-COR, 926-68070 (western blot, 1:10,000).

Cell lines

HeLa TREx cells (ThermoFisher) and Ampho293T (ThermoFisher) were maintained in DMEM (ThermoFisher) +10% FBS (Sigma-Aldrich). Cell lines containing tetracycline inducible constructs were cultured in DMEM +10% Tet System Approved FBS (TakaraBio). Cells were incubated at 37°C and 5% CO_2. Cells were used at early passage numbers (<20 passages). Cells were tested for mycoplasma using a PCR based method (Uphoff and Drexler 2014).

To generate HeLa cells with tetracycline-inducible control of γ-tubulin or GCP6 shRNA expression, we used retroviral transduction. First, retroviral particles containing the γ-tubulin shRNA were generated by transfecting Ampho293T cells via calcium phosphate with pSuperior.retro.puro-sh-γ-Tubulin. After a 48 hour incubation, the media from the Ampho293T containing retroviral particles was harvested and filtered using a 0.45µm filter, supplemented with 4µg/mL polybrene, and then added to HeLa TREx cells. This process was repeated the following day, once in the morning and once in the evening. 48 hours after the first application, stably transduced cells were selected with 2µg/mL

puromycin. Cells were maintained in puromycin until plated for an experiment. To induce shRNA expression, cells were allowed to adhere overnight, and then treated for 72 hours with 1µg/mL doxycycline (Sigma).

To generate cells with inducible expression of shRNA-resistant γ-tubulin or GCP6 constructs, we transfected the pCDNA5/FRT/TO plasmids (listed above) into HeLa TREx cells using Lipofectamine 2000 according to the manufacturer's recommendations (Invitrogen). Hygromycin B (Invitrogen) was used to select for cells that had stably incorporated the construct into the Flp-In site. Cells were maintained in Hygromycin B until plated for an experiment. This method was performed using non-transduced HeLa TREx cells, or with HeLa TREx cells already transduced to stably incorporate inducible γ-tubulin shRNA. Expression of WT and ΔGTP γ-tubulin$^{\text{RNAi-resistant}}$-GFP was induced by allowing the cells to adhere overnight, and subsequently treating the cells with 1µg/mL doxycycline for 48 hours.

Expression and purification of γ-TuRC$^{\text{γ-tub-WT}}$ and γ-TuRC$^{\text{γ-tubΔGTP}}$

γ-TuRC$^{\text{γ-tub-WT}}$ and γ-TuRC$^{\text{γ-tubΔGTP}}$ were purified using the same protocol, as described in Wieczorek et al. 2021. In brief, to purify γ-TuRC$^{\text{γ-tubΔGTP}}$, pACEBac1-γ-TuSC$^{\text{γ-tubΔGTP}}$ and pACEBac1-γ-TuRC$^{\text{γ-tubΔGTP}}$ were each transfected into SF9 cells using Cellfectin transfection reagent according to the manufacturer's protocol. Viruses from SF9 cells were amplified twice, after which they were used to infect Hi5 cells at a density of $3x10^6$ cells/mL.

After 60 hours, the Hi5 cells were lysed in Lysis Buffer (40 mM HEPES, pH 7.5, 150 mM KCl, 1 mM MgCl2, 10% glycerol [vol/vol], 0.1% Tween-20, 0.1 mM MgATP, 0.1

mM MgGTP, 1 mM β-mercaptoethanol, cOmplete EDTA-free Protease Inhibitor Cocktail tablets (Roche), 500 U benzonase, 2 mM PMSF, and 4 mM benzamidine-HCl) on ice using dounce homogenization. The lysate was clarified at 56,000rpm in a Type 70Ti rotor for 1 hour at 4°C. The clarified lysate was filtered, and loaded onto a 1mL NHS-Trap column pre-conjugated with rabbit IgG. The column was washed first with lysis buffer, and then with Gel Filtration Buffer (40 mM HEPES, pH 7.5, 150 mM KCl, 1 mM MgCl2, 10% glycerol [vol/vol], 0.1 mM MgGTP, 1 mM β-mercaptoethanol). 1mg of TEV protease, diluted in gel filtration buffer supplemented with 0.1mM MgGTP, was loaded onto the column and incubated for 1 hour at 4°C. The eluted fractions were pooled, and dialyzed against Dialysis Buffer (40 mM HEPES, pH 7.5, 150 mM KCl, 1 mM MgCl2, 60% sucrose [w/vol], 0.1 mM MgGTP, 2 mM β-mercaptoethanol) for 4 hours at 4°C, or until the volume was reduced to <1mL. The dialyzed eluate was then gel filtered using a Superose 6 increase 10/300 column (Cytvia) pre-equilibrated in Gel Filtration Buffer. The pACEBac1-γ-TuRC$^{\gamma\text{-tub}\Delta GTP}$ eluted at ~9mL.

The peak fraction was further purified by sucrose gradient centrifugation, by loading the eluate on a 2mL 10-40% sucrose (w/vol) gradient in. The sucrose for four gradient steps was dissolved in Gradient Buffer (40 mM HEPES, pH 7.5, 150 mM KCl, 1 mM MgCl2, 0.01% Tween-20 [vol/vol], 0.1 mM MgGTP, and 1 mM β-mercaptoethanol) The gradients were centrifuged for 3 hours at 50,000rpm at 4°C in a TLS-55 swing bucket rotor, with minimum acceleration and no break on the centrifuge. 10, 200µL fractions were collected from the top of the gradient manually using a cut P1000 tip. A sample from each was analyzed by SDS-PAGE followed by coomasie staining. Peak fractions

were aliquoted, snap-frozen, and stored in liquid N2 at -80°C. The concentration of the purified γ-TuRC was determined by quantitative western blotting.

γ-TuRC microtubule nucleation assay

TIRF-based microtubule nucleation assays using γ-TuRC$^{\gamma\text{-tub-WT}}$ and γ-TuRC$^{\gamma\text{-tub}\Delta\text{GTP}}$ were performed as described in Wieczorek et al. 2021. Assays using wild-type and mutant complexes were performed on the same days, using the same reagents.

For data analysis, time-lapse images were drift-corrected using the Multi-StackReg plugin in Fiji (Thevenaz, Ruttimann, and Unser 1998). To quantify the residence time of the γ-TuRC at minus-ends following a nucleation event, 15 µM tubulin was used in the reaction so that individual microtubules could be resolved over time. We generated kymographs for microtubules that were determined to have been nucleated from a surface-immobilized γ-TuRC, i.e., the initiation of microtubule growth off of a green γ-TuRC puncta was fully observed. A microtubule was considered dissociated from the γ-TuRC if the microtubule was released from the γ-TuRC, or if the microtubule minus-end grew following nucleation by γ-TuRC. Spontaneously nucleated microtubules, identified as microtubules growing at both ends or microtubules that appeared in the TIRF field of view after the initial growth phase, were not included in our analyses.

To compare the nucleation efficiencies of the γ-TuRC$^{\gamma\text{-tub-WT}}$ and γ-TuRC$^{\gamma\text{-tub}\Delta\text{GTP}}$, 1pM of γ-TuRC was adhered to the coverslip, and 20 µM tubulin was introduced to the flow chamber. Microtubules observed within the FOV (132x132 µm^2) at the indicated time points were counted manually and tracked using the Line tool together with the ROI manager tool in FIJI. The number of newly nucleated microtubules at each time point

was added to the number of microtubules counted at the previous time point to report the total number of microtubules.

Dynamic minus-end-capping TIRF assay

The TIRF microscope and flow cell setup were the same as described for the microtubule nucleation assay, with the following modifications. The flow cell was rinsed with BRB80 (80 mM K-PIPES, pH 6.8, 1 mM MgCl2, and 1 mM EGTA) containing 1 mM TCEP, followed by 0.2 mg/mL PLL-PEG-biotin (PLL(20)-g[3.5]- PEG(2)/PEG(3.4)-biotin(20%); SuSos) prepared in BRB80 + 1 mM TCEP. After 5 minutes, the flow cell was rinsed with BRB80 + 1 mM TCEP, and a mixture containing 0.5 mg/mL k-casein and 0.25 mg/mL neutravidin prepared in BRB80 + 1 mM TCEP was flowed in. After 5 minutes, GMPCPP seeds containing 12.5% X-rhodamine-labeled tubulin and 1% biotinylated tubulin, prepared with two cycles of polymerization as described (S. C. Ti et al. 2016), were flowed in. After 5 minutes, unbound seeds were rinsed off with room-temperature assay buffer (BRB80 + 1 mM TCEP, 50 mM KCl, 0.2 mg/mL k-casein, and 1 mM MgGTP). A reaction mixture containing 10-30 pM γ-TuRC, 15 µM tubulin (containing ~2.5% X-rhodamine-labeled tubulin), and oxygen scavengers (0.035 mg/mL catalase, 0.2 mg/mL glucose oxidase, 2.5 mM glucose, and 10 mM DTT) was prepared in assay buffer and introduced to the flow cell. Experiments with γ-TuRC$^{\gamma\text{-tub-WT}}$ and γ-TuRC$^{\gamma\text{-tub}\Delta\text{GTP}}$ were performed on the same days, using the same reagents. Soluble tubulin was prepared by mixing unlabeled and rhodamine-labeled tubulin on ice and clarifying at 90,000xg for 10 minutes at 4°C, and held on ice for no more than 2 hours, after which a new sample of soluble tubulin was prepared. The tubulin concentration was measured using a Bradford assay. The flow cell was sealed with VALAP and placed on the TIRF

microscope stage. The sample was imaged immediately in order to observe microtubule growth at both ends so that the plus-ends and minus-ends were distinguishable. Images were acquired for either 10 minutes at 3 second intervals or 30 minutes at 10 second intervals, and an exposure time of 500 ms for each laser channel. The microscope chamber was heated to ~35-37°C before image acquisition. Image acquisition was controlled using NIS- Elements AR 4.60.00 (Nikon).

Analysis of γ-TuRC capping at dynamic microtubule minus-ends

Time lapse images were drift-corrected using the MultiStackReg Fiji plugin (Thevenaz, Ruttimann, and Unser 1998). To quantify minus-end capping by γ-TuRCs, we generated kymographs for microtubules that met the following criteria: 1. Microtubules were determined to not be associated in parallel with another filament (i.e., a bundle), and 2. Both growing ends of the microtubule were within the FOV. Next, a capping event was scored if it met the following criteria: 1. Puncta persisted for two consecutive frames or greater, 2. The puncta was not present at the interaction site before the polymerizing microtubule reached that site. Distributions of the capping lifetimes were generated by measuring the length of time these criteria were met by first plotting the Z-axis profile of the γ-TuRC signal in FIJI, and then using the tDetector algorithm (Y. Chen et al. 2014) with an alpha value of 0.999 to detect the onset and end of the capping even. Since the γ-TuRC signal varied during the capping event due to drift and movement of the microtubule end, consecutive steps that were above the baseline signal were counted together, and visually confirmed for each independent event.

The landing rate was determined by counting the number of capping events within each experiment, and dividing by the total imaging time in minutes, the γ-TuRC concentration, and the number of GMPCPP seeds with polymerizing extensions in the field of view.

Expression and purification of Kinesin-1 1-560 (K560)

K560, a 560-amino acid N-terminal fragment of human conventional kinesin (kinesin-1) with a C-terminal His-tag (a gift from R. Vale, UCSF), was expressed in BL21 cells. After an induction with 1 mM IPTG at 18dC for 18 hours, cells were resuspended in lysis buffer (50 mM NaPO4, pH 8.0, 250 mM NaCl, 20 mM imidazole, 1 mM MgCl2, 0.5 mM MgATP, 1 mM TCEP) using 25mL of lysis buffer per 1L of cell culture. The cells were disrupted using a french press, and centrifuged at 35,000rpm for 45 minutes at 4°C using a Type 45 Ti rotor. The clarified lysate was incubated with 0.5mL Ni-NTA resin (Qiagen) per 1L of culture for 30 minutes. The resin was then washed with 100mL of lysis buffer. The protein was eluted in a stepwise manner using elution buffer (25mM Na-PIPES, pH 6.8, 150 mM NaCl, 400 mM imidazole, 1 mM MgCl2, 0.2 mM MgATP, 1 mM BME). Peak fractions, identified by performing a bradford assay, were pooled and diluted at least 5 time to <30 mM NaCl using dilution buffer (25mM Na-PIPES, pH 6.8, 2 mM MgCl2, 1 mM EGTA, 0.2 mM MgATP, 1 mM BME). The diluted sample was loaded onto a 2mL HiTrap SP FF, and washed with low salt buffer (25 mM Na-PIPES, pH 6.8, 50 mM NaCl, 2 mM MgCl2, 1 mM EGTA, 0.2 mM MgATP, 1 mM BME). The protein was eluted using a gradient of low to high salt buffer (25 mM Na-PIPES, pH 6.8, 1M NaCl, 2 mM MgCl2, 1 mM EGTA, 0.2 mM MgATP, 1 mM BME). Protein containing fractions were identified using SDS-PAGE followed by Coomasie staining. These fractions were pooled, and the sample was concentrated to <1mL. The sample was

further purified by gel filtration using a Superdex 200 16/60 column pre-equilibrated in gel filtration buffer (25 mM Na-PIPES, pH 6.8, 300 mM NaCl, 2 mM MgCl2, 1 mM EGTA, 0.2 mM MgATP, 1 mM BME). The peak fractions were pooled and dialyzed in storage buffer (25 mM Na-PIPES, pH 6.8, 350 mM NaCl, 2 mM MgCl2, 1 mM EGTA, 0.4 mM MgATP, 1 mM BME, 30% sucrose) for >2 hours.

Stable taxol or GMPCPP-microtubule minus-end-capping

Stable taxol microtubules were prepared by incubating 10 µM tubulin (with ~5% X-rhodamine-labeled tubulin) in BRB80 + 1 mM MgGTP +1 mM DTT. This tubulin mixture was incubated at 37°C for 2 minutes, after which increasing concentrations of taxol were added as follows: 1 µM taxol in DMSO at 1/10th the volume from 7 minutes, 10 µM taxol in DMSO at 1/10th the volume for 7 min, and 100 µM taxol in DMSO at 1/10th the volume for 15 minutes. After the final incubation period, the mixture was diluted 5 times with taxol buffer (BRB80 containing 10 µM taxol, 1% final DMSO concentration). The microtubules were centrifuged at 13,200 rcf for 15 minutes, at room temperature. The microtubule pellet was washed with 200uL of taxol buffer, and then resuspended in 100uL of taxol buffer. Taxol-stabilized microtubules were prepared fresh on each day of use, and stored at room temperature.

Stable GMPCPP microtubules were prepared by incubating 10 µM tubulin (with ~5% X-rhodamine-labeled tubulin) in BRB80 + 1 mM GMPCPP (Jena Biosciences) +1 mM DTT. The mixture was incubated on ice for 5 minutes, followed by 37°C for 30 minutes. The microtubules were then pelleted at 90,000rpm for 5 minutes at 37°C using a pre-heated TLA 120.2 rotor. The supernatant was removed, and the microtubules were

resuspended in BRB80 + 1 mM DTT. Following a 20 minute incubation on ice, 1 mM GMPCPP was added to the depolymerized tubulin. The mixture was transferred to 37°C and incubated for 1 hour. Microtubules were then centrifuged as before, and the obtained pellet was washed with 200uL BRB0 + 1 mM DTT, followed by resuspension in 50uL. GMPCPP-stabilized microtubules were used over the course of 4 days, and were stored at room temperature.

The TIRF microscope and flow cell setup were the same as described for the microtubule nucleation assay. All buffers were kept at room temperature. The flow cell was rinsed with BRB80 (80 mM K-PIPES, pH 6.8, 1 mM MgCl2, and 1 mM EGTA) containing 1 mM TCEP, followed by 700 nM of K560. After 5 minutes, the flow cell was washed with assay buffer (50 mM KCl, 0.2mg/mL k-casein, 1 mM MgGTP, 1 mM TCEP in BRB80). Next, 0.2 mg/mL PLL-PEG-biotin (PLL(20)-g[3.5]- PEG(2)/PEG(3.4)- biotin(20%); SuSos) + 0.5 mg/mL k-casein prepared in assay buffer were flowed in. After 5 minutes, taxol- or GMPCPP-stabilized microtubules diluted ~1:50 in assay buffer were flowed in. After 5 minutes, unbound microtubules were rinsed off with warm assay buffer. A reaction mixture containing 50 pM γ-TuRC, and oxygen scavengers (0.035 mg/mL catalase, 0.2 mg/mL glucose oxidase, 2.5 mM glucose, and 10 mM DTT) was prepared in assay buffer supplemented with 100 µM MgATP and introduced to the flow cell. For taxol stabilized microtubules, all buffers contained 10 µM taxol in 1% DMSO.

The flow cell was sealed with VALAP and placed on the TIRF microscope stage. Two-color images were acquired for at 2 second intervals and an exposure time of 150 ms. The microscope chamber was heated to ~35-37°C before image acquisition. Image acquisition was controlled using NIS- Elements AR 4.60.00 (Nikon). Experiments with γ-

TuRC$^{\gamma\text{-tub-WT}}$ and γ-TuRC$^{\gamma\text{-tub}\Delta GTP}$ were performed on the same days, using the same reagents.

Analysis of γ-TuRC capping at stabilized microtubule minus-ends

The number of capped minus-ends was manually counted and then divided by the total number of microtubules within a field of view, at approximately 3 minutes after the final reaction mixture was added to the flow cell. The microtubules were observed up to 20 seconds before and after 3 minutes in order to determine the directional movement of the microtubules. Bundled microtubules whose ends could not be determined were excluded from the analysis.

Kymographs were generated using the KymoResliceWide v.0.5 plugin for ImageJ *(https://github.com/ekatrukha/KymoResliceWide*).

Purification of recombinant γ-tubulin proteins

The protein sequences for C-terminally His-tagged Hs γ-tubulin WT or N229A was cloned into a pACEBAC1 backbone. The plasmids were transformed into DH10MultiBacTurbo cells (ATG:biosynthetics GmbH) and transposition-positive colonies were selected and used to generate recombinant bacmids. Bacmids were isolated using a phenol-chloroform extraction (S.-C. Ti, Wieczorek, and Kapoor 2020). Bacmids were transfected into Sf9 cells (Novagen) per the Bac-to-Bac manual (Invitrogen), baculoviruses were amplified twice, and fresh P3 virus was used to infect 2 liters of High Five cells (Thermo Fisher Scientific) at a 1:75 dilution and at a cell density of 2.5×10^6/ml for 60 h at 27°C.

The cells were centrifuged at 1000 rcf for 15 minutes at 4°C. After discarding the supernatant, the cells were resuspended in 40mL lysis buffer (50 mM KPO4, pH 8.0, 500 mM KCl, 1 mM MgCl2, 0.25 µM MgGTP, 5 mM BME, EDTA-free protease inhibitors (Roche), 250U benzonase, 1 mM PMSF) per liter of cell culture. The cells were lysed by dounce homogenization, by performing 20 strokes on ice. The lysate was centrifuged at 16,500 rpm for 15 minutes at 4°C in a Type 70 Ti rotor. The supernatant was then supplemented with 10% glycerol and 10 mM imidazole, and then further clarified at 40,000 rpm for 35 minutes at 4°C in a Type 70 Ti rotor. 1mL of pre-equilibrated Ni-NTA resin (Qiagen) was added to the clarified lysate, and incubated for 1 hour at 4°C with rotation. The resin was washed with 300mL wash buffer A (50 mM KPO4, pH 8.0, 500 mM KCl, 1 mM MgCl2, 10% glycerol, 25 mM imidazole, 0.25 µM MgGTP, 5 mM BME), followed by a second wash with 300mL wash buffer B (50 mM K-MES, pH 6.6, 500 mM KCl, 5 mM MgCl2, 10% glycerol, 25 mM imidazole, 0.25 µM MgGTP, 5 mM BME). The protein was eluted in a stepwise manner in elution buffer (50 mM K-MES, pH 6.6, 500 mM KCl, 5 mM MgCl2, 5% glycerol, 250 mM imidazole, 0.25 µM MgGTP, 5 mM BME). Peak fractions were identified using a bradford assay (BioRad), then pooled and concentrated to ~0.5mL. The sample was further purified by gel filtration, using a pre-equilibrated Superdex 200 increase 10/300 column (Cytvia). The peak fractions were pooled, and the protein concentration was determined by bradford assay. The protein was aliquoted, frozen in liquid nitrogen, and stored at -80.

Quantitative Western blotting

γ-TuRC concentrations were estimated using quantitative western blotting against purified γ-tubulin. Serial dilutions of γ-tubulin were used to calculate a standard curve, from which the concentration of γ-tubulin in each γ-TuRC was calculated. As each complex contains 14 γ-tubulins, the derived γ-tubulin concentration was then divided by 14 in order to calculate the final γ-TuRC concentration. Densitometry analysis was performed using the standard features in FIJI.

Native mass spectrometry (nMS) analysis

The purified protein samples were buffer-exchanged into nMS solution (500 mM ammonium acetate, 0.01% Tween-20) using Zeba desalting microspin columns with a 40-kDa molecular weight cut-off (Thermo Scientific). For nucleotide incubation, the buffer-exchanged sample was incubated with five-fold molar excess of Mg-GTP (1 µM protein:5-10 µM Mg-GTP) on ice for 2 min prior to nMS analysis. Each nMS sample was loaded into a gold-coated quartz capillary tip that was prepared in-house and was electrosprayed into an Exactive Plus EMR instrument (Thermo Fisher Scientific) using a modified static nanospray source (Olinares and Chait 2020). The MS parameters used included: spray voltage, 1.22 kV; capillary temperature, 150 °C; S-lens RF level, 200; resolving power, 8,750 at *m/z* of 200; AGC target, 1 x 10^6; number of microscans, 5; maximum injection time, 200 ms; in-source dissociation (ISD), 10 V; injection flatapole, 8 V; interflatapole, 4 V; bent flatapole, 4 V; high energy collision dissociation (HCD), 125 V; ultrahigh vacuum pressure, 4.5×10^{-10} mbar; total number of scans, 100. Mass calibration in positive EMR mode was performed using cesium iodide. Raw nMS spectra were visualized using Thermo

Xcalibur Qual Browser (version 4.2.47). Data processing and spectra deconvolution were performed using UniDec version 4.2.0 (Reid et al. 2019; Marty et al. 2015). The UniDec parameters used were m/z range: 2,000 – 7,000; mass range: 10,000 – 200,000 Da; sample mass every 1 Da; smooth charge state distribution, on; peak shape function, Gaussian; and Beta softmax function setting, 20. The expected masses for the wild-type and GTP-deficient mutant (N229A) γ-tubulin with N-terminal methionine removed were 52,713 Da and 52,670 Da, respectively. The measured masses for these proteins were within ± 2 Da from the expected mass.

Negative stain EM

Purified γ-TuRC$^{\gamma\text{-tub}\Delta GTP}$ was applied to glow- discharged carbon-coated copper grids (EMS; CF-400-Cu) and incubated for 1 minute per application at room temperature. Protein solution was removed by manual blotting with Whatman No. 1 filter paper. The application was repeated as necessary to improve particle density, depending on the concentration of γ-TuRC. The final application was not blotted off. Freshly filtered 1% uranyl acetate (wt/vol) was then applied to exchange the solution, and then incubated on the grid for 1 minute. The grid was blotted to remove the stain. The grid was air-dried for at least 24 hours in a sealed container with desiccant before imaging.

Particles on grids were imaged and processed as described previously (Wieczorek et al. 2021). In brief, ~300,000 Auto-picked particles were binned by two and subjected to reference-free 2D classification to remove particles likely corresponding to contaminants. Next, a random subset of these particles were used to generate an ab initio model. Then, the ab initio model was used as a reference to perform a 3D auto-refinement step. Re-

extracted particles were used to generate 4 3D classes. ~4,300 particles in the 3D class with the highest level of detail were re-extracted from CTF- corrected micrographs at the unbinned pixel size (3.036 Å) and subjected to a final round of 3D auto-refinement using one of the 3D classes as a reference model. A composite model of the native human γ-TuRC was then rigid body–fitted into density maps using the "Fit in map" function of Chimera. Protein models were generated using UCSF Chimera (Pettersen et al. 2004) or UCSF ChimeraX (Goddard et al. 2018).

Liquid chromatography-mass spectrometry

40-µls of γ-TuRC$^{\gamma\text{-tub}\Delta GTP}$ in 1x SDS sample buffer was loaded on a 10-well, 4–20% Tris-glycine precast gel with "wide wells" (Novex). A current of 150V was applied until the sample migrated ∼1cm into the gel. A ∼1 cm × 1 cm gel "plug" was cut out, and further cut into ~1-mm cubes. Proteins in gel were reduced and alkylated, and then digested with trypsin (Promega) and lysC (Wako). The generated peptides were analyzed using an Orbitrap Fusion Lumos LC-MS/MS using a 70-minute gradient on a pulled-emitter column. The mass spectrometer was operated in high resolution/high mass acquisition mode.

Mass spectrometry data were processed and searched using Proteome Discoverer/Mascot with the swissprot database.

Immunofluorescence

Cells were grown on pre-sterilized 12-mm-diameter glass coverslips (Fisher). For fixation, the coverslips were transferred into Fixation Buffer (80 mM K-Pipes pH 6.8, 0.8

mM MgCl2, 0.8 mM EDTA, 0.5% Triton X-100, 0.1% glutaraldehyde, and 3.2% paraformaldehyde) prewarmed to 37°C for 20 minutes. The cells were incubated in Fixation Buffer at 37°C for 10 minutes, and then reduced in 10 mM $NaBH_4$ (dissolved in water for) 5 minutes at room temperature. After one wash with PBS, the cells were incubated in Blocking Buffer (1x PBS, 3% BSA, 0.5% Triton X-100, 0.05% NaN_3) for 1.5 hr at room temperature. Coverslips were then incubated with primary antibody diluted in Blocking Buffer for 1.5 hr at room temperature. After three washes with 1× PBS for 5 minutes at room temperature, the coverslips were incubated for 1.5 hr at room temperature with secondary antibodies diluted in Blocking Buffer. After three washes in 1xPBS for 5 minutes, the coverslips were mounted (20 mM Tris-HCl, pH 8, 0.5% propyl gallate, and 90% glycerol), and sealed with nail polish.

Imaging was performed on a Nikon Eclipse Ti2-E equipped with a Yokogawa W1 confocal scanning unit, a z piezo stage, and a 100X oil objective (Plan Apo, 1.45 NA) at room temperature. Fluorescence was directed onto a Prime 95B sCMOS camera (Photometrics) and images were recorded using NIS-Elements software (Nikon).

Cell lysate preparation and western blotting

Cell lysates were prepared in Lysis Buffer (25 mM Tris-HCL, pH 7.4, 0.5% IGEPAL-CA-630, 100 mM NaCl, 5 mM MgCl2, 20 mM β-glycerophasphate, 1 mM EDTA) supplemented with 1 mM DTT, 1x cOmplete EDTA-free protease inhibitors (Roche), and 1 mM PMSF. Total lysate concentration was measured by Bradford assay and adjusted with Lysis Buffer. Lysates were denatured in sample buffer and boiled at 95°C for 10 minutes. Lysates were run on 4–20% Tris-glycine precast gels at 185V until the sample buffer reached the bottom of the gel. Proteins were then transferred onto Immobilon-P

PVDF 0.45 µm membrane (IPVH00010; Merck Millipore) using a wet-tank transfer system (Bio-Rad) in Tris-Glycine transfer buffer (25 mM Tris-HCl, 175 mM Glycine, 20% MeOH). The membrane was blocked in Intercept (TBS) Blocking Buffer (LICOR) for 45 minutes, and incubated in primary antibody diluted in Antibody Buffer (1xTBS, 5% BSA, 0.02% NaN_3) overnight at 4°C. Membranes were then washed 3x, 5 minutes per wash, in 1x TBS-T. Membranes were then incubated in secondary antibody, diluted in Antibody Buffer, for 1 hour. The membrane was again washed 3x, 5 minutes per wash, in 1x TBS-T, before imaging on the Odyssey imaging system (LICOR). Densitometry was performed using ImageJ. Densitometry was restricted to a comparison of lanes from the same exposure and run on the same gel. Intensity was normalized to loading control.

Sucrose gradient centrifugation of whole cell lysates

3.5-ml sucrose gradients were prepared as follows: 500uL of 5%, 10.85%, 16.7%, 22.72%, 28.3%, 34.15%, and 40% sucrose (wt/vol) in gradient buffer (40 mM HEPES, pH 7.5, 150 mM KCl, 1 mM MgCl2, 0.01% Tween-20 [vol/vol], 0.1 mM MgGTP, and 1 mM 2- mercaptoethanol) were layered into a 5 mL centrifuge tube using a cut-off P1000 tip. The gradient was allowed to equilibrate overnight at 4°C.

150uL of cell lysate at a concentration of 2ug/mL was layered at the top of the gradient. The gradient was centrifuged at 55,000 rpm in a SW-55 rotor at 4°C for 3.5 h with minimum acceleration and no break. 16 x ~220 µl fractions were manually collected by inserting a needle to the bottom of the gradient, and drawing the sample up using a peristaltic pump. Fractions were denatured in 5X sample buffer and boiled at 95°C for 10 minutes. Samples from each fraction were run on NuPAGE 4–20% Bis-Tris 17-well precast gels at 200V using NuPAGE MOPS SDS running buffer until the sample buffer

reached the bottom of the gel. Proteins were then transferred onto Immobilon-P PVDF 0.45 µm membrane (IPVH00010; Merck Millipore) using a wet-tank transfer system (Bio-Rad) in NuPAGE Transfer Buffer (Invitrogen). The membrane was processed as described above, before imaging on the ChemiDoc Imaging System (Bio-Rad). Densitometry was performed using ImageJ.

For quantitative analysis, the signal intensity of γ-tubulin in each fraction was divided by the sum of the signal intensities of γ-tubulin in all of the fractions.

Fixed cell microtubule regrowth assay

Cells were grown on pre-sterilized 12-mm-diameter glass coverslips (Fisher) in a 10cm-tissue culture dish. Coverslips for individual time-points were taken from the same culture dish. One coverslip for each experiment was fixed in Fixation Buffer (described above) prior to nocodazole treatment to confirm the phenotype of the cell sample. To minimize the loss of mitotic cells, coverslips were transferred to new dishes containing the indicated buffers. First, coverslips were incubated in 10 µM nocodazole diluted in DMEM +10% FBS +1 µg/mL Dox for 1 hour at 37°C. Coverslips were then transferred to an ice block for an additional 1 hour incubation. Coverslips were then washed 4x, 15 seconds per wash, in warm (37°C) Wash Media (DMEM +10% FBS +1 µg/mL Dox +0.1% DMSO), after which the coverslips were incubated at 37°C, followed by fixation at the indicated time points. One coverslip for each experiment was fixed prior to the wash step to confirm complete microtubule depolymerization (indicated as time point 0 in Figure S2I). Cells were processed for immunofluorescence as described above.

Western blot analysis of cells processed for microtubule regrowth assays confirmed that nocodazole treatment and ice incubation did not affect the expression patterns of the shRNA targeting endogenous γ-tubulin or of γ-tubulin-GFP (WT and ΔGTP).

Live cell imaging

Imaging was performed on a Nikon Eclipse Ti2-E equipped with a Yokogawa W1 confocal scanning unit, a z piezo stage, and a 100X oil objective (Plan Apo, 1.45 NA). The microscope was fitted with an environmental chamber enclosure and heated to 37°C with the AirTherm SMT heating system (WPI). Fluorescence from the GFP and SiR-Tubulin channels were excited with a 100mW 488 nm (Coherent) and 75mW 640 nm (Coherent) laser respectively. Both lasers were transmitted to the sample using a custom Yokogawa quad notch filter (405-480-561-640) and fluorescence was filtered using an ET 520/40m (Chroma Technology) and ET 670/50m (Chroma Technology) for the GFP and SiR-Tubulin channels respectively. Fluorescence was directed onto a Prime 95B sCMOS camera (Photometrics) and images were recorded using NIS-Elements software (Nikon).

Live cell microtubule regrowth assay

Cells were grown on pre-sterilized 22x22-mm square glass coverslips (Fisher) in a 10cm-tissue culture dish. To minimize the loss of mitotic cells, coverslips were transferred to new dishes containing the indicated buffers. First, coverslips were incubated in 10 µM nocodazole diluted in DMEM +10%FBS +1 µg/mL Dox for 1 hour at 37°C. Coverslips were then washed 4x, 15 seconds per wash, in cold (4°C) Wash Media (Leibovitz's L-15 (Gibco) +10% FBS +1 µg/mL Dox +0.1% DMSO). Coverslips were then incubated on an

ice block in cold (0°C) Leibovitz's L-15 media +1 µg/mL Dox +100 nM SiR-Tubulin (Cytoskeleton) for 1 hour. Coverslips were then assembled in a custom Rose chamber in warm (37°C) Leibovitz's L-15 media +10% FBS +1 µg/mL Dox +100 nM SiR-Tubulin. Imaging was initiated within 3 minutes after the coverslips were removed from the ice incubation. The positions of several cells on a coverslip were recorded by imaging with DIC, and these cells were imaged every 5 minutes. With 0.3-µm spacing between Z-planes, images were taken through 5 µm in the center of the cell, with 50-ms exposure in the GFP channel, and 150-ms exposure in the SiR-Tubulin channel. DIC images were used to align cells throughout each time point.

Live cell imaging of mitotic transition in GCP6 cell lines

Cells were grown on pre-sterilized 22x22-mm square glass coverslips (Fisher) in a 10cm-tissue culture dish. ~1 hour preceding imaging, the live cell DNA dye JF-646 Hoechst (Janelia) was added to the culture media at a 1:8000 dilution. Coverslips were then assembled in a custom Rose chamber in warm (37°C) Leibovitz's L-15 media +10% FBS +1 µg/mL Dox +JF-646 Hoechst. The position of cells with compacted chromosomes entering prophase were identified by DIC and recorded, and these cells were imaged every 3-5 minutes. With 0.3-µm spacing between Z-planes, images were taken through 10 µm in the center of the cell, with 50-ms exposure in the GFP channel, and 150-ms exposure in the JF-646 Hoechst channel. DIC images were used to align cells throughout each time point.

Counting microtubule foci

The raw images of cells undergoing live microtubule regrowth were compiled as MIPs. To quantify the number of microtubule foci, the following standard FIJI tools were applied. First, a signal intensity threshold of >90% was applied, followed by binarization of the image. The signal was then segmented using the Watershed plugin. A segmented particle greater than 1 μm^2 was counted as a microtubule foci.

Purification of GFP nanobody

6 liters of BL21 cells expressing pET21-PelB-GFP nanobody clone LaG16 were induced with 0.1mM IPTG for 18 hours at 18°C. Cells were harvested at 5,000xg for 10 minutes at 4°C using a JLA 8.100 rotor. Cell pellets were immediately resuspended in 10mL of TES buffer (200 mM Tris-HCl, pH 8, 0.5 mM EDTA, 500 mM sucrose) per pellet equivalent to 1 liter of culture. 15 mL of TES diluted 1:4 in H_2O was added to the resuspended pellets, followed by incubation on ice for 30 minutes. The resuspended pellets were then centrifuged at 6,000xg for 10 min at 4°C using a JLA 8.100 rotor. The supernatant was further clarified at 48,000xg for 15 minutes at 4°C using a Type 45 Ti rotor. After the supernatant was collected, NaCl was added to 150mM from a 5M stock, after which it was incubated with Ni-NTA resin (Qiagen) pre-equilibrated in binding buffer (20 mM Tris-HCl, pH 8, 150mM NaCl) for 30 min at 4°C. The resin was then washed with 40mL of wash buffer 1 (20 mM Tris-HCl, pH 8, 900mM NaCl), followed by 40mL of wash buffer 2 (20 mM Tris-HCl, pH 8, 150mM NaCl, 10mM imidazole). 1mL elution buffer (20 mM Tris-HCl, pH 8, 150mM NaCl, 250mM imidazole) was added to the resin and collected, for a total of ~15 fractions. Peak fractions were identified using Bradford reagent (Bio-Rad) and concentrated to <500µL using a 10kDa molecular weight cut off filter (Millipore). The concentrated eluate was then gel filtered on a Superdex 10/300 column pre-

equilibrated in gel filtration buffer (100mM $NaHCO_3$, pH 8.0, 150mM NaCl), and the GFP nanobody eluted at ~7-8mL. The GFP nanobody was coupled to the indicated resin either immediately or the next day.

Coupling GFP nanobody to NHS-sepharose

Coupling of purified GFP nanobady to NHS-sepharose resin was performed as described in (Widlund et al. 2012). Briefly, 1mL of NHS-sepharose FastFlow resin (Sigma, H8280) was centrifuged for 5 min at 500xg at 4°C. The supernatant was discarded, and the resin was resuspended in 1mL of ice cold 1mM HCl. The resin was centrifuged for 5 min at 500xg at 4°C. The resin was then resuspended in a volume equivalent to >10mg of GFP nanobody and incubated with rotation for 30 minutes at room temperature. Unreacted NHS groups were blocked by incubating the resin in 3mL blocking buffer (0.5mM ethanolamine, pH 8, 0.5M NaCl) for 30 minutes at room temperature with rotation. The resin was washed with 3mL 6x PBS, and then resuspended in 1x PBS supplemented with 80% glycerol. The coupled resin was stored at -20°C.

Coupling GFP nanobody to M270 Epoxy Dynabeads

M270 Epoxy Dynabeads (ThermoFisher, 14301) were diluted to 30mg/mL in DMF and stored at 4°C until ready for coupling. 25mg of beads were resuspended and washed 2x in 1mL freshly prepared 0.1M $NaPO_4$. During each wash, the beads were vortexed on low speed for ~10 seconds, and then incubated at room temperature for 10 minutes. In a separate tube, 450µL of GFP nanobody (~2-3mg/mL) were mixed with 883µL of 0.1M $NaPO_4$. 667µL of freshly prepared 3M NH_4SO_4 was added to the antibody mix dropwise, while mixing using a vortex. 500µL of antibody mix was then incubated with 25mg of washed beads overnight at 37°C with rotation. The beads were separated from the antibody

mix using a magnetic tube rack. The antibody mix was aspirated, and the beads were quickly washed 1mL of 100mM glycine, followed by 1mL Tris, pH 8.8. The beads were then quickly washed with 100mM triethylamine, followed by 1x PBS. The beads were washed 2x with PBS + 0.5% Triton-X 100, first for 5 minutes and then for 15 minutes with rotation. The beads were resuspended in storage buffer (PBS, pH 7.4, 0.5mg/mL BSA, 0.02% NaN_3, 50% glycerol), aliquoted and stored at -20°C.

Affinity purification of γ-tubulin-GFP

HeLa TREx cells harboring inducible expression of RNAi-resistant γ-tubulin-GFP and shRNA targeting endogenous γ-tubulin were grown in the presence of doxycycline (1μg/mL) for 60-72 hours. ~5g of cells (equivalent to 60x15cm^2 circular plates) were collected by scraping the cells in the culture media, pelleting the cells at 1000xg for 3 minutes at 4°C, washing the cell pellet in PBS, and pelleting the cells again. The cell pellet was resuspended in ~1mL of PBS in a 3mL syringe. The cells were pelleted inside the syringe by centrifugation at 1000xg for 3 minutes at 4°C. After aspirating the supernatant, the cells were slowly ejected from the syringe into a container of liquid nitrogen in order to form small frozen pellets of cells. These pellets were then cryomilled into a fine cell powder in a planetary ball mill PM 100 (Retsch; see http://lab.rockefeller.edu/rout/protocols and LaCava, Jiang, and Rout 2016). 100mg of cell powder was resuspended in 500 μL extraction buffer (40 mM HEPES, pH 7.5, 150 mM NaCl, 1 mM MgCl2, 1mM EGTA, 1mM DTT, 0.5% NP-40, 0.1 mM MgGTP, cOmplete EDTA-free Protease Inhibitor Cocktail tablets (Roche), 1 mM PMSF). After two consecutive clarification steps at 16,000xg for 10 minutes each, the lysate was incubated with 15μL of GFP nanobody-conjugated dynabeads for 1 hour at 4°C with rotation. The

beads were washed 3x in extraction buffer, and moved to a new tube after the second wash. Proteins were eluted from the beads in 45µL extraction buffer with 1.1x LDS buffer (Invitrogen, NP0007) at 70°C for 10 minutes while shaking at 1000rpm. The eluate was moved to a separate tube, and supplemented with a final concentration of 50mM DTT. All samples were then boiled at 95°C, followed by SDS-PAGE. For western blot analysis, the samples were run for 45 minutes at 185V, and processed as described above.

Label-free quantitative mass spectrometry

For mass spectrometry analyses, samples were heated at 70ºC for 10 minutes with agitation and allowed to cool to room temperature. To alkylate reduced cysteines, add 1µl of 1M iodoacetamide was added per 10 µL of sample. Alkylation was allowed to proceed for 30 minutes at room temperature, protected from light. The samples were then run on 12-well NuPAGE 10% Tris-Bis gels in MOPS running buffer with antioxidant, at 180V for ~5 minutes until the samples entered the gel as a single "plug." The gel was then placed in a sterile 15cm^2 tissue culture plate, and stained and fixed with coomasie solution (0.5% R250 coomassie in 45%/45%/10% of H2O/Methanol/Acetic acid) for 5 min. The gel was then rinsed with destain solution (16% methanol, 10% acetic acid) overnight.

The sample was further processed for mass spectrometry analysis by Dr. Wenzhu Zhang in the lab of Dr. Brian Chait. In brief, the gel plug was excised, cut into small pieces with a sharp blade, destained using 50mM NH_4HCO_3 in 50% MeOH: 50% H_2O to efficiently remove the Coomassie blue, and digested with trypsin. The resulting peptides were extracted from the gel using a sequential process involving the use of 200µl ACN followed by 40µl of 10% Formic acid in 50%ACN:50%H2O, and then adding 200µl 0.2%TFA in 50%ACN:50%H2O. The pooled peptide solution was subjected to repeated centrifugation

to remove gel debris and depletion of ACN using a SpeedVac vacuum concentrator. The peptides were then bound to C18 StageTips, which were produced in-house. Peptides eluted from the StageTip were loaded onto an Easy-Spray reversed phase HPLC column (ES800A, Thermo Fisher Scientific) and analyzed by liquid chromatography–mass spectrometry (LCMS) using an Orbitrap Q Exactive Plus mass spectrometer (Thermo Fisher Scientific) coupled with an Easy-nLC system (Thermo Fisher Scientific). Protein identification was performed using the GPM software (Beavis 2006) by searching against a human protein sequence database. Label-free quantification of the core γ-TuRC proteins was calculated by the SpectroMine software (Biognosys AG, Schlieren, Switzerland), and normalized to the known stoichiometries of GCP2, GCP3, GCP5, and GCP6.

Proteins listed in Tables 3.1 and 3.2 were identified in 4 individual replicates (2 biological replicates, each with 2 technical replicates) with an E value cutoff of 10^{-90}, unless otherwise indicated. One replicate was performed with pre-treatment of the cells with 10 μM nocodazole for 2 hours in order to depolymerize microtubules and limit indirect interactions with the γ-TuRC. The reported values are from the nocodazole treated replicate, although no significant differences were found between the proteins identified in the nocodazole treated or DMSO treated samples.

Affinity purification and sucrose gradient analysis of GCP6-PreScission-GFP

The following protocol was used to affinity purify GFP-tagged GCP6 from the $GCP6^{FL}$, $GCP6^{\Delta NHD}$, and $GCP6^{\Delta N\text{-}Belt}$ cell lines. A cell pellet equivalent to 1x 500cm^2 plate (collected as described previously) was resuspended in 1mL of lysis buffer (40 mM HEPES, pH 7.5, 150 mM KCl, 1 mM MgCl2, 1mM EGTA, 1mM DTT, 0.1% NP-40, 0.1 mM MgGTP, cOmplete EDTA-free Protease Inhibitor Cocktail tablets (Roche), 1 mM PMSF) on ice.

The cells were lysed by dounce homogenization, 50 strokes on ice. The lysates were clarified for 20 minutes at 16,000xg at 4°C. 20µL of GFP nanobody-conjugated sepharose resin were added to the lysate and incubated for 30 minutes at 4°C with rotation. The resin was washed 2x with 1mL of wash buffer (40 mM HEPES, pH 7.5, 150 mM KCl, 1 mM MgCl2, 1mM EGTA, 1mM DTT, 0.01% NP-40, 0.1 mM MgGTP), and then incubated with 100µL of 200µg/mL PreScission Protease (diluted 1:4 in wash buffer) for 2 hours at 4°C with rotation. The supernatant was then loaded onto a 2mL 5-40% sucrose gradient, prepared as described above in the wash buffer. The sucrose gradients were centrifuged at 50,000rpm for 3 hours in a TLS55 rotor, with slow acceleration and no brake. The sucrose gradients were fractionated manually using a cut p1000 pipette tip. The fractionated samples were analyzed by western blot, as described above.

References

Aher, Amol, Maurits Kok, Ashwani Sharma, Ankit Rai, Natacha Olieric, Ruddi Rodriguez-Garcia, Eugene A. Katrukha, et al. 2018. "CLASP Suppresses Microtubule Catastrophes through a Single TOG Domain." *Developmental Cell* 46 (1): 40–58.e8.

Akhmanova, Anna, and Casper C. Hoogenraad. 2015. "Microtubule Minus-End-Targeting Proteins." *Current Biology: CB* 25 (4): R162–71.

Akhmanova, Anna, and Lukas C. Kapitein. 2022. "Mechanisms of Microtubule Organization in Differentiated Animal Cells." *Nature Reviews. Molecular Cell Biology* 23 (8): 541–58.

Akhmanova, Anna, and Michel O. Steinmetz. 2015. "Control of Microtubule Organization and Dynamics: Two Ends in the Limelight." *Nature Reviews. Molecular Cell Biology* 16 (12): 711–26.

Aldaz, Hector, Luke M. Rice, Tim Stearns, and David A. Agard. 2005. "Insights into Microtubule Nucleation from the Crystal Structure of Human γ-Tubulin." *Nature* 435 (7041): 523–27.

Alfaro-Aco, Raymundo, Akanksha Thawani, and Sabine Petry. 2017. "Structural Analysis of the Role of TPX2 in Branching Microtubule Nucleation." *The Journal of Cell Biology* 216 (4): 983–97.

Anders, K. R., and D. Botstein. 2001. "Dominant-Lethal Alpha-Tubulin Mutants Defective in Microtubule Depolymerization in Yeast." *Molecular Biology of the Cell* 12 (12): 3973–86.

Atherton, Joseph, Yanzhang Luo, Shengqi Xiang, Chao Yang, Ankit Rai, Kai Jiang, Marcel Stangier, et al. 2019. "Structural Determinants of Microtubule Minus End Preference in CAMSAP CKK Domains." *Nature Communications* 10 (1). https://doi.org/10.1038/s41467-019-13247-6.

Ayaz, Pelin, Xuecheng Ye, Patrick Huddleston, Chad a. Brautigam, and Luke M. Rice. 2012. "A TOG : αβ-Tubulin Complex Structure." *Science* 337 (6096): 857–60.

Bahi-Buisson, Nadia, Karine Poirier, Franck Fourniol, Yoann Saillour, Stéphanie Valence, Nicolas Lebrun, Marie Hully, et al. 2014. “The Wide Spectrum of Tubulinopathies: What Are the Key Features for the Diagnosis?” *Brain: A Journal of Neurology* 137 (Pt 6): 1676–1700.

Bahtz, Ramona, Joerg Seidler, Marc Arnold, Uta Haselmann-Weiss, Claude Antony, Wolf D. Lehmann, and Ingrid Hoffmann. 2012. “GCP6 Is a Substrate of Plk4 and Required for Centriole Duplication.” *Journal of Cell Science* 125 (2): 486–96.

Ballinger, Mandy L., Swetansu Pattnaik, Piyushkumar A. Mundra, Milita Zaheed, Emma Rath, Peter Priestley, Jonathan Baber, et al. 2023. “Heritable Defects in Telomere and Mitotic Function Selectively Predispose to Sarcomas.” *Science* 379 (6629): 253–60.

Baumgart, Johannes, Marcel Kirchner, Stefanie Redemann, Alec Bond, Jeffrey B. Woodruff, Jean-Marc Verbavatz, Frank Jülicher, Thomas Müller-Reichert, Anthony A. Hyman, and Jan Brugués. 2019. “Soluble Tubulin Is Significantly Enriched at Mitotic Centrosomes.” *The Journal of Cell Biology* 218 (12): jcb.201902069.

Beavis, Ronald C. 2006. “Using the Global Proteome Machine for Protein Identification.” In *New and Emerging Proteomic Techniques*, edited by Dobrin Nedelkov and Randall W. Nelson, 217–28. Totowa, NJ: Humana Press.

Benaud, Christelle, Gaëlle Le Dez, Svetlana Mironov, Federico Galli, David Reboutier, and Claude Prigent. 2015. “Annexin A2 Is Required for the Early Steps of Cytokinesis.” *EMBO Reports* 16 (4): 481–89.

Berman, Adi Y., Michal Wieczorek, Amol Aher, Paul Dominic B. Olinares, Brian T. Chait, and Tarun M. Kapoor. 2023. “A Nucleotide Binding–independent Role for γ-Tubulin in Microtubule Capping and Cell Division.” *The Journal of Cell Biology* 222 (3). https://doi.org/10.1083/jcb.202204102.

Bond, Jacquelyn, Emma Roberts, Kelly Springell, Sofia B. Lizarraga, Sheila Scott, Julie Higgins, Daniel J. Hampshire, et al. 2005. “A Centrosomal Mechanism Involving CDK5RAP2 and CENPJ Controls Brain Size.” *Nature Genetics* 37 (4): 353–55.

Brilot, Axel F., Andrew S. Lyon, Alex Zelter, Shruthi Viswanath, Alison Maxwell, Michael J. Maccoss, Eric G. Muller, Andrej Sali, Trisha N. Davis, and David A. Agard. 2021. “CM1-Driven Assembly and Activation of Yeast g-Tubulin Small Complex Underlies Microtubule Nucleation” 1: 1–35.

Brock, Stefanie, Katrien Stouffs, Emmanuel Scalais, Marc D’Hooghe, Kathelijn Keymolen, Renzo Guerrini, William B. Dobyns, Nataliya Di Donato, and Anna C. Jansen. 2018. “Tubulinopathies Continued: Refining the Phenotypic Spectrum Associated with Variants in TUBG1.” *European Journal of Human Genetics: EJHG* 26 (8): 1132–42.

Brouhard, Gary J., and Luke M. Rice. 2018. “Microtubule Dynamics: An Interplay of Biochemistry and Mechanics.” *Nature Reviews. Molecular Cell Biology* 19 (7): 451–63.

Brown, C. Randell, Stephen J. Doxsey, Ly Q. Hong-Brown, Robert L. Martin, and William J. Welch. 1996. “Molecular Chaperones and the Centrosome: A role for TCP-1 in microtubule nucleation.” *The Journal of Biological Chemistry* 271 (2): 824-832.

Bucciarelli, Elisabetta, Claudia Pellacani, Valeria Naim, Antonella Palena, Maurizio Gatti, and Maria Patrizia Somma. 2009. “Drosophila Dgt6 Interacts with Ndc80, Msps/XMAP215, and γ-Tubulin to Promote Kinetochore-Driven MT Formation.” *Current Biology: CB* 19 (21): 1839–45.

Carlier, Marie-France, and Shashank Shekhar. 2017. “Global Treadmilling Coordinates Actin Turnover and Controls the Size of Actin Networks.” *Nature Reviews. Molecular Cell Biology* 18 (6): 389–401.

Chaaban, Sami, and Gary J. Brouhard. 2017. “A Microtubule Bestiary: Structural Diversity in Tubulin Polymers.” *Molecular Biology of the Cell* 28: 2924-2931.

Chaaban, Sami, Shashank Jariwala, Chieh Ting Hsu, Stefanie Redemann, Justin M. Kollman, Thomas Müller-Reichert, David Sept, Khanh Huy Bui, and Gary J. Brouhard. 2018. “The Structure and Dynamics of C. Elegans Tubulin Reveals the Mechanistic Basis of Microtubule Growth.” *Developmental Cell* 47 (2): 191–204.e8.

Cheeseman, Iain M., and Arshad Desai. 2008. “Molecular Architecture of the Kinetochore-Microtubule Interface.” *Nature Reviews Molecular Cell Biology*. https://doi.org/10.1038/nrm2310.

Chen, Fangrui, Jingchao Wu, Malina K. Iwanski, Daphne Jurriens, Arianna Sandron, Milena Pasolli, Gianmarco Puma, et al. 2022. “Self-Assembly of Pericentriolar Material in Interphase Cells Lacking Centrioles.” *eLife* 11 (July). https://doi.org/10.7554/eLife.77892.

Chen, Yalei, Nathan C. Deffenbaugh, Charles T. Anderson, and William O. Hancock. 2014. “Molecular Counting by Photobleaching in Protein Complexes with Many Subunits: Best Practices and Application to the Cellulose Synthesis Complex.” *Molecular Biology of the Cell* 25 (22): 3630–42.

Choi, Yuk-Kwan, Pengfei Liu, Siu Kwan Sze, Chao Dai, and Robert Z. Qi. 2010. “CDK5RAP2 Stimulates Microtubule Nucleation by the γ-Tubulin Ring Complex.” *The Journal of Cell Biology* 191 (6): 1089–95.

Chrétien, D., S. D. Fuller, and E. Karsenti. 1995. “Structure of Growing Microtubule Ends: Two-Dimensional Sheets Close into Tubes at Variable Rates.” *The Journal of Cell Biology* 129 (5): 1311–28.

Consolati, Tanja, Julia Locke, Johanna Roostalu, Zhuo Angel Chen, Julian Gannon, Jayant Asthana, Wei Ming Lim, et al. 2020. “Microtubule Nucleation Properties of Single Human γ-TuRCs Explained by Their Cryo-EM Structure.” *Developmental Cell* 53: 1–15.

Coquand, Laure, Guiliana Soraya Victoria, Alice Tata, Jacopo Amerigo Carpentieri, Jean-Baptiste Brault, Fabien Guimiot, Vincent Fraisier, and Alexandre D. Baffet. 2021. “CAMSAPs Organize an Acentrosomal Microtubule Network from Basal Varicosities in Radial Glial Cells.” *The Journal of Cell Biology* 220 (8): 1-12.

David, Ana F., Philippe Roudot, Wesley R. Legant, Eric Betzig, Gaudenz Danuser, and Daniel W. Gerlich. 2019. “Augmin Accumulation on Long-Lived Microtubules Drives Amplification and Kinetochore-Directed Growth.” *The Journal of Cell Biology*: 2150-2168.

Delgehyr, Nathalie, James Sillibourne, and Michel Bornens. 2005. “Microtubule Nucleation and Anchoring at the Centrosome Are Independent Processes Linked by Ninein Function.” *Journal of Cell Science* 118 (Pt 8): 1565–75.

De Wever, Veerle, David C. Lloyd, Isha Nasa, Mhairi Nimick, Laura Trinkle-Mulcahy, Robert Gourlay, Nick Morrice, and Greg B. G. Moorhead. 2012. “Isolation of Human Mitotic Protein Phosphatase Complexes: Identification of a Complex between Protein Phosphatase 1 and the RNA Helicase Ddx21.” *PloS One* 7 (6): e39510.

Di Bartolomeo, Sabrina, Marco Corazzari, Francesca Nazio, Serafina Oliverio, Gaia Lisi, Manuela Antonioli, Vittoria Pagliarini, et al. 2010. “The Dynamic Interaction of AMBRA1 with the Dynein Motor Complex Regulates Mammalian Autophagy.” *The Journal of Cell Biology* 191 (1): 155–68.

Dictenberg, J. B., W. Zimmerman, C. A. Sparks, A. Young, C. Vidair, Y. Zheng, W. Carrington, F. S. Fay, and S. J. Doxsey. 1998. “Pericentrin and γ-Tubulin Form a Protein Complex and Are Organized into a Novel Lattice at the Centrosome.” *The Journal of Cell Biology* 141 (1): 163–74.

Dobrynin, Grzegorz, Oliver Popp, Tina Romer, Sebastian Bremer, Michael H. A. Schmitz, Daniel W. Gerlich, and Hemmo Meyer. 2011. “Cdc48/p97-Ufd1-Npl4 Antagonizes Aurora B during Chromosome Segregation in HeLa Cells.” *Journal of Cell Science* 124 (9): 1571–80.

Ducat, Daniel, Shin Ichi Kawaguchi, Hongbin Liu, John R. Yates, and Yixian Zheng. 2008. “Regulation of Microtubule Assembly and Organization in Mitosis by the AAA+ ATPase Pontin.” *Molecular Biology of the Cell* 19 (7): 3097–3110.

Dumont, Julien, and Arshad Desai. 2012. “Acentrosomal Spindle Assembly and Chromosome Segregation during Oocyte Meiosis.” *Trends in Cell Biology* 22 (5): 241–49.

Efimov, Andrey, Alexey Kharitonov, Nadia Efimova, Jadranka Loncarek, Paul M. Miller, Natalia Andreyeva, Paul Gleeson, et al. 2007. “Asymmetric CLASP-Dependent Nucleation of Noncentrosomal Microtubules at the Trans-Golgi Network.” *Developmental Cell* 12 (6): 917–30.

Elting, Mary Williard, Christina L. Hueschen, Dylan B. Udy, and Sophie Dumont. 2014. “Force on Spindle Microtubule Minus Ends Moves Chromosomes.” *The Journal of Cell Biology* 206 (2): 245–56.

Ennulat, D. J., R. K. Liem, G. A. Hashim, and M. L. Shelanski. 1989. “Two Separate 18-Amino Acid Domains of Tau Promote the Polymerization of Tubulin.” *The Journal of Biological Chemistry* 264 (10): 5327–30.

Euteneuer, U., and J. R. McIntosh. 1981. “Structural Polarity of Kinetochore Microtubules in PtK1 Cells.” *The Journal of Cell Biology* 89 (2): 338–45.

Farache, Dorian, Alain Jauneau, Cécile Chemin, Marine Chartrain, Marie Hélene Rémy, Andreas Merdes, and Laurence Haren. 2016. “Functional Analysis of γ-Tubulin Complex Proteins Indicates Specific Lateral Association via Their N-Terminal Domains.” *The Journal of Biological Chemistry* 291 (44): 23112–25.

Fielding, Andrew B., Iveta Dobreva, Paul C. McDonald, Leonard J. Foster, and Shoukat Dedhar. 2008. “Integrin-Linked Kinase Localizes to the Centrosome and Regulates Mitotic Spindle Organization.” *The Journal of Cell Biology* 180 (4): 681–89.

Fong, Ka-Wing, Yuk Kwan Choi, Jerome B. Rattner, and Robert Z. Qi. 2008. “CDK5RAP2 Is a Pericentriolar Protein That Functions in Centrosomal Attachment of the γ-Tubulin Ring Complex.” *Molecular Biology of the Cell* 19 (January): 115–25.

Fridy, Peter C., Yinyin Li, Sarah Keegan, Mary K. Thompson, Ilona Nudelman, Johannes F. Scheid, Marlene Oeffinger, et al. 2014. “A Robust Pipeline for Rapid Production of Versatile Nanobody Repertoires.” *Nature Methods* 11 (12): 1253–60.

Fuchs, Elaine, and Iakowos Karakesisoglou. 2001. “Bridging Cytoskeletal Intersections.” *Genes & Development* 15: 1-14.

Gaglio, T., A. Saredi, and D. A. Compton. 1995. “NuMA Is Required for the Organization of Microtubules into Aster-like Mitotic Arrays.” *The Journal of Cell Biology* 131 (3): 693–708.

Gavilan, Maria P., Pablo Gandolfo, Fernando R. Balestra, Francisco Arias, Michel Bornens, and Rosa M. Rios. 2018. “The Dual Role of the Centrosome in Organizing the Microtubule Network in Interphase.” *EMBO Reports* 19 (11): 1-21.

Ginsburg, Avi, Asaf Shemesh, Abigail Millgram, Raviv Dharan, Yael Levi-Kalisman, Israel Ringel, and Uri Raviv. 2017. “Structure of Dynamic, Taxol-Stabilized, and GMPPCP-Stabilized Microtubule.” *The Journal of Physical Chemistry. B* 121 (36): 8427–36.

Goddard, Thomas D., Conrad C. Huang, Elaine C. Meng, Eric F. Pettersen, Gregory S. Couch, John H. Morris, and Thomas E. Ferrin. 2018. “UCSF ChimeraX: Meeting Modern Challenges in Visualization and Analysis.” *Protein Science: A Publication of the Protein Society* 27 (1): 14–25.

Goldberg, Jonathan. 1998. “Structural Basis for Activation of ARF GTPase: Mechanisms of Guanine Nucleotide Exchange and GTP–Myristoyl Switching.” *Cell* 95 (2): 237–48.

Gombos, Linda, Annett Neuner, Mykhaylo Berynskyy, Luca L. Fava, Rebecca C. Wade, Carsten Sachse, and Elmar Schiebel. 2013. “GTP Regulates the Microtubule Nucleation Activity of γ-Tubulin.” *Nature Cell Biology* 15 (11): 1317–27.

Goshima, Gohta, Mirjam Mayer, Nan Zhang, Nico Stuurman, and Ronald D. Vale. 2008. “Augmin: A Protein Complex Required for Centrosome-Independent Microtubule Generation within the Spindle.” *The Journal of Cell Biology* 181 (3): 421–29.

Gruss, Oliver J., Malte Wittmann, Hideki Yokoyama, Rainer Pepperkok, Thomas Kufer, Herman Silljé, Eric Karsenti, Iain W. Mattaj, and Isabelle Vernos. 2002. “Chromosome-Induced Microtubule Assembly Mediated by TPX2 Is Required for Spindle Formation in HeLa Cells.” *Nature Cell Biology* 4 (11): 871–79.

Gudimchuk, Nikita B., Evgeni V. Ulyanov, Eileen O’Toole, Cynthia L. Page, Dmitrii S. Vinogradov, Garry Morgan, Gabriella Li, et al. 2020. “Mechanisms of Microtubule Dynamics and Force Generation Examined with Computational Modeling and Electron Cryotomography.” *Nature Communications* 11 (1): 3765.

Gunawardane, Ruwanthi N., Ona C. Martin, Kan Cao, Lijun Zhang, Kimberly Dej, Akihiro Iwamatsu, and Yixian Zheng. 2000. “Characterization and Reconstitution of Drosophila γ-Tubulin Ring Complex Subunits.” *The Journal of Cell Biology* 151 (7): 1513–24.

Hallen, Mark A., Jianghai Ho, Christine D. Yankel, and Sharyn A. Endow. 2008. “Fluorescence Recovery Kinetic Analysis of γ-Tubulin Binding to the Mitotic Spindle.” *Biophysical Journal* 95 (6): 3048–58.

Hannak, Eva, Karen Oegema, Matthew Kirkham, Pierre Gönczy, Bianca Habermann, and Anthony A. Hyman. 2002. “The Kinetically Dominant Assembly Pathway for Centrosomal Asters in Caenorhabditis Elegans Is γ-Tubulin Dependent.” *The Journal of Cell Biology* 157 (4): 591–602.

Haren, Laurence, Dorian Farache, Laurent Emorine, and Andreas Merdes. 2020. “A Stable Sub-Complex between GCP4, GCP5 and GCP6 Promotes the Assembly of Tubulin Ring Complexes.” *Journal of Cell Science* 133 (11): 1-14.

Haren, Laurence, Marie Hélène Remy, Ingrid Bazin, Isabelle Callebaut, Michel Wright, and Andreas Merdes. 2006. “NEDD1-Dependent Recruitment of the γ-Tubulin Ring Complex to the Centrosome Is Necessary for Centriole Duplication and Spindle Assembly.” *The Journal of Cell Biology* 172 (4): 505–15.

Haren, Laurence, Tim Stearns, and Jens Lüders. 2009. “Plk1-Dependent Recruitment of γ-Tubulin Complexes to Mitotic Centrosomes Involves Multiple PCM Components.” *PloS One* 4 (6): 1-10.

Heald, Rebecca, and Alexey Khodjakov. 2015. “Thirty Years of Search and Capture: The Complex Simplicity of Mitotic Spindle Assembly.” *The Journal of Cell Biology* 211 (6): 1103–11.

Heald, Rebecca, Regis Tournebize, Thiemo Blankt, Raphael Sandaltzopoulost, Peter Beckert, Anthony Hyman, and Eric Karsenti. 1996. “Self-Organization of Microtubules into Bipolar Spindles around Artificial Chromosomes in Xenopus Egg Extracts.” *Nature* 382: 420-425.

He, Liu, Lotte van Beem, Berend Snel, Casper C. Hoogenraad, and Martin Harterink. 2022. “PTRN-1 (CAMSAP) and NOCA-2 (NINEIN) Are Required for Microtubule Polarity in Caenorhabditis Elegans Dendrites.” *PLoS Biology* 20 (11): e3001855.

Henkin, Gil, Cláudia Brito, Claire Thomas, and Thomas Surrey. 2023. “The Minus End Depolymerase KIF2A Drives Flux-like Treadmilling of γ-TuRC-Uncapped Microtubules.” *bioRxiv*. https://doi.org/10.1101/2023.04.06.535808.

Hernández-Vega, Amayra, Marcus Braun, Lara Scharrel, Marcus Jahnel, Susanne Wegmann, Bradley T. Hyman, Simon Alberti, Stefan Diez, and Anthony A. Hyman. 2017. “Local Nucleation of Microtubule Bundles through Tubulin Concentration into a Condensed Tau Phase.” *Cell Reports* 20 (10): 2304–12.

Hoffmann, Ingrid. 2021. “Centrosomes in Mitotic Spindle Assembly and Orientation.” *Current Opinion in Structural Biology* 66 (February): 193–98.

Hooikaas, Peter Jan, Maud Martin, Tobias Mühlethaler, Gert Jan Kuijntjes, Cathelijn A. E. Peeters, Eugene A. Katrukha, Luca Ferrari, et al. 2019. “MAP7 Family Proteins Regulate Kinesin-1 Recruitment and Activation.” *The Journal of Cell Biology* 218 (4): 1298–1318.

Huang, Tzu Lun, Hsiu Jung Wang, Ya Chieh Chang, Shao Win Wang, and Kuo Chiang Hsia. 2020. “Promiscuous Binding of Microprotein Mozart1 to γ-Tubulin Complex Mediates Specific Subcellular Targeting to Control Microtubule Array Formation.” *Cell Reports* 31 (13): 107836.

Hueschen, Christina L., Samuel J. Kenny, Ke Xu, and Sophie Dumont. 2017. “NuMA Recruits Dynein Activity to Microtubule Minus-Ends at Mitosis.” *eLife* 6: 1–26.

Hutchins, James R. A., Yusuke Toyoda, Björn Hegemann, Ina Poser, Jean-Karim Hériché, Martina M. Sykora, Martina Augsburg, et al. 2010. “Systematic Analysis of Human Protein Complexes Identifies Chromosome Segregation Proteins.” *Science* 328 (5978): 593–99.

Isokane, Mayumi, Thomas Walter, Robert Mahen, Bianca Nijmeijer, Jean-Karim Hériché, Kota Miura, Stefano Maffini, et al. 2016. “ARHGEF17 Is an Essential Spindle Assembly Checkpoint Factor That Targets Mps1 to Kinetochores.” *The Journal of Cell Biology* 212 (6): 647–59.

Jiang, Hao, Xiaonan He, Di Feng, Xueliang Zhu, and Yixian Zheng. 2015. “RanGTP Aids Anaphase Entry through Ubr5-Mediated Protein Turnover.” *The Journal of Cell Biology* 211 (1): 7–18.

Jiang, Kai, Shasha Hua, Renu Mohan, Ilya Grigoriev, Kah Wai Yau, Qingyang Liu, Eugene A. Katrukha, et al. 2014. “Microtubule Minus-End Stabilization by Polymerization-Driven CAMSAP Deposition.” *Developmental Cell* 28 (3): 295–309.

Jiang, Kai, Lenka Rezabkova, Shasha Hua, Qingyang Liu, Guido Capitani, A. F. Maarten Altelaar, Albert J. R. Heck, Richard A. Kammerer, Michel O. Steinmetz, and Anna Akhmanova. 2017. “Microtubule Minus-End Regulation at Spindle Poles by an ASPM-Katanin Complex.” *Nature Cell Biology* 19 (5): 480–92.

Jiang, Xueer, Dac Bang Tam Ho, Karan Mahe, Jennielee Mia, Guadalupe Sepulveda, Mark Antkowiak, Linhao Jiang, Soichiro Yamada, and Li-En Jao. 2021. “Condensation of Pericentrin Proteins in Human Cells Illuminates Phase Separation in Centrosome Assembly.” *Journal of Cell Science* 134 (14).

Johmura, Yoshikazu, Nak-Kyun Soung, Jung-Eun Park, Li-Rong Yu, Ming Zhou, Jeong K. Bang, Bo-Yeon Kim, Timothy D. Veenstra, Raymond L. Erikson, and Kyung S. Lee. 2011. “Regulation of Microtubule-Based Microtubule Nucleation by Mammalian Polo-like Kinase 1.” *Proceedings of the National Academy of Sciences of the United States of America* 108 (28): 11446–51.

Kapoor, Tarun M. 2017. “Metaphase Spindle Assembly.” *Biology* 6 (1): 8.

Kapust, R. B., J. Tözsér, J. D. Fox, D. E. Anderson, S. Cherry, T. D. Copeland, and D. S. Waugh. 2001. “Tobacco Etch Virus Protease: Mechanism of Autolysis and Rational Design of Stable Mutants with Wild-Type Catalytic Proficiency.” *Protein Engineering* 14 (12): 993–1000.

Karsenti, E., J. Newport, and M. Kirschner. 1984. “Respective Roles of Centrosomes and Chromatin in the Conversion of Microtubule Arrays from Interphase to Metaphase.” *The Journal of Cell Biology* 99 (1 Pt 2): 47s – 54s.

Keating, Thomas J., and Gary G. Borisy. 2000. “Immunostructural Evidence for the Template Mechanism of Microtubule Nucleation.” *Nature Cell Viology* 2: 352-357.

Kettenbach, Arminja N., Devin K. Schweppe, Brendan K. Faherty, Dov Pechenick, Alexandre A. Pletnev, and Scott A. Gerber. “Quantitative Phosphoproteomics Identifies Substrates and Functional Modules of Aurora and Polo-Like Kinase Activities in Mitotic Cells.” *Science Signaling* 4(179).

Khodjakov, Alexey, Richard W. Cole, Berl R. Oakley, and Conly L. Rieder. 1999. “Centrosome-Independent Mitotic Spindle Formation in Vertebrates.” *Current Biology: CB*, no. 10: 59–67.

Khodjakov, Alexey, and Conly L. Rieder. 1999. “The Sudden Recruitment of γ-Tubulin to the Centrosome at the Onset of Mitosis and Its Dynamic Exchange Throughout the Cell Cycle, Do Not Require Microtubules.” *The Journal of Cell Biology* 146(3): 585-596.

King, Brianna R., Michelle Moritz, Haein Kim, David A. Agard, Charles L. Asbury, and Trisha N. Davis. 2020. “XMAP215 and γ-Tubulin Additively Promote Microtubule Nucleation in Purified Solutions.” *Molecular Biology of the Cell* 31 (20): 2187–94.

King, Matthew R., and Sabine Petry. 2020. “Phase Separation of TPX2 Enhances and Spatially Coordinates Microtubule Nucleation.” *Nature Communications* 11 (1): 270.

Kirschner, Marc, and Timothy J. Mitchison. 1986. “Beyond Self-Assembly: From Microtubules to Morphogenesis.” *Cell* 45 (3): 329–42.

Kitamura, Etsushi, Kozo Tanaka, Shinya Komoto, Yoko Kitamura, Claude Antony, and Tomoyuki U. Tanaka. 2010. “Kinetochores Generate Microtubules with Distal plus Ends: Their Roles and Limited Lifetime in Mitosis.” *Developmental Cell* 18 (2): 248–59.

Klopfenstein, D. R., F. Kappeler, and H. P. Hauri. 1998. “A Novel Direct Interaction of Endoplasmic Reticulum with Microtubules.” *The EMBO Journal* 17 (21): 6168–77.

Kollman, Justin M., Andreas Merdes, Lionel Mourey, and David A. Agard. 2011. "Microtubule Nucleation by γ-Tubulin Complexes." *Nature Reviews. Molecular Cell Biology* 12 (11): 709–21.

Kollman, Justin M., Jessica K. Polka, Alex Zelter, Trisha N. Davis, and David A. Agard. 2010. "Microtubule Nucleating γ-TuSC Assembles Structures with 13-Fold Microtubule-like Symmetry." *Nature* 466 (7308): 879–82.

Kress, Elsa, Françoise Schwager, René Holtackers, Jonas Seiler, François Prodon, Esther Zanin, Annika Eiteneuer, et al. 2012. "The UBXN-2/p37/p47 Adaptors of CDC-48/p97 Regulate Mitosis by Limiting the Centrosomal Recruitment of Aurora A." *The Journal of Cell Biology* 201 (4): 559–75.

Kwiatkowska, Maria, Katarzyna Popłońska, Dariusz Stepiński, and Zygmunt Hejnowicz. 2006. "Microtubules with Different Diameter, Protofilament Number and Protofilament Spacing in Ornithogalum Umbellatum Ovary Epidermis Cells." *Folia Histochemica et Cytobiologica / Polish Academy of Sciences, Polish Histochemical and Cytochemical Society* 44 (2): 133–38.

LaCava, John, Hua Jiang, and Michael P. Rout. 2016. "Protein Complex Affinity Capture from Cryomilled Mammalian Cells." *Journal of Visualized Experiments: JoVE* 2016 (118). https://doi.org/10.3791/54518.

Lampson, Michael A., and Iain M. Cheeseman. 2011. "Sensing Centromere Tension : Aurora B and the Regulation of Kinetochore Function." *Trends in Cell Biology* 21 (3): 133–40.

Lappalainen, Pekka, Tommi Kotila, Antoine Jégou, and Guillaume Romet-Lemonne. 2022. "Biochemical and Mechanical Regulation of Actin Dynamics." *Nature Reviews. Molecular Cell Biology* 23 (12): 836–52.

Lechler, Terry, and Elaine Fuchs. 2007. "Desmoplakin: An Unexpected Regulator of Microtubule Organization in the Epidermis." *The Journal of Cell Biology* 176 (2): 147–54.

Lecland, Nicolas, and Jens Lüders. 2014. "The Dynamics of Microtubule Minus Ends in the Human Mitotic Spindle." *Nature Cell Biology* 16 (8): 770–78.

Liu, Bo, and Yuh-Ru Julie Lee. 2022. "Spindle Assembly and Mitosis in Plants." *Annual Review of Plant Biology* 73 (May): 227–54.

Liu, P., Yuk Kwan Choi, and Robert Z. Qi. 2014. "NME7 Is a Functional Component of the γ-Tubulin Ring Complex." *Molecular Biology of the Cell* 25 (13): 2017–25.

Liu, Peng, Martin Würtz, Erik Zupa, Stefan Pfeffer, and Elmar Schiebel. 2021. "Microtubule Nucleation: The Waltz between γ-Tubulin Ring Complex and Associated Proteins." *Current Opinion in Cell Biology* 68: 124-131.

Liu, Peng, Erik Zupa, Annett Neuner, Anna Böhler, Justus Loerke, Dirk Flemming, Thomas Ruppert, et al. 2019. "Insights into the Assembly and Activation of the Microtubule Nucleator γ-TuRC." *Nature* 578: 467–471.

Lüders, Jens. 2021. "Nucleating Microtubules in Neurons: Challenges and Solutions." *Developmental Neurobiology* 81 (3): 273–83.

Lüders, Jens, Urvashi K. Patel, and Tim Stearns. 2006. "GCP-WD Is a γ-Tubulin Targeting Factor Required for Centrosomal and Chromatin-Mediated Microtubule Nucleation." *Nature Cell Biology* 8 (2): 137–47.

Lüders, Jens, and Tim Stearns. 2007. "Microtubule-Organizing Centres: A Re-Evaluation" *Nature Reviews Molecular and Cell Biology* 8: 161–167.

Lukinavičius, Gražvydas, Luc Reymond, Elisa D'este, Anastasiya Masharina, Fabian Göttfert, Haisen Ta, Angelika Güther, et al. 2014. "Fluorogenic Probes for Live-Cell Imaging of the Cytoskeleton." *Nature Methods* 11 (7): 731–33.

Mahoney, Nicole M., Gohta Goshima, Adam D. Douglass, and Ronald D. Vale. 2006. "Making Microtubules and Mitotic Spindles in Cells without Functional Centrosomes." *Current Biology: CB* 16 (6): 564–69.

Maiani, Emiliano, Giacomo Milletti, Francesca Nazio, Søs Grønbæk Holdgaard, Jirina Bartkova, Salvatore Rizza, Valentina Cianfanelli, et al. 2021. "AMBRA1 Regulates Cyclin D to Guard S-Phase Entry and Genomic Integrity." *Nature* 592 (7856): 799–803.

Maiato, Helder, Conly L. Rieder, and Alexey Khodjakov. 2004. "Kinetochore-Driven Formation of Kinetochore Fibers Contributes to Spindle Assembly during Animal Mitosis." *The Journal of Cell Biology* 167 (5): 831–40.

Manka, Szymon W., and Carolyn A. Moores. 2018. "The Role of Tubulin–tubulin Lattice Contacts in the Mechanism of Microtubule Dynamic Instability." *Nature Structural & Molecular Biology* 25 (7): 607–15.

Martin, Maud, and Anna Akhmanova. 2018. "Coming into Focus: Mechanisms of Microtubule Minus-End Organization." *Trends in Cell Biology* 28 (7): 574–88.

Marty, Michael T., Andrew J. Baldwin, Erik G. Marklund, Georg K. A. Hochberg, Justin L. P. Benesch, and Carol V. Robinson. 2015. "Bayesian Deconvolution of Mass and Ion Mobility Spectra: From Binary Interactions to Polydisperse Ensembles." *Analytical Chemistry* 87 (8): 4370–76.

Matunis, M. J., E. Coutavas, and G. Blobel. 1996. “A Novel Ubiquitin-like Modification Modulates the Partitioning of the Ran-GTPase-Activating Protein RanGAP1 between the Cytosol and the Nuclear Pore Complex.” *The Journal of Cell Biology* 135 (6 Pt 1): 1457–70.

Maver, Aleš, Goran Čuturilo, Anja Kovanda, Aleksandra Miletić, and Borut Peterlin. 2019. “Rare Missense TUBGCP5 Gene Variant in a Patient with Primary Microcephaly.” *European Journal of Medical Genetics* 62 (12): 103598.

McGill, M., and B. R. Brinkley. 1975. “Human Chromosomes and Centrioles as Nucleating Sites for the in Vitro Assembly of Microtubules from Bovine Brain Tubulin.” *The Journal of Cell Biology* 67 (1): 189–99.

McKinley, Kara L., and Iain M. Cheeseman. 2017. “Large-Scale Analysis of CRISPR/Cas9 Cell-Cycle Knockouts Reveals the Diversity of p53-Dependent Responses to Cell-Cycle Defects.” *Developmental Cell* 40 (4): 405–20.

Melki, Ronald, Irina E. Vainberg, Robert L. Chow, and Nicholas J. Cowan. 1993. “Chaperonin-Mediated Folding of Vertebrate Actin-Related Protein and γ-Tubulin.” *The Journal of Cell Biology* 122 (6): 1301–10.

Meng, Wenxiang, Yoshimi Mushika, Tetsuo Ichii, and Masatoshi Takeichi. 2008. “Anchorage of Microtubule Minus Ends to Adherens Junctions Regulates Epithelial Cell-Cell Contacts.” *Cell* 135 (5): 948–59.

Merdes, A., K. Ramyar, J. D. Vechio, and D. W. Cleveland. 1996. “A Complex of NuMA and Cytoplasmic Dynein Is Essential for Mitotic Spindle Assembly.” *Cell* 87 (3): 447–58.

Meunier, Sylvain, and Isabelle Vernos. 2016. “Acentrosomal Microtubule Assembly in Mitosis: The Where, When, and How.” *Trends in Cell Biology* 26 (2): 80–87.

Miki, Harukata, Yasushi Okada, and Nobutaka Hirokawa. 2005. “Analysis of the Kinesin Superfamily: Insights into Structure and Function.” *Trends in Cell Biology* 15 (9): 467–76.

Mishra, Ram Kumar, Papia Chakraborty, Alexei Arnaoutov, Beatriz M. A. Fontoura, and Mary Dasso. 2010. “The Nup107-160 Complex and γ-TuRC Regulate Microtubule Polymerization at Kinetochores.” *Nature Cell Biology* 12 (2): 164–69.

Mitani, Tadahiro, Jaya Punetha, Ibrahim Akalin, Davut Pehlivan, Mateusz Dawidziuk, Zeynep Coban Akdemir, Sarenur Yilmaz, et al. 2019. “Bi-Allelic Pathogenic Variants in TUBGCP2 Cause Microcephaly and Lissencephaly Spectrum Disorders.” *American Journal of Human Genetics* 105 (5): 1005–15.

Murphy, S. M., a. M. Preble, U. K. Patel, K. L. O'Connell, D. P. Dias, Michelle Moritz, David A. Agard, J. T. Stults, and Tim Stearns. 2001. "GCP5 and GCP6: Two New Members of the Human γ-Tubulin Complex." *Molecular Biology of the Cell* 12 (11): 3340–52.

Murphy, S. M., L. Urbani, and T. Stearns. 1998. "The Mammalian γ-Tubulin Complex Contains Homologues of the Yeast Spindle Pole Body Components spc97p and spc98p." *The Journal of Cell Biology* 141 (3): 663–74.

Nagai, Tomoaki, Masanori Ikeda, Shuhei Chiba, Shin-Ichiro Kanno, and Kensaku Mizuno. 2013. "Furry Promotes Acetylation of Microtubules in the Mitotic Spindle by Inhibition of SIRT2 Tubulin Deacetylase." *Journal of Cell Science* 126 (Pt 19): 4369–80.

Needleman, Daniel, Aaron Groen, Ryoma Ohi, Thomas Maresca, Leonid Mirny, and Tim Mitchison. 2009. "Fast Microtubule Dynamics in Meiotic Spindles Measured by Single Molecule Imaging: Evidence That the Spindle Environment Does Not Stabilize Microtubules." *Molecular Biology of the Cell* 21: 1033–46.

Neumann, Beate, Thomas Walter, Jean-Karim Hériché, Jutta Bulkescher, Holger Erfle, Christian Conrad, Phill Rogers, et al. 2010. "Phenotypic Profiling of the Human Genome by Time-Lapse Microscopy Reveals Cell Division Genes." *Nature* 464 (7289): 721–27.

Noordstra, Ivar, Qingyang Liu, Wilco Nijenhuis, Shasha Hua, Kai Jiang, Matthijs Baars, Sanne Remmelzwaal, Maud Martin, Lukas C. Kapitein, and Anna Akhmanova. 2016. "Control of Apico-Basal Epithelial Polarity by the Microtubule Minus-End-Binding Protein CAMSAP3 and Spectraplakin ACF7." *Journal of Cell Science* 129 (22): 4278–88.

Oakley, Berl R., Vitoria Paolillo, and Yixian Zheng. 2015. "γ-Tubulin Complexes in Microtubule Nucleation and beyond." *Molecular Biology of the Cell* 26 (17): 2957–62.

Oakley, C. Elizabeth, and Berl R. Oakley. 1989. "Identification of γ-Tubulin, a New Member of the Tubulin Superfamily Encoded by mipA Gene of Aspergillus Nidulans." *Nature* 338: 662–64.

Oegema, Karen, Christiane Wiese, Ona C. Martin, Ronald A. Milligan, Akihiro Iwamatsu, Timothy J. Mitchison, and Yixian Zheng. 1999. "Characterization of Two Related Drosophila γ-Tubulin Complexes That Differ in Their Ability to Nucleate Microtubules." *The Journal of Cell Biology* 144 (4): 721–33.

Ohba, T., M. Nakamura, H. Nishitani, and T. Nishimoto. 1999. "Self-Organization of Microtubule Asters Induced in Xenopus Egg Extracts by GTP-Bound Ran." *Science* 284 (5418): 1356–58.

Oh, Won Jun, and Estela Jacinto. 2011. “mTOR Complex 2 Signaling and Functions.” *Cell Cycle* 10 (14): 2305–16.

Olinares, Paul Dominic B., and Brian T. Chait. 2020. “Native Mass Spectrometry Analysis of Affinity-Captured Endogenous Yeast RNA Exosome Complexes.” *Methods in Molecular Biology* 2062: 357–82.

O’Toole, Eileen, Garrett Greenan, Karen I. Lange, Martin Srayko, and Thomas Müller-Reichert. 2012. “The Role of γ-Tubulin in Centrosomal Microtubule Organization.” *PloS One* 7 (1).

Park, Elizabeth M., Phillip M. Scott, Kevin Clutario, Katelyn B. Cassidy, Kevin Zhan, Scott A. Gerber, and Andrew J. Holland. 2020. “WBP11 Is Required for Splicing the TUBGCP6 Pre-mRNA to Promote Centriole Duplication.” *The Journal of Cell Biology* 219 (1).

Paz, Joel, and Jens Lüders. 2017. “Microtubule-Organizing Centers: Towards a Minimal Parts List.” *Trends in Cell Biology* 28 (3): 176–87.

Petry, Sabine, Aaron C. Groen, Keisuke Ishihara, Timothy J. Mitchison, and Ronald D. Vale. 2013. “Branching Microtubule Nucleation in Xenopus Egg Extracts Mediated by Augmin and TPX2.” *Cell* 152 (4): 768–77.

Pettersen, Eric F., Thomas D. Goddard, Conrad C. Huang, Gregory S. Couch, Daniel M. Greenblatt, Elaine C. Meng, and Thomas E. Ferrin. 2004. “UCSF Chimera--a Visualization System for Exploratory Research and Analysis.” *Journal of Computational Chemistry* 25 (13): 1605–12.

Piemonte, Katrina M., Lindsey J. Anstine, and Ruth A. Keri. 2021. “Centrosome Aberrations as Drivers of Chromosomal Instability in Breast Cancer.” *Endocrinology* 162 (12).

Poirier, Karine, Nicolas Lebrun, Loic Broix, Guoling Tian, Yoann Saillour, Cécile Boscheron, Elena Parrini, et al. 2013. “Mutations in TUBG1, DYNC1H1, KIF5C and KIF2A Cause Malformations of Cortical Development and Microcephaly.” *Nature Genetics* 45 (6): 639–47.

Pollard, Thomas D. 2016. “Actin and Actin-Binding Proteins.” *Cold Spring Harbor Perspectives in Biology* 8 (8).

Prosser, Suzanna L., and Laurence Pelletier. 2017. “Mitotic Spindle Assembly in Animal Cells: A Fine Balancing Act.” *Nature Reviews Molecular Cell Biology* 18: 187-201.

Rai, Ankit, Tianyang Liu, Eugene A. Katrukha, Juan Estévez-Gallego, Szymon W. Manka, Ian Paterson, J. Fernando Díaz, Lukas C. Kapitein, Carolyn A. Moores, and Anna Akhmanova. 2021. “Lattice Defects Induced by Microtubule-Stabilizing Agents Exert a Long-Range Effect on Microtubule Growth by Promoting Catastrophes.” *Proceedings of the National Academy of Sciences of the United States of America* 118 (51).

Rai, Dipti, Shasha Hua, Jooske L. Monster, Riccardo Stucchi, Kelly Stecker, Yaqian Zhang, Eugene A. Katrukha, et al. 2022. “CAMSAP-Driven Microtubule Release from γ-TuRC and Its Regulation by Nucleation-Promoting Factors.” *bioRxiv*. https://doi.org/10.1101/2022.08.03.502613.

Raman, Malavika, Mikhail Sergeev, Maija Garnaas, John R. Lydeard, Edward L. Huttlin, Wolfram Goessling, Jagesh V. Shah, and J. Wade Harper. 2015. “Systematic Proteomics of the VCP-UBXD Adaptor Network Identifies a Role for UBXN10 in Regulating Ciliogenesis.” *Nature Cell Biology* 17 (10): 1356–69.

Ramírez Cota, Rosa, N. Teixido-Travesa, Artur Ezquerra, Susana Eibes, Cristina Lacasa, Joan Roig, and Jens Lüders. 2017. “MZT1 Regulates Microtubule Nucleation by Linking γ-TuRC Assembly to Adapter-Mediated Targeting and Activation.” *Journal of Cell Science* 130 (2): 406–19.

Reck-Peterson, Samara L., William B. Redwine, Ronald D. Vale, and Andrew P. Carter. 2018. “The Cytoplasmic Dynein Transport Machinery and Its Many Cargoes.” *Nature Reviews. Molecular Cell Biology* 19 (6): 382–98.

Reid, Deseree J., Jessica M. Diesing, Matthew A. Miller, Scott M. Perry, Jessica A. Wales, William R. Montfort, and Michael T. Marty. 2019. “MetaUniDec: High-Throughput Deconvolution of Native Mass Spectra.” *Journal of the American Society for Mass Spectrometry* 30 (1): 118–27.

Renda, Fioranna, Christopher Miles, Irina Tikhonenko, Rebecca Fisher, Lina Carlini, Tarun M. Kapoor, Alex Mogilner, and Alexey Khodjakov. 2022. “Non-Centrosomal Microtubules at Kinetochores Promote Rapid Chromosome Biorientation during Mitosis in Human Cells.” *Current Biology: CB* 32 (5): 1049–63.

Rice, Luke M., Elizabeth A. Montabana, and David A. Agard. 2008. “The Lattice as Allosteric Effector: Structural Studies of αβ- and γ-Tubulin Clarify the Role of GTP in Microtubule Assembly.” *Proceedings of the National Academy of Sciences of the United States of America* 105 (14): 5378–83.

Rice, Luke M., Michelle Moritz, and David A. Agard. 2021. “Microtubules Form by Progressively Faster Tubulin Accretion, Not by Nucleation–elongation.” *The Journal of Cell Biology* 220 (5).

Roostalu, Johanna, Nicholas I. Cade, and Thomas Surrey. 2015. “Complementary Activities of TPX2 and chTOG Constitute an Efficient Importin-Regulated Microtubule Nucleation Module” 17 (11).

Roostalu, Johanna, and Thomas Surrey. 2017. “Microtubule Nucleation: Beyond the Template.” *Nature Reviews. Molecular Cell Biology* 18 (11): 702–10.

Sanchez, Ariana D., and Jessica L. Feldman. 2017. “Microtubule-Organizing Centers: From the Centrosome to Non-Centrosomal Sites.” *Current Opinion in Cell Biology* 44: 93–101.

Sankaran, Satish, Lea M. Starita, Aaron C. Groen, Min Ji Ko, and Jeffrey D. Parvin. 2005. “Centrosomal Microtubule Nucleation Activity Is Inhibited by BRCA1-Dependent Ubiquitination.” *Molecular and Cellular Biology* 25 (19): 8656–68.

Scheidecker, Sophie, Christelle Etard, Laurence Haren, Corinne Stoetzel, Sarah Hull, Gavin Arno, Vincent Plagnol, et al. 2015. “Mutations in TUBGCP4 Alter Microtubule Organization via the γ-Tubulin Ring Complex in Autosomal-Recessive Microcephaly with Chorioretinopathy.” *American Journal of Human Genetics* 96(4): 666-674.

Shearer, Robert F., Kari Anne Myrum Frikstad, Jessie McKenna, Rachael A. McCloy, Niantao Deng, Andrew Burgess, Trond Stokke, Sebastian Patzke, and Darren N. Saunders. 2018. “The E3 Ubiquitin Ligase UBR5 Regulates Centriolar Satellite Stability and Primary Cilia.” *Molecular Biology of the Cell* 29 (13): 1542–54.

Shin, Ji-Yeon, and Howard J. Worman. 2022. “Molecular Pathology of Laminopathies.” *Annual Review of Pathology* 17 (January): 159–80.

Sillibourne, James Edward, Bénédicte Delaval, Sambra Redick, Manisha Sinha, and Stephen John Doxsey. 2007. “Chromatin Remodeling Proteins Interact with Pericentrin to Regulate Centrosome Integrity.” *Molecular Biology of the Cell* 18 (9): 3667–80.

So, Chun, K. Bianka Seres, Anna M. Steyer, Eike Mönnich, Dean Clift, Anastasija Pejkovska, Wiebke Möbius, and Melina Schuh. 2019. “A Liquid-like Spindle Domain Promotes Acentrosomal Spindle Assembly in Mammalian Oocytes.” *Science* 364 (6447). https://doi.org/10.1126/science.aat9557.

Strome, Susan, James Powers, Melanie Dunn, Kimberly Reese, Christian J. Malone, John White, Geraldine Seydoux, and William Saxton. 2001. “Spindle Dynamics and the Role of γ-Tubulin in Early Caenorhabditis Elegans Embryos.” *Molecular Biology of the Cell* 12: 1751–64.

Sulimenko, Vadym, Eduarda Dráberová, and Pavel Dráber. 2022. “γ-Tubulin in Microtubule Nucleation and beyond.” *Frontiers in Cell and Developmental Biology* 10: 880761.

Sung, M., and P. Giannakakou. 2014. “BRCA1 Regulates Microtubule Dynamics and Taxane-Induced Apoptotic Cell Signaling.” *Oncogene* 33 (11): 1418–28.

Teixido-Travesa, N., J. Villen, C. Lacasa, M. T. Bertran, M. Archinti, S. P. Gygi, C. Caelles, J. Roig, and Jens Lüders. 2010. “The γ-TuRC Revisited: A Comparative Analysis of Interphase and Mitotic Human γ-TuRC Redefines the Set of Core Components and Identifies the Novel Subunit GCP8.” *Molecular Biology of the Cell* 21: 3963–72.

Thevenaz, P., U. E. Ruttimann, and M. Unser. 1998. “A Pyramid Approach to Subpixel Registration Based on Intensity.” *IEEE Transactions on Image Processing: A Publication of the IEEE Signal Processing Society* 7 (1): 27–41.

Ti, Shih Chieh, Melissa C. Pamula, Stuart C. Howes, Christian Duellberg, Nicholas I. Cade, Ralph E. Kleiner, Scott Forth, Thomas Surrey, Eva Nogales, and Tarun M. Kapoor. 2016. “Mutations in Human Tubulin Proximal to the Kinesin-Binding Site Alter Dynamic Instability at Microtubule Plus- and Minus-Ends.” *Developmental Cell* 37 (1): 72–84.

Ti, Shih-Chieh, Michal Wieczorek, and Tarun M. Kapoor. 2020. “Purification of Affinity Tag-Free Recombinant Tubulin from Insect Cells.” *STAR Protocols* 1: 100011.

Tovey, Corinne A., Chloe E. Tubman, Eva Hamrud, Zihan Zhu, Anna E. Dyas, Andrew N. Butterfield, Alex Fyfe, Errin Johnson, and Paul T. Conduit. 2018. “γ-TuRC Heterogeneity Revealed by Analysis of Mozart1.” *Current Biology: CB* 28 (14): 2314–23.e6.

Tsuchiya, Kenta, and Gohta Goshima. 2021. “Microtubule-Associated Proteins Promote Microtubule Generation in the Absence of γ-Tubulin in Human Colon Cancer Cells.” *The Journal of Cell Biology* 220 (12).

Tulu, U. Serdar, Carey Fagerstrom, Nick P. Ferenz, and Patricia Wadsworth. 2006. “Molecular Requirements for Kinetochore-Associated Microtubule Formation in Mammalian Cells.” *Current Biology: CB*, 536–41.

Tungadi, Elsa A., Ami Ito, Tomomi Kiyomitsu, and Gohta Goshima. 2017. “Human Microcephaly ASPM Protein Is a Spindle Pole-Focusing Factor That Functions Redundantly with CDK5RAP2.” *Journal of Cell Science* 130 (21): 3676–84.

Uphoff, Cord C., and Hans G. Drexler. 2014. “Detection of Mycoplasma Contamination in Cell Cultures.” *Current Protocols in Molecular Biology*. 106: 28.4.1–14.

Valdez, Venecia A., Lila Neahring, Sabine Petry, and Sophie Dumont. 2023. “Mechanisms Underlying Spindle Assembly and Robustness.” *Nature Reviews. Molecular Cell Biology*. https://doi.org/10.1038/s41580-023-00584-0.

Verma, Vikash, and Thomas J. Maresca. 2019. “Direct Observation of Branching MT Nucleation in Living Animal Cells” 218 (9): 2829–40.

Verma, Vikash, and Thomas J. Maresca. 2022. “A Celebration of the 25th Anniversary of Chromatin-Mediated Spindle Assembly.” *Molecular Biology of the Cell* 33 (2): 1–6.

Vineethakumari, Chithran, and Jens Lüders. 2022. “Microtubule Anchoring: Attaching Dynamic Polymers to Cellular Structures.” *Frontiers in Cell and Developmental Biology* 10: 867870.

Walker, R. A., E. T. O’Brien, N. K. Pryer, M. F. Soboeiro, W. A. Voter, H. P. Erickson, and E. D. Salmon. 1988. “Dynamic Instability of Individual Microtubules Analyzed by Video Light Microscopy: Rate Constants and Transition Frequencies” 107: 1437–48.

Wang, Huanxi, Xizi Jiang, Yu Cheng, Hongjiu Ren, Yujiao Hu, Yao Zhang, Hongbo Su, et al. 2021. “MZT2A Promotes NSCLC Viability and Invasion by Increasing Akt Phosphorylation via the MOZART2 Domain.” *Cancer Science* 112 (6): 2210–22.

Watanabe, Sadanori, Franz Meitinger, Andrew K. Shiau, Karen Oegema, and Arshad Desai. 2020. “Centriole-Independent Mitotic Spindle Assembly Relies on the PCNT – CDK5RAP2 Pericentriolar Matrix” 219 (12).

Widlund, Per O., Marija Podolski, Simone Reber, Joshua Alper, Marko Storch, Anthony A. Hyman, Jonathon Howard, David N. Drechsel, and David G. Drubin. 2012. “One-Step Purification of Assembly-Competent Tubulin from Diverse Eukaryotic Sources.” *Molecular Biology of the* Cell 23(22): 4393-4401.

Widlund, Per O., Jeffrey H. Stear, Andrei Pozniakovsky, Marija Zanic, Simone Reber, Gary J. Brouhard, Anthony A. Hyman, and Jonathon Howard. 2011. “XMAP215 Polymerase Activity Is Built by Combining Multiple Tubulin-Binding TOG Domains and a Basic Lattice-Binding Region.” *Proceedings of the National Academy of Sciences of the United States of America* 108 (7): 2741–46.

Wieczorek, Michal, Susanne Bechstedt, Sami Chaaban, and Gary J. Brouhard. 2015. “Microtubule-Associated Proteins Control the Kinetics of Microtubule Nucleation.” *Nature Cell Biology* 17 (7): 907–16.

Wieczorek, Michal, Tzu-Lun Huang, Linas Urnavicius, Kuo-Chiang Hsia, and Tarun M. Kapoor. 2020. “MZT Proteins Form Multi-Faceted Structural Modules in the γ-Tubulin Ring Complex.” *Cell Reports* 31 (107791).

Wieczorek, Michal, Shih Chieh Ti, Linas Urnavicius, Kelly R. Molloy, Amol Aher, Brian T. Chait, and Tarun M. Kapoor. 2021. “Biochemical Reconstitutions Reveal Principles of Human γ-TuRC Assembly and Function.” *The Journal of Cell Biology* 220 (3).

Wieczorek, Michal, Linas Urnavicius, Shih Chieh Ti, Kelly R. Molloy, Brian T. Chait, and Tarun M. Kapoor. 2020. “Asymmetric Molecular Architecture of the Human γ-Tubulin Ring Complex.” *Cell*, 1–11.

Wiese, Christiane, and Yixian Zheng. 2000. “A New Function for the γ-Tubulin Ring Complex as a Microtubule Minus-End Cap.” *Nature Cell Biology* 2 (6): 358–64.

Wilde, A., and Y. Zheng. 1999. “Stimulation of Microtubule Aster Formation and Spindle Assembly by the Small GTPase Ran.” *Science* 284 (5418): 1359–62.

Witt, P. L., H. Ris, and G. G. Borisy. 1980. “Origin of Kinetochore Microtubules in Chinese Hamster Ovary Cells.” *Chromosoma* 81 (3): 483–505.

Wojcik, Cezary, Mihiro Yano, and George N. DeMartino. 2004. “RNA Interference of Valosin-Containing Protein (VCP/p97) Reveals Multiple Cellular Roles Linked to Ubiquitin/proteasome-Dependent Proteolysis.” *Journal of Cell Science* 117 (2): 281–92.

Woodruff, Jeffrey B., Beatriz Ferreira Gomes, Per O. Widlund, Julia Mahamid, Alf Honigmann, and Anthony A. Hyman. 2017. “The Centrosome Is a Selective Condensate That Nucleates Microtubules by Concentrating Tubulin.” *Cell* 169 (6): 1066–71.e10.

Woodruff, Jeffrey B., O. Wueseke, and Anthony A. Hyman. 2014. “Pericentriolar Material Structure and Dynamics.” *Philosophical Transactions of the Royal Society of London. Series B, Biological Sciences* 369 (1650): 20130459–20130459.

Wu, Jingchao, and Anna Akhmanova. 2017. “Microtubule-Organizing Centers.” *Annual Reviews in Cell and Dev. Biol.*, no. 33: 51–75.

Wu, Jingchao, Cecilia de Heus, Qingyang Liu, Benjamin P. Bouchet, Ivar Noordstra, Kai Jiang, Shasha Hua, et al. 2016. “Molecular Pathway of Microtubule Organization at the Golgi Apparatus.” *Developmental Cell* 39 (1): 44–60.

Wu, Jingchao, Ainhoa Larreategui-Aparicio, Maaike L. A. Lambers, Dani L. Bodor, Sjoerd J. Klaasen, Eveline Tollenaar, Marta de Ruijter-Villani, and Geert J. P. L. Kops. 2023. “Microtubule Nucleation from the Fibrous Corona by LIC1-Pericentrin Promotes Chromosome Congression.” *Current Biology: CB* 33 (5): 912–25.e6.

Würtz, Martin, Anna Böhler, Annett Neuner, Erik Zupa, Lukas Rohland, Peng Liu, Bram J. A. Vermeulen, Stefan Pfeffer, Sebastian Eustermann, and Elmar Schiebel. 2021. “Reconstitution of the Recombinant Human γ-Tubulin Ring Complex.” *Open Biology* 11: 200325.

Würtz, Martin, Erik Zupa, Enrico S. Atorino, Annett Neuner, Anna Böhler, Ariani S. Rahadian, Bram J. A. Vermeulen, et al. 2022. “Modular Assembly of the Principal Microtubule Nucleator γ-TuRC.” *Nature Communications*, no. 2022.

Yan, Xiumin, Robert Habedanck, and Erich A. Nigg. 2006. “A Complex of Two Centrosomal Proteins, CAP350 and FOP, Cooperates with EB1 in Microtubule Anchoring.” *Molecular Biology of the Cell* 17 (2): 634–44.

Yau, Kah Wai, Sam F. B. vanBeuningen, Inês Cunha-Ferreira, Bas M. C. Cloin, Eljo Y. vanBattum, Lena Will, Philipp Schätzle, et al. 2014. “Microtubule Minus-End Binding Protein CAMSAP2 Controls Axon Specification and Dendrite Development.” *Neuron* 82 (5): 1058–73.

Yokoyama, Hideki, Birgit Koch, Rudolf Walczak, Fulya Ciray-Duygu, Juan Carlos González-Sánchez, Damien P. Devos, Iain W. Mattaj, and Oliver J. Gruss. 2014. “The Nucleoporin MEL-28 Promotes RanGTP-Dependent γ-Tubulin Recruitment and Microtubule Nucleation in Mitotic Spindle Formation.” *Nature Communications* 5: 3270.

Young, A., J. B. Dictenberg, A. Purohit, R. Tuft, and S. J. Doxsey. 2000. “Cytoplasmic Dynein-Mediated Assembly of Pericentrin and Gamma Tubulin onto Centrosomes.” *Molecular Biology of the Cell* 11 (6): 2047–56.

Zhang, Yaqian, Xing Hong, Shasha Hua, and Kai Jiang. 2022. “Reconstitution and Mechanistic Dissection of the Human Microtubule Branching Machinery.” *The Journal of Cell Biology* 221 (7).

Zheng, Yixian, Mei Lie Wong, Bruce Alberts, and Timothy J. Mitchison. 1995. “Nucleation of Microtubule Assembly by a γ-Tubulin-Containing Ring Complex.” *Nature* 378 (6557): 578–83.

Zhu, Hui, Judith A. Coppinger, Chang-Young Jang, John R. Yates, and Guowei Fang. 2008. “FAM29A Promotes Microtubule Amplification via Recruitment of the NEDD1–γ-Tubulin Complex to the Mitotic Spindle.” *The Journal of Cell Biology* 183 (5): 835–48.

Zhu, Mei, Florian Settele, Sachin Kotak, Luis Sanchez-Pulido, Lena Ehret, Chris P. Ponting, Pierre Gönczy, and Ingrid Hoffmann. 2013. “MISP Is a Novel Plk1 Substrate Required for Proper Spindle Orientation and Mitotic Progression.” *The Journal of Cell Biology* 200 (6): 773–87.

Zimmermann, Fabian, Marina Serna, Artur Ezquerra, Rafael Fernandez-leiro, Oscar Llorca, and Jens Lüders. 2020. “Assembly of the Asymmetric Human γ-Tubulin Ring Complex by RUVBL1-RUVBL2 AAA ATPase.” *Science Advances*, 1–20.

Zimmerman, Wendy C., James Sillibourne, Jack Rosa, and Stephen J. Doxsey. 2004. "Mitosis-Specific Anchoring of γ-Tubulin Complexes by Pericentrin Controls Spindle Organization and Mitotic Entry." *Molecular Biology of the Cell* 15 (8): 3642–57.

Zupa, Erik, Martin Würtz, Annett Neuner, Thomas Hoffmann, Mandy Rettel, Anna Böhler, Bram J. A. Vermeulen, Sebastian Eustermann, Elmar Schiebel, and Stefan Pfeffer. 2022. "The Augmin Complex Architecture Reveals Structural Insights into Microtubule Branching." *Nature Communications* 13 (1): 5635.